NASA-CR-192356

NAG 3-831

# GENERATION OF MONODISPERSE DROPLETS BY SPONTANEOUS CONDENSATION OF FLOW IN NOZZLES

by

DER-SHAIUN LAI
and
J.R. KADAMBI

FINAL TECHNICAL REPORT
NASA GRANT NAG 3-831

Department of Mechanical and Aeropsace Engineering

CASE WESTERN RESERVE UNIVERSITY
Cleveland, Ohio 44106

January 1993

REPORT #NAG-3-831 FR1.

GENERATION OF MONODISPERSE DROPLETS BY SPONTANEOUS CONDENSATION OF FLOW IN NOZZLES

## Abstract

Submicron size monodisperse particles are of interest in many industrial and scientific applications. These include the manufacture of ceramic parts using fine ceramic particles, the production of thin films by deposition of ionized clusters, monodisperse seed particles for laser anemometry, and the study of size dependence of cluster chemical and physical properties. An inexpensive and relatively easy way to generate such particles is by utilizing the phenomenon of spontaneous condensation. The phenomenon occurs when the vapor or a mixture of a vapor and a noncondensing gas is expanded at a high expansion rate. The saturation line is crossed with the supercooled vapor behaving like a gas, until all of a sudden at so called the Wilson point, condensation occurs, resulting in a large number of relatively monodisperse droplets. The droplet size is a function of the expansion rate, inlet conditions, mass fraction of vapor, gas properties, etc.

In this dissertation, spontaneous condensation of (a) steam and (b) water vapor and air mixture in one dimensional nozzle has been modeled and the resulting equations solved numerically. The classical (Frenkel and Volmer) and Deich's nucleation theories were used. Unlike classical theory, Deich's theory also accounts for the critical droplet size dependence upon the expansion rate in the nozzle. The droplet size distribution at the exit of various one dimensional nozzles and the flow characteristics such as pressure ratio, mean droplet radius, vapor and droplet temperatures, nucleation flux, supercooling, wetness etc., along the axial distance were obtained. The numerical results compared very well with the available experimental data. Both nucleation theories predicted the pressure ratio properly but the classical theory tended to overestimate the droplet sizes. Additionally, since the classical theory cannot be used for obtaining a correlation for surface tension ratio, Deich's theory is preferred for analyzing and designing new nozzles.

The effect of inlet conditions, nozzle expansion rates and vapor mass fractions on droplet mean radius, droplet size distribution and pressure ratio were examined. By manipulating the various parameters, different mean radius and pressure ratio can be obtained. However, this only has minor impact on the relatively monodisperse droplet size distribution.

TABLE OF CONTENTS

LIST OF TABLES

table

LIST OF FIGURES

figure

NOMENCLATURE

| | |
|---|---|
| $A(x)$ | Area ($m^2$) at location x |
| $C(x)$ | Velocity (m/sec) at location x |
| $c_p$ | Specific heat at constant pressure for vapor phase (J/kg/K) |
| $c_f$ | Specific heat of liquid phase (J/kg/K) |
| $h$ | Enthalpy (J/kg) |
| $h_0$ | Stagnation (total) enthalpy (J/kg) |
| $J$ | Nucleation flux (no. of nuclei per sec. per kg of mixture) |
| $k$ | Thermal conductivity (J/sec/m/K) |
| $M$ | Mach Number |
| $\bar{N}$ | No. of molecules per kg |
| $p$ | Pressure (Pa) |
| $\dot{p}$ | Expansion rate (1/sec) |
| $r_i(x_i;x)$ | Radius of droplet formed at location $x_i$ and currently located at location x |
| $R$ | Gas constant (J/kg/K) |
| $s$ | supersaturation |
| $T$ | Temperature (K) |
| $T_f$ | Droplet mean temperature (K) |
| $T_{f,i}(x_i;x)$ | Temperature of droplet formed at location $x_i$ and currently located at location x (K) |

| | |
|---|---|
| $\Delta T$ | Supercooling (K) |
| $v_{sg}$ | Specific volume of saturated steam ($m^3/kg$) |
| $w$ | Total wetness (kg of liquid phase/kg of mixture) |
| $w_i(x_i;x)$ | Wetness due to droplets formed at location $x_i$ and currently located at location x (kg of liquid phase/kg of mixture) |
| $w_0$ | mass fraction of the condensing vapor contained in the mixture before expansion |
| $x$ | Axial location along the nozzle downstream of the throat (m) |

Greek

| | |
|---|---|
| $\alpha_i(x_i;x)$ | Heat transfer coefficient between vapor phase and droplet formed at location $x_i$ currently located at location x ($J/sec/m^2/K$) |
| $\gamma$ | Ratio of specific heat |
| $\rho$ | Density ($kg/m^3$) |
| $\Lambda$ | ln(s) |
| $\mu$ | Viscosity ($N \cdot sec/m^2$) |
| $\sigma$ | Surface tension (N/m) |

Subscript

| | |
|---|---|
| f | Liquid phase |
| g | Vapor phase |
| s | Saturation |

# CHAPTER 1 INTRODUCTION

Submicron size monodisperse particles are of interest in many industrial, as well as scientific applications. These include the manufacture of ceramic parts using ceramic particles, the production of thin metal, semiconductor and organic films by deposition of ionized clusters, and the study of the size of dependence of cluster chemical and physical properties [1.01]. Monodisperse seed particles are also of great importance in laser anemometry. The ultimate accuracy of particle scattering based laser velocimetry measurement depends upon the ability of the light scattering seed particles to faithfully track the local flow field. For achieving maximum measurement efficiency, the control of seed particle size, size distribution, shape and a specific material density is desired [1.02]. Edwards [1.03] suggests that all possible bias problems in laser anemometry would be easier to be dealt with if there existed an inexpensive seeder that was capable of generating monodisperse seed particles fast enough to provide acceptable levels of data density. The size ranges of 0.1 to 1 μm are of great interest in seeding high speed flows such as high subsonic, transonic, supersonic and hypersonic flows.

The phenomenon of spontaneous condensation, also called homogeneous condensation, can be utilized for generating monodisperse particles. The phenomenon occurs when the vapor or the mixture of vapor and gas is expanded at a high expansion rate through a nozzle, such that the saturation line on the Mollier chart is crossed with the supercooled vapor behaving like a gas until all of a sudden at a certain point called the Wilson point, condensation occurs, and the condensate separates out, resulting in a large number of nearly monodisperse droplets. The droplet size is a function of the expansion rate, nozzle geometry, inlet total conditions, mass fraction of vapor in case of vapor gas mixture, gas properties, etc.

The phenomenon of spontaneous condensation is also of much interest in the problem of wetness loss in the low pressure as well as high pressure stages [1.04], [1.05], [1.06] of steam turbines. The latter case was stimulated by the advent of the light-water-cooled reactors which supplies dry saturated steam at inlet to the high pressure cylinder of the turbine. The same phenomenon was found important in the supersonic and hypersonic wind tunnels [1.07], [1.08], [1.09] and free-jet expansions [1.10]. Condensation is usually undesirable in these applications, and therefore a better understanding and prediction

of the phenomenon are crucial to the control or even elimination of the condensation.

Experimental and theoretical studies of expansion of steam through supersonic nozzles has been conducted by various investigators [1.11], [1.12], [1.13], [1.14], [1.15], [1.16]. Experiments conducted by Gyarmathy and Meyer [1.13] show a strong relationship between the rate of expansion in the nozzle and the spontaneous condensation process. The theoretical investigation of steam nozzle flows [1.13], [1.14], [1.16], [1.17] have mostly been conducted from the point of view of obtaining the pressure rise, moisture levels and the decrease in the nozzle efficiency associated with the spontaneous condensation process. More recently, Turner et al. [1.01] have investigated the use of subsonic nozzles for the formation of monodisperse particles in a system of interest for industrial powder production. A mixture of nitrogen and aluminum sec-butoxide vapor was considered.

While several theories have been proposed for obtaining the nucleation rate during spontaneous condensation, the two main theories of interest are the classical theory (known as the Frenkel and Volmer theory) and the theory developed by Deich et al. The most widely adopted classical nucleation theory is discussed by many authors [1.18], [1.06], [1.19], [1.20]. Deich's

nucleation theory is reviewed by Moore [1.16] and Kadambi and Whirlow [1.14]. The derivation of the classical theory is based upon the kinetic theory [1.18]. The nucleation rate can be expressed as a function of thermodynamic properties and the surface tension coefficient. Deich's theory accounts for two components of the formation of nuclei. The first one arises from the so-called "heterophase fluctuations", which means that statistically a number of molecules will clump together and form a droplet size equal to or greater than the critical size necessary for survival and subsequent growth. This component corresponds to the classical theory but considers more realistic conditions about the steadiness of the droplet generation and is considerably smaller in magnitude than the classical theory. The second component arises from the fact that the critical size depends upon the vapor condition in a fashion such that during expansion in the nozzle, the critical droplet size decreases. As a result, some droplets formed at subcritical sizes are transported, before they can evaporate, to a downstream region where their sizes become super critical. The final nucleation rate is the addition of the two components. It can be shown that the second component is usually of order of magnitude much higher than the first one and is directly proportioned to the expansion rate in the nozzle.

One of the major drawback of the classical theory is that it does not directly account for the effect of the rate of expansion on the nucleation rate, while Deich's theory does. According to Gyarmathy [1.13], the experimental observation shows that expansion rate has strong effects on the nucleation rate. It is also noted that all nucleation theories cannot achieve satisfactory agreement with experimental data without using any correction factors. One of the unknown parameters in the nucleation theory equations, which also has substantial effects on the nucleation rate, is the surface tension for small droplets. By using surface tension ratio as correcting factor, Moore [1.16] showed that the classical theory cannot obtain agreement with the experimental data of pressure ratio and mean droplet radius simultaneously. The other drawback of the classical theory is that it can not establish usable correlations between the flow conditions and the correcting factor. Such correlation is especially desirable if the method has to be utilized for predicting various new flow conditions. Saltanov [1.17] has used surface tension for flat surface in his study and uses a correction coefficient in the exponential term for the nucleation rate in the classical theory equations. He varied the value of the coefficient to obtain agreement with experimental pressure ratio and obtained a correlation between the correction coefficient and the inlet total pressure. However, only three

data points were considered in a pressure range $P_t$ < 40 psia and there was considerable scatter.

## 1.1 Objectives

The objective of this work was to develop a theoretical/numerical model of the flow of vapor and vapor/inert gas mixture in a supersonic nozzle with spontaneous condensation, capable of predicting droplet size distribution. The model would be a useful tool to design nozzles to obtain desired micron sized droplets. Steam was selected as the vapor because of availability of experimental data to verify the model. The classical and the Deich's nucleation theories were used in this study to provide a comparison between the two.

# CHAPTER 2 DESCRIPTION OF SPONTANEOUS CONDENSATION PHENOMENA

## 2.1 Introduction

To generate relatively monodisperse particles, a spontaneous condensation based monodisperse particle generator is proposed. The analysis will consist of the expansion process of both the supercooled vapor phase and condensed liquid phase. The variables which define the characteristics of the two phases are related by the conservation laws of mass, momentum and energy of the whole system as well as the "life history" of the condensate: when are the droplets born? what are their sizes and number when first born? how will they grow? Before we present all the governing equations and calculation procedures, it is beneficial to define some of the fundamental concepts and outline the specific problem we will be dealing with in the later analysis.

## 2.2 Homogeneous Condensation In A Supersonic Nozzle Flow

Let us consider a vapor expanded from a superheated state such that it crosses the saturation line. If the expansion is

relatively fast, the vapor will not have enough time to adjust itself immediately for the condensation. Rather, it will remain as vapor even after crossing the saturation line. This vapor phase which is in a meta-stable equilibrium condition and behaves like superheated vapor is referred to as "supercooled vapor". Very often, the name "supersaturated" or "subcooled" is also used.

When a vapor or a mixture of vapor and gas is expanded in a nozzle in a relatively high expansion rate, condensation may be delayed with respect to the equilibrium states (as described in the previous paragraph, no condensation occurs even after crossing the saturation line). The supercooled vapor continues to expand just like a superheated vapor. At certain point called Wilson point where the supercooled vapor can no longer hold its meta stable equilibrium condition, further expansion causes a sudden collapse of the supersaturation with the formation of nearly monodisperse droplets appearing in the form of a fog. This process is called spontaneous condensation or homogeneous condensation which takes place in absence of any foreign nuclei. This phenomenon is also observed in supersonic wind tunnels (when humidity is high and the moisture separates out all of a sudden in the form of a fog), wet steam nozzles and steam turbine blade passages. The release of latent heat during condensation results

in a diabatic flow with an increase in pressure.

The phenomenon for steam or any other vapor flow in a condensing Laval nozzle is shown in Figure 2.1. The enthalpy-entropy diagram shows the isentropic expansion vapor from initial stagnation conditions to crossing the saturation line and staying in a supersaturated state until at pressure $p_w$ when suddenly spontaneous condensation occurs. The release of latent heat causing an increase in temperature and pressure as well as entropy. This pressure rise is often misinterpreted as the condensation shock. As will be shown later, the steepness of the pressure rise depends mainly on the expansion rate as well as the stagnation conditions of the vapor prior to expansion. At low expansion rate the pressure rise is not appreciable. The supercooling decreases as the vapor temperature, pressure and entropy increase. Consequently, the supercooled vapor becomes closer and closer to its equilibrium state. The spontaneous condensation process takes place in a very short time. Eventually, at the end of spontaneous condensation shown by pressure $P_E$ in Figure 2.1, the supercooled vapor will almost achieve its equilibrium state and further expansion would take place almost like an equilibrium isentropic expansion again. There will still be a very small amount of supercooling at the end of spontaneous condensation, and the supercooled vapor will

gradually recover back to the equilibrium state as the expansion continues or the adjustment would occur in the form of either weak oblique shock or expansion wave at the exit of the nozzle depending on whether the atmosphere pressure is smaller or larger than the exit pressure. Since the degree of supercooling at this stage is so small (usually only a few degree F), the deviation from the equilibrium case is usually negligible. Besides, the complex non-equilibrium phenomena occurs at the exit of the nozzle is not our main interests thus will not be discussed in this work.

A lot of information which would serve for different applications can be obtained from the simulation of the process described above. For example, the information about velocity and Mach number variation, as well as the Wilson point and the pressure distribution would be useful in wind tunnel application; the wetness level would be useful in examining the erosion on turbine blades; the entropy increase would be valuable in calculating the loss in total pressure or the efficiency on turbine application; etc. Our main interest is to obtain the mean droplet size and size distribution and proper correlation between the crucial parameter and the inlet condition so that one can design the nozzle to give us the desired size and distribution.

## 2.3 Fundamental Definitions

We have illustrated the physical phenominon and the model we will be analyzing in the last setion. Before we can go on to the mathematical simulation equations, we need to quantitatively define the degree of supersaturation and some of the important physical qantities.

### 2.3.1 supercooling

By assuming isentropic expansion and treating the vapor phase as an ideal gas with constant specific heat at constant pressure $c_{pg}$ and constant specific heat ratio $\gamma$, we can greatly simplify our analysis without losing the essence of the phenomena. As shown in Figure 2.2, suppose the vapor is expanded isentropically from the superheated state noted as point T, across the saturation line at point A to a certain supercooled state B on the Mollier chart (enthalpy-entropy chart). The location of point B on the Mollier chart can be determined by the enthalpy drop $\Delta h$ between the two states A and B

$$\Delta h = \frac{\gamma}{\gamma - 1} RT_A \left[ 1 - \left( \frac{p_B}{p_A} \right)^{\frac{\gamma - 1}{\gamma}} \right] \qquad (2.1)$$

By shifting the expansion line to the right and left, we can eventually construct the isobar passing point B which intersects the saturation line at point C as shown in Figure 2.2. For ideal gas, the isotherms coincide with the constant enthalpy line. Since the supercooled vapor is considered to behave just like the superheated vapor, the isotherm crossing point B will be the extension of the isotherm in the superheated region. This isotherm shown in Figure 2.2 has the intersection with saturation line at point D. Therefore, the saturation temperature corresponding to the supercooled vapor pressure $p_B$ will be $T_s(p_B) = T_C$ . From Figure 2.2, we can see that

$$T_B < T_C = T_s(p_B) \qquad (2.2)$$

The temperature of the supercooled vapor is always lower than the saturation temperature corresponding to its own pressure. The supercooling $\Delta T$ is defined to be the temperature difference between the two:

$$\Delta T = T_s(p_B) - T_B \qquad (2.3)$$

Supercooling represents the deviation of the state of the supercooled vapor from the equilibrium condition. The higher the supercooling, the larger the extent of the non-equilibrium.

### 2.3.2 supersaturation

From Figure 2.2, we can also see that the saturation pressure corresponding to temperature $T_B$ is the same as the pressure at point D, $p_s(T_B) = p_D$ . The isobar passing point D lies below the isobar passing point C which is corresponding to $p_B$, therefore, we have

$$p_B > p_D = p_s(T_B) \tag{2.4}$$

The pressure of the supercooled vapor is always higher than the saturation pressure corresponding to its own temperature. The supersaturation s is defined as the ratio:

$$s = \frac{p_B}{p_s(T_B)} \tag{2.5}$$

The natural logarithm of the supersaturation $\Lambda$ is usually more useful

$$\Lambda = \ln\left( \frac{p_g}{p_s(T_g)} \right) \tag{2.6}$$

2.3.3 critical radius

The stability of a spherical droplet surrounded by the vapor phase was studied by Thompson (1870), Helmholtz (1886) and Gibbs (1878) [1.18]. Though their work proceeded largely independently, by considering the chemical potential and mechanical equilibrium, they found the radius of a droplet in equilibrium with its vapor can be expressed as

$$r_{cr} = \frac{2\sigma}{\rho_f R T_g \Lambda} \tag{2.7}$$

An alternative expression shown by Kirillov et al. [1.06] is

$$r_{cr} = \frac{2\sigma}{\rho_f h_{fg} \ln\left( \frac{T_s}{T_g} \right)} \tag{2.8}$$

The detail derivation can be found from Kirillov et al. [1.06], and will not be presented here.

The significance of the critical radius is that it defines the minimum size of the droplet able to survive under the given vapor conditions. If the droplet radius is below the critical radius, the chemical potential of the liquid phase increases, and the liquid phase tends to convert to vapor, i.e. the droplet will vaporize. On the other hand, if the droplet radius is beyond critical, the chemical potential of the vapor phase increases, and the vapor tends to convert to the liquid phase, i.e. the droplet will grow. If the droplet radius is equal to the critical radius, its size will remain unchanged provided the pressure and temperature of the vapor phase remain the same. Thus, only those droplets which have reached the critical size can serve as the condensation nuclei. As shown by Kirillov et al. [1.06], the critical radius is primarily affected by the supercooling $\Delta T$ (or $\Lambda$ which is closely related to $\Delta T$) and is insensitive to the change of pressure.

# CHAPTER 3 NUCLEATION THEORIES

Though it is not the purpose of this work to review the development and status of the spontaneous nucleation theory in detail, it is important to consider the basic concepts and do a comparison of the two theories used in this work. The detailed historical evolution and discussion can be found in various books and articles [3.01], [1.18], [1.20], and it is sufficient to say that the the theoretical prediction of the nucleation rate is still in doubt by several orders of magnitude.

In the absence of foreign nuclei or during the rapid expansion where the condensate accumulation on the foreign nuclei is small enough to be negligible, the condensation will be delayed with respect to equilibrium state. As will be discussed later, the spontaneous condensation process can be viewed to start from the formation of very small droplets of critical size whose typical order of magnitude is around $10^{-9}$ m. These droplets serve as the "condensation center", on which the supercooled steam condenses thus causing the droplets to grow. The nucleation theories predict the rate of formation of such nuclei providing the number of nuclei per unit time per unit volume or mass.

## 3.1 Classical Theory

The most commonly used classical nucleation theory was derived by Volmer [3.02]. Frenkel [3.03] using a different approach also derived the identical equation. The basic idea is to postulate [3.04] that the probable number of molecular clusters formed by random collisions is proportional to Boltzmann factor, $\exp(-\Delta S/k)$, where $\Delta S$ is the entropy decrease associated with the formation of such cluster. $\Delta S$ can be related to the work associated with the formation of the cluster W as $\Delta S = W/T$. W can be further calculated from the sum of different contributions of the change of Gibbs free enthalpy $\Delta G$ associated with the formation of such cluster. Furthermore, Farkas [3.05] introduced a hypothetical quasi-steady process model, in which clusters are thought to be continually removed and replaced by single molecules, and there exists a net flux of clusters growing into critical size. Detailed derivation is described by Wegener [1.18], or in the original work by Volmer [3.02] and Frenkel [3.03]. The final expression for the nucleation rate is

$$J = Z_o \exp\left(-\frac{Z_1^2}{\Lambda^2}\right) \qquad (3.1)$$

where

$$Z_o = \frac{p}{RT_g \rho_f} \sqrt{\frac{2\bar{N}^3 \sigma}{\pi}}$$

$$Z_1^2 = \frac{16\pi \bar{N} \sigma^3}{3\rho_f^2 (RT_g)^3}$$

$$\Lambda = \ln \left( \frac{p}{p_s(T_g)} \right)$$

With the same basic concepts mentioned above, different authors [1.18], [1.04] derived various revised versions of the nucleation theories by modifying some of the physical assumptions and mathematical simplifications. Nevertheless, except Lothe and Pound [3.06] whose theory predicted $10^{17}$ times higher nucleation rate, all the other theories result in nucleation rate of similar order of magnitude as Volmer and Frenkel's theory. None of these theories, including the theory derived by Lothe and Pound, can explain the discrepancy between the experimental data and the theoretical prediction.

## 3.2 Deich's Nucleation Theory

Deich et al. [3.07] concluded that the classical theory and Lothe-Pound theory are both unsound. They proposed a nucleation

theory which consists of two components. The first component is due to the so called "heterophase fluctuations". Due to the fluctuation of the density in the vapor, two or more molecules may collide and attach together for a short period. Some of them happen to be droplets of critical size or larger. Two assumptions were made during the derivation:

1. The vapor has an equilibrium nuclei number distribution before the expansion.
2. The expansion is so rapid such that the number distribution of the droplets does not have enough time to adjust, and thus remains at the initial equilibrium distribution.

This component is similar to the classical theory yet considers more realistic conditions: a non-equilibrium distribution was used instead of the equilibrium one. The second component is directly related to the expansion rate. As explained in chapter 2, the critical cluster size is a function of the state of the vapor. Suppose some droplets of subcritical size are formed at certain point during the expansion, if the condition of the vapor remains the same, these droplets would have been evaporated. However, since the supersaturation increases and the pressure decreases during the expansion, the local critical cluster size may be smaller than the radii of the subcritical droplets formed previously. As a result, these subcritical droplets are

transported, before they can completely evaporate, to a downstream region where their size is considered to be supercritical. These droplets then also serve as the condensation nuclei and constitute the second component of Deich's nucleation theory. Since there are some mistakes in the original paper by Deich [3.07] and the equation presented by Moore [1.16], a detailed derivation is described in Appendix A. The final equations may be expressed as below:

Deich's_theory_(first_component)

$$J_1 = \frac{3\Lambda\bar{N}p\sqrt{RT_g}}{\sqrt{8\pi}\,\sigma}\left(\frac{T_g\Lambda\sigma_0/\sigma - T_0\Lambda_0}{T_0}\right)\exp\left[-\frac{Z_1^2}{\Lambda^2}\,\frac{3T_g\Lambda\sigma_0/\sigma - 2T_0\Lambda_0}{T_0\Lambda}\right] \tag{3.2}$$

where subscript 0 stands for the condition before expansion.

Deich's_theory_(second_component)

$$J_2 = \frac{3\,\bar{N}}{T_g \ln\left(\frac{T_s}{T_g}\right)}\,\frac{d\Delta T}{dt}\exp\left[-\frac{Z_1^2}{\Lambda^2}\,\frac{3T_g\Lambda\sigma_0/\sigma - 2T_{g0}\Lambda_0}{T_0\Lambda}\right] \tag{3.3}$$

The total nucleation rate is:

$$J = J_1 + J_2 \tag{3.4}$$

When expanding from superheated vapor, $\Lambda_0 = 0$ , thus the two components can be further simplified respectively as:

$$J_1 = \frac{3\Lambda^2 \bar{N} p \sqrt{RT_g}\, T\sigma_0}{\sqrt{8\pi}\ \sigma^2 T_0} \exp\left[ - \frac{Z_1^2}{\Lambda^2} \frac{3T_g \sigma_0}{T_0 \sigma} \right] \tag{3.5}$$

$$J_2 = \frac{3\ \bar{N}}{T_g \ln\left( \frac{T_s}{T_g} \right)} \frac{d\Delta T}{dt} \exp\left[ - \frac{Z_1^2}{\Lambda^2} \frac{3T_g \sigma_0}{T_0 \sigma} \right] \tag{3.6}$$

In most instances, except in the case of very low expansion rate, the magnitude of $J_2$ is several orders greater than $J_1$, [1.14] thus the total nucleation rate can be approximated by:

$$J \cong J_2 \tag{3.7}$$

### 3.2.1 Relation between the nucleation rate and the expansion rate

One of the important term in the dominant component $J_2$ in Deich's nucleation theory is $\frac{d\Delta T}{dt}$ . As we mentioned before, the

condensation process is strongly affected by the expansion rate $\dot{p}$. Therefore, it is interesting to see how these two term could be related. For isentropic expansion, the two terms can be related [3.08] as:

$$\frac{d\Delta T}{dt} = \left( T_g \frac{(\gamma - 1)}{\gamma} - \frac{pv_{sg} T_s}{h_{fg}} \right) \dot{p} \qquad (3.8)$$

Detailed derivation is shown in Appendix B. Equation 3.8 shows that $\frac{d\Delta T}{dt}$ and therefore nucleation flux J is directly proportional to the expansion rate $\dot{p}$.

## 3.3 Surface Tension Of The Droplet With Small Radius

The accuracy which can be achieved in calculating non-equilibrium condensing nozzle flow depends ultimately on the accuracy of the nucleation theory and the droplet growth. The accuracy of the practical computation of the nucleation rate, however, depends on the accuracy of the properties of the droplets with small radius. The most important property which has very strong effect on the nucleation rate is the surface tension $\sigma$. According to many different investigators [3.09], [3.10], [3.11], [3.12], [3.13], the value of surface tension for a highly curved surface, $\sigma_r$ may

be considerably different from $\sigma_\infty$ , surface tension for a flat surface. Some researchers suggest that $\sigma_r > \sigma_\infty$ [3.09], [3.10], while others claim $\sigma_r < \sigma_\infty$ [3.11], [3.12], [3.13]. Since no definite conclusion can be made yet, so we adopted a correction factor, surface tension ratio $\sigma_r / \sigma_\infty$ , to obtain agreement between the calculations for the pressure ratio with the available experiment data.

Although the two nucleation theories are substantially different, both need the value of the surface tension for droplets with small radius. As will be shown in chapter 6, for both nucleation theories, only a small change in the surface tension ratio results in substantial change in the pressure ratio, mean droplet radius, and droplet size distribution. A higher surface tension ratio tends to delay the onset of spontaneous condensation (indicated by pressure rise) thus decreasing the Wilson pressure, increasing the mean droplet radius and causing a slightly larger variation in droplet radius. The results are relatively very sensitive to the change in surface tension ratio. It will be shown later, although the correlations for surface tension ratio of the two nucleation theories have similar trend, the one obtained using classical nucleation theory is not an acceptable correlation due to relatively large scatter in the correlation data.

It has to be noted that $\sigma$ is a strong function of temperature ($\sigma(T)$). To interpret it properly, the vapor temperature $T_g$, instead of the saturation temperature $T_s(p)$, should be used, because the droplet has the same temperature as the vapor when it is freshly formed. Hence, the surface tension should be $\sigma = \sigma(T_g)$. The equation listed by Leinhard [3.14] with slight modification in the coefficient was used to account for the temperature dependence of $\sigma$ of water. It may be expressed as:

$$\sigma = 235.3(1 - T_R)^{1.256} [1 - 0.625(1 - T_R)] \times 10^{-3} \quad Nm^{-1} \tag{3.9}$$

where reduced temperature is defined as

$$T_R = \frac{T_g}{647.286} \tag{3.10}$$

and $T_g$ is in K.

# CHAPTER 4. DROPLET GROWTH PHENOMENA

## 4.1 Droplet Growth Rate (Heat Transfer Coefficient)

The preceding chapters treated the birth of the droplets, their size and number. The next step of the analysis would be how will they grow? We have pointed out in the previous chapter that the temperature of the freshly formed droplet is equal to the vapor temperature. However, as expansion continues, the vapor temperature decreases faster than the temperature of the droplets. Thus, a temperature gradient is established between the droplet and the surrounding supercooled vapor. Consequently, heat transfer occurs between the two phases, which causes the droplet to grow. The detailed microscopic mechanism of the condensation process of a supercooled vapor is quite involved and beyond the scope of this work. However, the process can be simply illustrated by the following.

Let us consider a control volume of the vapor immediately adjacent to the droplet in Figure 4.1 with temperature distribution T(r). If the droplet temperature is higher than the surrounding supercooled vapor temperature $T_f > T_g$, without knowing

the detail distribution of T(r), it is reasonable to say that $T_f > T(r_1)$ and $T(r_2) > T_g$. Hence, heat is transfered from the droplet to the adjacent vapor $Q(r_1)$ as well as from the adjacent vapor to the surrounding supercooled vapor $Q(r_2)$. When the adjacent vapor rejects more heat than it receives $Q(r_2) > Q(r_1)$, phase change occurrs and the adjacent vapor condenses. Accordingly, the rate of condensation depends on the rate at which the latent heat can be carried away from the vapor adjacent to the droplet surface into the cooler vapor. If $Q(r_2) < Q(r_1)$, then the adjacent vapor will be heated up and there will have no condensation.

Similarly, in the case of evaporation, the vapor temperature is higher than the droplet surface temperature which is higher than the droplet bulk temperature. When the droplet surface receives more heat than it rejects, phase change occurrs and the droplet surface evaporates.

The growth rate (positive for condensation, negative for evaporation) can be calculated from the energy balance of the droplet

$$\rho_f c_f \frac{4}{3} \pi r^3 \frac{dT_f}{dt} + 4\pi r^2 \rho_f \frac{dr}{dt} \left[ h_f(T_f) - h_g(T_g) \right] = 4\pi r^2 \alpha (T_g - T_f) \tag{4.1}$$

The heat capacity term in Equation (4.1) is negligible compared with the latent heat released as shown by Gyarmathy [1.04], thus the droplet growth equation can be expressed as

$$4\pi r^2 \rho_f \frac{dr}{dt}\left[h_g(T_g) - h_f(T_f)\right] = 4\pi r^2 \alpha (T_f - T_g) \qquad (4.2)$$

To correctly compute the droplet growth rate, a proper expression of the heat transfer coefficient $\alpha$ is important. Since the order of magnitude of the droplet diameter when it is first born (typically, critical radius of steam $r_{cr} \cong 10^{-9}$m) is smaller than the typical value of mean free path (for steam, $l \cong 10^{-7}$m at atmospheric pressure), the effect of molecular interaction has to be taken into account when evaluating $\alpha$. As droplet grows, the droplet diameter may eventually become greater than the mean free path. Hence, the molecular interaction is less important and the continuum flow prevails. While the transition from rarefied flow to continuum flow is really gradual rather than sharply defined, the different flow regimes may be represented by different range of Knudsen Number

$$Kn = \frac{l}{2r} = \frac{3\mu\sqrt{RT_g}}{4rp}\sqrt{\frac{\pi}{2}} \qquad (4.3)$$

where mean free path $l$ can be found from kinetics theory [4.01]

$$l = \sqrt{\frac{\pi RT_g}{8}}\ \frac{3\mu}{p} \qquad (4.4)$$

4.1.1 continuous flow regime

For Kn < 0.01, the mean free path is much smaller than the droplet radius, therefore, the equations of continuum mechanics apply [4.02]. Since the droplet travels in the same velocity as the surrounding vapor, the heat transfer process between the droplet and the surrounding vapor can be approximated by free convection of a sphere at uniform temperature. The Nusselt number can be calculated as [4.03]

$$Nu_m = \frac{\alpha(2r)}{k_g} = 2 + 0.43(Gr\ Pr)^{0.25} \qquad (4.5)$$

where

$$Gr = \frac{g\beta(T_f - T_g)(2r)^3}{\nu^2} = \frac{g(T_f - T_g)(2r)(3Kn)^2\pi}{8RT_g^2}$$

$$Pr = \frac{c_p\mu}{k_g}$$

For most vapors, Pr is of order 1, R $\cong 10^3$ — $10^4$ J/(Kg K), and r

is no larger than $10^{-6}$ m in most spontaneous condensation processes. Suppose the temperature difference and the vapor temperature are both of order $10^{2}$ K, and Kn is at the limit $10^{-2}$, the order of magnitude of the last term in Equation (4.5) for the most conservative case would be $10^{-4}$ which can be safely neglected compared with 2. Thus the Nusselt number will be

$$Nu_m = \frac{\alpha(2r)}{k_g} = 2 \tag{4.6}$$

or

$$\alpha_c = \frac{k_g}{r} \tag{4.7}$$

Equation (4.2) can now be expressed as

$$\rho_f \frac{dr}{dt} \left[ h_g(T_g) - h_f(T_f) \right] = \frac{k_g}{r} (T_f - T_g) \tag{4.8}$$

4.1.2 free molecular flow regime

Opposite to continuum flow, the other extreme is the free molecular flow regime where Kn > 3. Hill [1.19] has derived the energy transfer equation under high Kn condition, Young [1.05] rewrites it with an alternative expression as

$$\rho_f \frac{dr}{dt}\left[h_g(T_g) - h_f(T_f)\right] = \frac{p(\gamma + 1)c_p}{\sqrt{2\pi RT_g}\ 2\gamma}(T_f - T_g) \qquad (4.9)$$

From Equation (4.9), the heat transfer coefficient for free molecular flow $\alpha_{fm}$ is

$$\alpha_{fm} = \frac{p(\gamma + 1)c_p}{\sqrt{2\pi RT_g}\ 2\gamma} \qquad (4.10)$$

which is practically the same expression presented by Gyarmathy in reference [1.09] utilizing the derivation by Gyarmathy [4.04] and Kang [4.05]

$$\alpha_{fm} = \alpha_c \frac{1}{\sqrt{8\pi}} \frac{\gamma + 1}{\gamma} \frac{3\ Pr}{4\ Kn'} \qquad (4.11)$$

However, the expression of the Knudsen number Kn' in Equation (4.11) is misrepresented as

$$Kn' = \frac{3\mu\sqrt{RT_g}}{4rp} \qquad (4.12)$$

in Gyarmathy's derivation. Therefore, symbol Kn' instead of Kn is used in Equation (4.11).

4.1.3 slip and transition flow regime

There is no simple analysis which can describe the complex molecular interactions occurred in the flow of intermediate Knudsen number $0.01 < Kn < 0.1$ (slip flow) and $0.1 < Kn < 3$ (transition flow). A simple analytical model suggested by Young [1.05] postulates that free molecular flow is valid within a few mean free path of the droplet surface, while continuum theory prevails outside this region. The model is illustrated in Figure 4.2. The interface separating the two flow regimes is at radius $(r + al)$ where the suitable value of parameter $a$ is suggested by Fuchs [4.06] to be 2. According to this model, Equation (4.8) is valid outside the interface, and Equation (4.9) is valid within the interface. By replacing $T_f$ with $T_i$ at the right hand side of Equation (4.8), we obtain Equation (4.13). By replacing $T_g$ with $T_i$ at the right hand side of Equation (4.9), we obtain Equation (4.14). The two equations are shown as follows:

$$4\pi r^2 \rho_f \frac{dr}{dt}\left[h_g(T_g) - h_f(T_f)\right] = 4\pi(r + al)^2 \frac{k_g}{r}(T_i - T_g) \qquad (4.13)$$

$$\rho_f \frac{dr}{dt}\left[h_g(T_g) - h_f(T_f)\right] = \frac{p(\gamma + 1)c_p}{\sqrt{2\pi RT_g}\, 2\gamma}(T_f - T_i) \qquad (4.14)$$

Note that the latent heat part remains the same as Equation (4.8)

and (4.9), for the transition region in the vicinity of the droplet is considered to retain the same condition and propagate as the droplet grows. As a result, the net energy change of phase transformation is the enthalpy change between the droplet and the surrounding supercooled vapor at infinity. Combining Equation (4.13) and (4.14) by eliminating $T_i$, we get

$$\rho_f \frac{dr}{dt}\left[h_g(T_g) - h_f(T_f)\right] = \frac{\alpha_c (T_f - T_g)}{\left[\frac{1}{(1 + 2a\mathrm{Kn})} + \frac{16}{3}\frac{\gamma}{\gamma + 1}\frac{\mathrm{Kn}}{\mathrm{Pr}}\right]} \qquad (4.15)$$

This equation is identical to the one derived by Young [1.05] except the more realistic enthalpy change $h_g(T_g) - h_f(T_f)$ is used rather than latent heat, and the expression of Kn is also misrepresented as Equation (4.12) in Young's equation. With $a$ = 0, the equation is identical to that derived by Gyarmathy [1.09] except Kn should be replaced by Kn'. Equation (4.15) not only correctly approaches the limit of the two extreme flow regimes, but also provides a smooth transition between the two as well. Therefore, it is thought that Equation (4.15) can be used for all values of Kn. It is also noted by Young [1.05] that Gyarmathy's equation

$$\alpha = \frac{\alpha_c}{1 + 3.18\mathrm{Kn}'} \qquad (4.16)$$

which is widely used in many low pressure steam studies is actually an incorrect deduction. For steam at low pressure $\gamma$ = 1.3, Pr ≅ 0.95, Gyarmathy's equation (with a = 0) should be

$$\alpha = \frac{\alpha_c}{1 + 3.98Kn'} \tag{4.17}$$

The difference between the current model with $a$ = 2 and Gyarmathy's model is shown in Figure 4.3. It shows that while negligible error is incurred for both high and low values of Kn, significant deviation exists for moderate Kn.

## 4.2 Droplet Temperature

The droplet growth rate can also be found by molecular kinetic considerations [1.09], [1.19] as

$$\rho_f \frac{dr}{dt} = \xi_c \frac{p}{\sqrt{2\pi RT_g}} - \xi_e \frac{p_s(T_f)}{\sqrt{2\pi RT_f}} \exp\left(\frac{-2\sigma}{r\rho_f RT_f}\right) \tag{4.18}$$

With the modification which accounts for the vapor moving toward the droplet with a finite bulk velocity and the condensation

coefficient different from the evaporation coefficient [4.07], [4.08], the equation is presented by Young [1.05] as

$$\rho_f \frac{dr}{dt} = \frac{2\xi_c}{2 - \xi_c} \left[ \frac{p}{\sqrt{2\pi R T_g}} - \frac{\xi_e}{\xi_c} \frac{p_s(T_f)}{\sqrt{2\pi R T_f}} \exp\left( \frac{-2\sigma}{r \rho_f R T_f} \right) \right] \qquad (4.19)$$

By equating the growth rate found from kinetic theory Equation (4.18), or (4.19) with the general Equation (4.15), and eliminating dr/dt, we can obtain an equation for droplet temperature as done by Gyarmathy [1.09], Campbell and Bakhtar [4.09], and Young [1.05]. However, the expressions are quite complicated, and the solution requires an iterative procedure. A much simpler equation proposed by Gyarmathy [1.09] can also yield the droplet temperature without the iteration procedure previously mentioned

$$T_f = T_s(p) - \Delta T \frac{r_{cr}}{r} \qquad (4.20)$$

Young [1.05] argued that a net condensation is occurring and the droplet may not be in equilibrium with the vapor, yet Gyarmathy's equation will only be valid by assuming the pressure of the droplet (after corrected for surface curvature) be the same as the vapor pressure. Nevertheless, it is shown by Gyarmathy [1.09]

that Equation (4.20) yields essentially the same result as the previous procedure discussed in the beginning of this paragraph. In addition, Equation (4.20) will reflect the physical meaning of the critical radius. If the droplet radius is grater than critical radius $r > r_{cr}$, then $T_f > T_g$, the vapor will continue condensing on the droplet; If the droplet radius is less than critical radius $r < r_{cr}$, then $T_f < T_g$, the droplet will evaporate. When $r = r_{cr}$, $T_f = T_g$, the droplet size will remain the same as long as the vapor condition does not change. Also, the value of condensation coefficient and the relation between the condensation coefficient and evaporation coefficient remains unclear. Thus even with the complex iteration procedure, the final solution is still uncertain. Hence, Equation (4.20) will be used in the current model.

## 4.3 Droplet Radius and Spectrum

With Equation (4.2), (4.15) and (4.20), we have the complete information to calculate the droplet radius. Since droplets are continuously generated in different sizes by spontaneous nucleation during the expansion, we would divide the expansion process into many intervals, and the droplets generated in each interval will be treated as one group. Different groups of

droplet then would have different numbers, sizes and temperatures, i.e. droplet spectrum. Before we can derive the equations for accounting of different groups, two questions have to be answered. First, will the droplets collide with each other thus affects the spectrum? Second, what is the effect of the foreign particles?

### 4.3.1 coagulation

Coagulation means the formation of larger droplet by collision of small droplets. Thermal (Brownian) motion is the main cause of the coagulation. Stein [4.10] has shown that for a typical transit time through a condensation zone of $10^2$ μsec, a droplet of radius 30 Å will undergo approximately one collision with another droplet, which is a frequency considered to be negligibly low to result in coagulation. Wu [4.11] also estimated and concluded that time for coagulation process is longer than the nucleation process, thus the effect of coagulation is negligible.

### 4.3.2 effect of foreign particles

Oswatitsch [4.12] first showed that the condensation by heterogeneous nucleation does not contribute significantly to the amount of condensate during rapid expansion in supersonic nozzle.

It is found that even by assigning generous growth laws on foreign nuclei, the time available is too short for the formation of appreciable amount of condensate. The number of nuclei generated by spontaneous nucleation far exceeds the number of existing foreign particles. In an interesting experiment, Buckle and Pouring [4.13] artificially introduced a large number of smoke particles (up to $10^8$ particles) at the inlet of a supersonic nozzle. The result showed that there was no effect of seeding on the condensation process in the nozzle. It is worth mentioning here that condensation on the nozzle wall surface was estimated by Gyarmathy [4.04] to be negligible.

### 4.3.3 equations for droplet accounting

The radius of a group of droplets formed at location $x_i$ and currently located at location x can be found by integrating Equation (4.2) from $x_i$ to x

$$r_i(x_i;\, x) = r_{cr}(x_i) + \int_{x'=x_i}^{x} \frac{\alpha_i(x_i;x')\ [T_{f,i}(x_i;x')-T_g(x')]\ dx'}{\rho_f[h_g(T_g(x'))-h_f(T_{f,i}(x_i;x'))]C(x')} \tag{4.21}$$

From Equation (4.15), heat transfer coefficient can be expressed

as

$$\alpha_i(x_i;\ x) = \frac{k_g \,/\, r_i(x_i;\ x)}{\frac{1}{(1 + 4\ Kn)} + \frac{16}{3}\ \frac{\gamma}{\gamma + 1}\ \frac{Kn}{Pr}} \tag{4.22}$$

From Equation (4.20), the droplet temperature can be expressed as

$$T_{f,i}(x_i;\ x) = T_g(x) + \Delta T(x) \left[1 - \frac{r_{cr}(x_i)}{r_i(x_i;\ x)}\right] \tag{4.23}$$

If we denote wetness as

$$w_i(x_i;\ x) = J(x_i)\ \frac{4}{3}\ \pi\ r_i^3(x_i;\ x)\ \rho_f\ \frac{1}{c(x_i)} \tag{4.24}$$

, the average droplet temperature can be defined as

$$T_f(x) = \frac{\int_{x_i=0}^{x} w_i(x_i;\ x)\ T_{f,i}(x_i;\ x)\ dx_i}{w(x)} \tag{4.25}$$

, and the total wetness will be

$$w(x) = \int_{x_i=0}^{x} w_i(x_i;\ x)\ dx_i \tag{4.26}$$

# CHAPTER 5. MATHEMATICAL FORMULATION OF MODEL AND NUMERICAL SOLUTION TECHNIQUE

A model of supersonic flow of a vapor in a Laval nozzle was developed. Coagulation, as discussed in chapter 4 is not significant for nozzle flow and therefore was not considered. It was also assumed that the effect of foreign nuclei is negligible in the flow. The model consists of the constitutive equations, nucleation theory equations and equations for droplet growth and accounting.

## 5.1 Nucleation Rate

The equations of nucleation rate were derived in chapter 3 and will not be presented here again. Equation (3.1) is for classical theory, and Equations (3.2), (3.3) and (3.4) are for Deich's theory. In the cases where expansion starts from superheated vapor, Equations (3.5) and (3.6) are used for Deich's theory.

## 5.2 Droplet Growth and Accounting

For obtaining the droplet growth and accounting the number of droplets of various sizes, the equations for critical radius, $r_{cr}$, (minimum radius of a droplet which can survive); droplet temperature, $T_{f,i}$; droplet radius, $r_i$; average droplet temperature, $T_f$; heat transfer coefficient, $\alpha_i$; wetness, $w_i$; total wetness, w, are needed. These equations have been derived and discussed in chapter 2 and chapter 4. A summary of the equations to be used is presented as follows.

Critical Radius $r_{cr}(x)$ : Equation (2.7)

Droplet Radius $r_i(x_i; x)$ : Equation (4.21)

Heat Transfer Coefficient $\alpha_i(x_i; x)$ : Equation (4.22)

Droplet Temperature $T_f(x_i; x)$ : Equation (4.23)

Wetness $w_i(x_i; x)$ : Equation (4.24)

Average Droplet Temperature $T_f(x)$ : Equation (4.25)

Total Wetness w(x) : Equation (4.26)

## 5.3 Constitutive Equations

Instead of using the differential form as in most investigations,

the integral form equations are used whenever possible. This greatly improves the computational efficiency. The equation for axial velocity, c, was obtained using the differential form of the continuity, momentum and energy equations. Detailed derivation can be found in Appendix D. It is assumed that the droplet travels with the same velocity as the vapor phase, and the vapor phase can be treated as an ideal gas. There are some instances where real gas effect play an important role in the expansion process such as condensation of carbon-dioxide [1.19], high pressure steam [1.05], [5.01] etc. However, this effect is not important for low pressure steam as in the cases for experimental data used for comparison with the theory and the real gas effect can be included into the analysis and computation without difficulty whenever necessary.

The temperature dependence of the various properties are considered in the analysis. The temperature range of interest for the study cases in this work is between 0 to 130 $^{\circ}$C. The temperature dependent properties needed in the analysis include $c_p$, $c_f$, $\rho_f$, $\mu$, $\sigma$, and $k_g$. Among them, the constant value $c_f$ = 4198 J/(Kg·m) is used. Compared with $c_f$ at the saturation line [5.01], this will give the maximum error < +0.5% between 0 — 100 $^{\circ}$C, and < -1.5% between 100 — 130 $^{\circ}$C. The choice of such value

is justifiable, for the higher temperature range is rarely encountered in the current cases studied. Also, since the actual $c_p$ of the compressed liquid droplet tends to be lower than that at the saturation line, the average error between 100 — 130 °C will be even smaller. For similar reason and simplicity, the constant $c_p$ = 1998 J/(Kg·m) is also used. Nevertheless, the temperature dependence can be incorporated into the analysis without difficulty when different temperature range is of interest. Surface tension $\sigma(T_g)$ is described by Equation (3.9) to an accuracy of ±0.2% between 0 — 130 °C (compared with data adopted from [5.02]). Thermal conductivity $k_g(T_g)$ can be calculated to an accuracy of ±0.5% in the temperature range 0 — 130 °C (compared with data adopted from [5.03]) as

$$k_g(T_g) = 1.82 \times 10^{-2} + 5.8343014 \times 10^{-5}\, T_g - 5.888523 \times 10^{-8}\, T_g^2 - 4.51 \times 10^{-11}\, T_g^3 \quad \frac{W}{K \cdot m} \tag{5.1}$$

where $T_g$ is in °C. Viscosity $\mu(T_g)$ can be calculated to an accuracy of ±0.4% in the temperature range 0 — 130 °C (compared with data adopted from [5.03]) as

$$\mu(T_g) = (0.398\, T_g + 80.2) \times 10^{-7} \quad \text{Pa·s} \tag{5.2}$$

where $T_g$ is in $^{\circ}C$. The liquid phase density $\rho_f(T_f)$ can be expressed to an accuracy of ±0.1% in the temperature range 0 — 130 $^{\circ}C$ (compared with data adopted from [5.03]) by the following equation [5.04].

$$\rho_f(T_f) = \rho_c \left[ 1 + \sum_{i=1}^{8} D_i \left( 1 - \frac{T_f}{T_c} \right)^{i/3} \right] \qquad (5.3)$$

where $\rho_c = 317.0\ Kg/m^3$

$T_c = 647.286\ K$

$D_1 = 3.6711257$

$D_2 = -2.8512396 \times 10^1$

$D_3 = 2.2265240 \times 10^2$

$D_4 = -8.8243852 \times 10^2$

$D_5 = 2.0002765 \times 10^3$

$D_6 = -2.6122557 \times 10^3$

$D_7 = 1.8297674 \times 10^3$

$D_8 = -5.3350520 \times 10^2$

The constitutive equations are listed for both single component condensing vapor and two component (condensing vapor and inert gas) models.

5.3.1 single component model

Continuity $\rho_g$:

$$\rho_g = \frac{c_{in}}{c} \frac{A_{in}}{A} \rho_{in}(1-w) \tag{5.4}$$

Equation of velocity c :

$$\frac{dc}{dx} = \frac{c}{\left(\frac{M^2}{1-w} - 1\right)} \left[\frac{dA}{dx}\frac{1}{A} + \frac{wc_f}{(1-w)c_{p,g}T_g}\frac{dT_f}{dx} + \frac{c_{p,g}T_g - h'_{f,g}}{(1-w)c_{p,g}T_g}\frac{dw}{dx}\right] \tag{5.5}$$

where

$$M^2 = \frac{(c_p - R)c^2}{c_p R T_g}$$

$$h'_{f,g} = h_g(T_g) - h_f(T_f)$$

The derivative of total wetness $\frac{dw}{dx}$ in Equation (5.5) is derived in Appendix C to be

$$\frac{dw}{dx}(x) = \frac{1}{c(x)} \frac{4}{3} \pi r_{cr}^{3}(x) \rho_f J(x)$$

$$+ \frac{4\pi}{c(x)} \int_{x_i=0}^{x} \frac{r_i(x_i; x) \alpha_i(x_i; x) J(x_i) [T_{f,i}(x_i; x) - T_g(x)] dx_i}{[h_g(T_g(x)) - h_f(T_{f,i}(x_i; x))] c(x_i)} \tag{5.6}$$

Energy equation $T_g$:

$$\frac{c^2}{2} + (1-w) h_g(T_g) + w h_f(T_f) = h_0 \tag{5.7}$$

Equation of state $\rho$, (for vapor and supercooled region):

$$p = \rho_g R T_g \tag{5.8}$$

### 5.3.2 two component (condensing vapor and noncondensing gas) model

The two components considered here are the condensing vapor and the noncondensible gas which does not react with the condensing vapor, nor has condensation. It is assumed that vapor phase temperature for both components is the same and is represented as $T_g$. The pressure of each component is represented by partial

pressure. The mass fraction of the condensing vapor contained in the mixture at the beginning of the expansion is denoted by $w_0$. If subscripts n and v denote the noncondensible gas and the condensing vapor respectively, partial pressure can be defined as

$$p = p_v + p_n \tag{5.9}$$

$$p_v = y\ p \tag{5.10}$$

$$p_n = (1 - y)\ p \tag{5.11}$$

$$y = \frac{(w_0 - w)/ M_v}{(1 - w_0)/ M_n + (w_0 - w)/ M_v} \tag{5.12}$$

For two component model, the nucleation rate and droplet growth and accounting equations are the same as single component model except that partial pressure $p_v$ has to be used, and all the variables should now be referring to the condensing vapor in the two component case e.g. gas constant R, number of molecules per unit mass $\bar{N}$ etc. The supercooling and supersaturation will now be evaluated as

$$\Delta T = T_s(p_v) - T_g \tag{5.13}$$

$$\Lambda = \ln\left(p_v / p_s(T_g)\right) \tag{5.14}$$

The expressions of the constitutive equations are, however, somewhat different from the single component model. They are presented as follows.

Continuity $\rho_g$:

$$\rho_{in} C_{in} A_{in} = \frac{\rho_g}{1 - w} CA \tag{5.15}$$

Here $\rho_g$ is the density of the whole vapor phase including condensing vapor and inert gas. A mean molecular weight can be defined as (see Appendix E for derivation)

$$M_g = \frac{1 - w}{(1 - w_0)/ M_n + (w_0 - w)/ M_v} \tag{5.16}$$

The relationship between $\rho_g$ and $\rho_v$, $\rho_n$ can be shown to be (Appendix E)

$$\frac{\rho_g}{M_g} = \frac{\rho_v}{M_v} + \frac{\rho_n}{M_n} \tag{5.17}$$

Equation of velocity c :

The equation of velocity can be derived with the same procedure as one component case (explained in Appendix D)

$$\frac{dc}{dx} = \frac{c}{M^{+2} - 1}\left\{\frac{1}{A}\frac{dA}{dx} + \left[\frac{1 / M_v}{(1 - w_0)/ M_n + (w_0 - w)/ M_v} - \frac{h'_{fv}}{(c_{p0} - wc_{pv})T_g}\right]\frac{dw}{dx} + \frac{wc_f}{(c_{p0} - wc_{pv})T_g}\frac{dT_f}{dx}\right\} \tag{5.18}$$

where

$$M^{+2} = \frac{c^2}{T_g}\left\{\frac{1}{R[(1 - w_0)/ M_n + (w_0 - w)/ M_v]} - \frac{1}{c_{p0} - wc_{pv}}\right\}$$

$$h'_{fv} = h_v(T_g) - h_f(T_f)$$

$$c_{p0} = (1 - w_0)c_{pn} + w_0 c_{pv}$$

Energy equation $T_g$ :

$$\frac{c^2}{2} + c_{p0}(T_g - T_0) - w\, h'_{fv} = 0 \qquad (5.19)$$

Equation of state p :

$$p = \rho_g R \frac{(1 - w_0)/M_n + (w_0 - w)/M_v}{1 - w} T_g \qquad (5.20)$$

## 5.4 Numerical Solution Technique

The solution procedure used for solving these equations was as follows. Initial values of the temperatures, velocity c, density, etc., were known. Finite difference approximations were obtained for $d(\Delta T)/dx$ and $\frac{1}{A}\frac{dA}{dx}$ . The solution procedure consisted of guessing the values of $T_g$, pressure p, velocity c, and radius $r_i$, and using an iterative procedure to solve all the equations to get a new set of the values of the variables at the grid point. The procedure was then repeated for the next point. A fourth order Runge Kutta method was used for solving Equations (5.5) and (5.18).

It can be observed that Equations (5.5) or (5.18) will break down when the value of the term $M^2/(1 - w)$ or $(M^{*2} - 1)$ equals to 1. Numerically, problem arises even when $M^2/(1 - w)$ or $(M^{*2} - 1)$ is very close to 1. It is observed from Equations (5.5) and (5.18) that if wetness is not zero, this singular point would occur at a distance upstream of the actual nozzle throat. How large this distance is would depend on how large the wetness is. The nucleation usually starts somewhere upstream of the nozzle throat, hence, the wetness is usually greater than zero. However, the nucleation rate is usually not high there, and the wetness is usually small, consequently, this distance is usually small as well.

The singularity characteristic in two-phase flow equations was discussed by many investigators [5.05], [5.06], [5.07]. Due to this singular nature, a pure numerical scheme, if employed for solution, will either yield erroneous results or will become unstable and fail. Therefore, a remedial procedure must be adopted in this region. One way is to use the differential form of the momentum equation. The differential form of the momentum equation can be expressed as

$$c \frac{dc}{dx} + \frac{1 - w}{\rho_g} \frac{dp}{dx} = 0$$

With proper finite difference approximation (Appendix D), the velocity at next grid point 2 can be computed from the [illegible] grid point 1 as

$$c_2 = \sqrt{c_1 + \frac{(w_1 + w_2) - 4}{\rho_1 + \rho_2} (p_2 - p_1)} \qquad (5.22)$$

Although the above menticned method is easier to implement than using Runge-Kutta method on the equation of velocity, its accuracy is not as good. Fortunately, the axial range of nozzle where $M^2/(1 - w)$ or $(M^{+2} - 1)$ is very close to 1 is very short. Also, this usually occurs very close to the nozzle throat where nucleation rate and wetness are small. Therefore, this remedial procedure does not affect the final result.

In some of the cases studied, the aforementioned technique either will not converge or does not give the physically acceptable supersonic branch of solution. Under this circumstance, another technique has to be used. As we noticed that the pressure ratio always starts to deviate from the isentropic pressure ratio at

quite a distance downstream of the the singular point. Therefore, the pressure ratio can be taken as the isentropic pressure ratio at the singular point. The velocity is calculated utilizing the differential form of the momentum equation. Until the "dangerous zone" is passed, the computation is switched back to equation of velocity. Depending on the different cases studied, the length of this zone varies. Different machine accuracies associated with the different computers used do not make appreciable change on the length of this zone. Instead of using the isentropic pressure, the extrapolation of the properties can also be adopted to solve the singularity problem. When doing so, one has to make certain that the solution after extrapolation falls into the correct quadrant of the solution space. Usually, a criteria $\delta p < 0$ and $\delta x > 0$ is used [5.05] where $\delta x$ is the distance for extrapolation. In addition, assumptions of negligible nucleation rate and negligible change of droplet temperature between the extrapolation points have to be made, and a simplified droplet growth rate equation has to be applied. Some other techniques are discussed by Gyarmathy [1.09]. Some studies neglect the nucleation effect entirely before the throat and start the computation from the throat, thus avoiding the singularity point [5.08].

# CHAPTER 6 RESULTS AND DISCUSSION

## 6.1 Single Component Results

### 6.1.1 Pressure ratio and mean droplet radius

Although the two nucleation theories are substantially different, both need the value of the surface tension for droplets with small radius. The surface tension values for small radius droplets are not available. According to many investigators [3.09, 3.10, 3.11, 3.12, 6.01] the surface tension of a small droplet is different from that of a flat surface and one is not sure whether it decreases or increases. Therefore, various values of the surface tension ratio ($\sigma/\sigma_\infty$) were tried to obtain a good agreement between the calculated pressure ratio with the experimental results. Sixteen test cases for which experimental data were available were studied. A summary of inlet total conditions, Wilson pressure, surface tension ratio, the mean radius as well as the standard deviation at the end of computation (not necessarily the nozzle exit, depending upon the nozzle geometry information available) is presented in Table 6.1.

The pressure ratio along the nozzle length obtained using classical and Deich's nucleation theories compared reasonably well with the experimental data. Results of pressure ratio and droplet size distribution for all the sixteen cases are provided in Figures 6.1 to 6.48. It is observed that in all cases, the final droplet size distribution is quite monodisperse. However, Deich's theory gives slightly better agreement with experiments in general. Computation also shows that Deich's theory gives better monodispersion regarding the droplet size distribution and smaller mean radius (see Figure 6.6).

Experimental information on mean droplet size are scarce and only the data provided by Gyarmathy and Meyer [1.13] was available for comparison. Figure 6.49 shows the comparison between the mean radius predicted by using Deich and classical nucleation theories and the experiment (Gyarmathy and Meyer Nozzle data, Table 6.1). The mean droplet size obtained by using Deich's theory is reasonably close to the experimental data, while the classical theory tends to overestimate the droplet size. However, it should be noted that as mentioned earlier the surface tension ratio were varied to obtain good agreement with the experimental pressure ratio and the same value of the surface tension ratio was used for ascertaining the droplet sizes.

### 6.1.2 Typical results of some important variables

The results of the sixteen test cases investigated showed similar trends. Therefore, we will only present the result of Barschdorff nozzle test no. 7 as representative of the data. Figure 6.50 shows the variations of nucleation flux and supercooling along the nozzle axial distance. Nucleation starts after a certain amount of supercooling (in this case about 17°C) is reached. As steam expands, nucleation reaches its peak slightly upstream of the peak of supercooling and drops to zero suddenly after the supercooling peak where spontaneous condensation occurs due to large number of nuclei. Since most of the nucleation occurs around the nucleation flux peak, this accounts for the monodisperse nature of droplet size. The latent heat released due to this spontaneous condensation causes a sharp pressure increase, as shown in Figure 6.1 through 6.48. Note that pressure rise occurs at the peak of supercooling or right after the peak of nucleation rate, which is the start of the spontaneous condensation and is defined as the Wilson point. The latent heat also causes a sudden increase of the vapor temperature (Figure 6.51) and entropy increase (Figure 6.52), and results in bringing the vapor toward an equilibrium state rapidly

from a supercooled state. Consequently, supercooling decreases rapidly during spontaneous condensation. At the end of spontaneous condensation, usually defined at where supercooling stops to decrease and remain constant, the state of vapor is close enough to the equilibrium state (about 3°C supercooling in this typical example), and the expansion proceeds almost like normal equilibrium expansion. The pressure (Figure 6.1 through 6.48) and vapor temperature (Figure 6.51) decrease again similar to where normal equilibrium expansion takes place, and the entropy increases in a much slower pace (Figure 6.52).

Figure 6.51 shows the vapor temperature $T_g$, liquid temperature $T_f$, and the equilibrium saturation temperature at the vapor pressure $T_s(p)$, along the nozzle axis. The result indicates that the liquid temperature $T_f$ is the same as $T_g$ at the beginning of nucleation. At the end of spontaneous condensation, $T_f$ and $T_s$ are very close, which means that the liquid phase is almost in equilibrium, while the vapor phase remains at a constant supercooling (about 3°C). We can also observe from this figure that wetness becomes appreciable after the sudden pressure rise. Before the Wilson point is reached (i.e., sudden pressure rise or start of spontaneous condensation), the increase in the wetness is mainly due to the new nucleation which is so small that the steam is practically dry. After the Wilson point, which is also

the end of nucleation and the start of spontaneous condensation, the existing large amount of nuclei (nucleated around the nucleation flux peak) provide a large surface area for condensation which causes a rapid increase in wetness.

Mach number and entropy are shown in Figure 6.52. The variation in the Mach number and the entropy along the nozzle axis is similar to the pressure variation. Before the occurrence of spontaneous condensation, Mach number increases, entropy remains constant and expansion is isentropic. During spontaneous condensation, Mach number decreases and entropy increases because of the pressure rise and release of latent heat. After the end of spontaneous condensation the vapor is almost in a thermodynamic equilibrium state, the expansion is nearly isentropic and the Mach number increases again.

Figure 6.53 shows the growth of mean radius and Sauter mean radius of the droplets and the variation in critical radius along the nozzle axis. Mean radius is defined with the same amount of wetness and the same total number of droplets. Sauter mean radius is defined by the ratio of the total volume to the total area of all the droplets. Sauter mean is slightly larger than the mean radius in all the study cases here. It should be noted that the smaller the difference between the two mean, the better the

monodispersion would be. The droplet growth rate is basically proportional to the temperature difference between the droplet and supercooled vapor. In the nucleation zone (before the advent of spontaneous condensation) in spite of the increasing temperature difference (Figure 6.51), the droplet growth rate remains small due to the presence of the large number of newly formed small nuclei. At the end of nucleation and at the beginning of the spontaneous condensation, mean radius grows rapidly because no new small nuclei are being formed. Near the end of spontaneous condensation, the temperature difference becomes small, therefore, the growth rate slows down again. The critical radius decreases in the nucleation zone, which also justifies the consideration of the second component of nucleation in Deich's nucleation theory. The results of droplet size distribution at the end of the expansion are presented in Figure 6.1 to 6.48. From the figures, we can see that good monodispersion exists for all study cases.

The nozzle expansion rate and velocity for Barschdorff No. 7 are shown in Figure 6.54. The shape of the expansion rate curve of each case studied mainly depends on the nozzle geometry. The velocity curve displays similar trend as the Mach Number.

Figure 6.55 depicts the Knudsen Number and Prandtl Number. In all

the cases studied, Prandtl Number decreases before Wilson point is reached, rapidly increases during the spontaneous condensation, and stabilizes to remain nearly constant after the spontaneous condensation. The change in Prandtl Number is small, and the value is around .95 for all study cases. The Knudsen Number always increases at the early stage of the expansion where the pressure is decreasing and the droplet growth rate is very slow. When droplet growth rate starts to pick up, the value of Knudsen Number drops sharply until the droplet growth rate slows down. In most cases the effects of pressure drop and droplet growth eventually balance out, and the Knudsen Number would remain fairly constant through the rest of the expansion. The range of the value of Knudsen number varies nozzle by nozzle. In the cases studied, it ranges from one to a few hundreds. Thus we know that for most cases the flow is under free molecular flow regime (Kn > 3) and sometimes under slip and transition flow regime (0.01 < Kn < 3). The continuous flow regime (Kn < 0.01) is almost nonexistent.

The two components of the nucleation rate for Deich's nucleation theory are presented on Figure 6.56. The second component $J_2$ has always been a few order of magnitude smaller than the first component $J_1$ in all our study cases. However, depending on the condensing vapor used, expansion rate, and the initial condensing

vapor content, it is possible that the second component may overwhelm the first component.

### 6.1.3 Correlation for surface tension ratio

In this study the surface tension ratio values were varied to obtain agreement between the theoretical and experimental pressure ratios. It is therefore important to establish relevant correlation for the surface tension ratio so that a proper value can be used for designing new nozzles and analyzing nozzles for which experimental data does not exist. Thus, obtaining correlation for surface tension ratio for the nucleation theories is very important. Various correlations were tried and the results showing inlet total temperature, Wilson pressure, inlet total pressure and inlet total entropy for the two nucleation theories are presented in Figure 6.57 to 6.64. Apparently, inlet total temperature does not yield acceptable correlation for both nucleation theories. The correlation yielded by Wilson pressure seem to show a positive trend. However, since the Wilson pressure is not known *a priori*, a correct value of the surface tension ratio cannot be assigned. A more difficult iterative procedure is needed to implement the Wilson pressure correlation in nozzle design. On the other hand, the usage of inlet total entropy and

pressure correlations are rather straightforward and need no iteration procedure since the inlet conditions are always known. In addition, the Wilson pressure correlation data presents the larger scatter than inlet total pressure and inlet total entropy correlations.

The correlations utilizing inlet total pressure and inlet total entropy seem to be the most promising. However, the slope of the correlation based upon inlet total pressure at the region of small total pressure is so steep that a small uncertainty in the correlation would trigger a large error in the predicted surface tension ratio. As a result, the correlation between the inlet total entropy and surface tension ratio is chosen. From Figure 6.63 and 6.64 we found that the trends on the variation of surface tension ratio with inlet total entropy for Deich's and classical nucleation theories are similar. However the scatter for the classical theory data is larger than that for Deich's theory. The correlation coefficient (which is defined in Appendix G) for Deich's theory can be computed as -0.9394 and for classical theory to be -0.9337. The larger correlation coefficient for Deich's theory shows that it gives better correlation. In the next section it will be shown that the pressure ratio, mean droplet size and droplet size distribution are quite sensitive to the value of the surface tension ratio.

Therefore, the correlation for Deich's theory with less scatter was adopted. Additionally, the classical theory, as indicated earlier, tends to overestimate the droplet size.

### 6.1.4 Effects of parameters

#### A. effect of surface tension ratio

The effect of the variation of surface tension ratio on pressure rise associated with spontaneous condensation, mean radius and droplet size distributions are shown in Figures 6.65, 6.66 and 6.67 respectively. These results were obtained by using different values of surface tension ratio for the Barschdorff nozzle No. 7 for the same inlet conditions $p_0$ = 78323 Pa, $T_0$ = 388.44 K. Higher surface tension ratio which gives a smaller nucleation rate and broader nucleation zone will delay the onset of spontaneous condensation (indicated by pressure rise) thus decreasing the Wilson pressure. The total amount of heat transfer can be roughly measured by the extent of the pressure rise. From Figure 6.65 we found that the total amount of heat transfer is about the same for different surface tension ratios. The mean droplet radius is smaller at first in the case of larger surface tension ratio since the nucleation starts later compared with the

case of smaller surface tension ratio. When spontaneous condensation takes place later, the mean radius starts to grow rapidly. With the approximately same amount of total heat transfer and the smaller number of nuclei given by larger surface tension ratio, more heat transfer takes place on each individual droplet. Consequently, the mean droplet radius of larger surface tension ratio eventually outgrows those of smaller surface tension ratio (see Figure 6.66), and causes a slightly larger variation in droplet radius (Figure 6.67). The results are relatively very sensitive to the change in surface tension ratio. This reaffirms our previous statement concerning the inability to obtain an acceptable correlation for surface tension ratio using classical nucleation theory due to relatively large scatter in correlation data.

B. effect of inlet total temperature

The effect of inlet total temperature is investigated by comparing Barschdorff's nozzle test No. 4, 7 and 10 at an inlet total pressure of 11.36 psia. From Figures 6.68, 6.69 and 6.70, it is observed that for a given nozzle geometry and inlet total pressure, a higher value of inlet total temperature delays the onset of spontaneous condensation and therefore decreases the

Wilson pressure and mean droplet size and gives a relatively smaller variation in droplet radius. The inlet total temperature in general does not affect the nucleation rate. Thus, the mean droplet radius for higher inlet total temperature does not have the outgrown effect similar to the cases of different surface tension ratio.

C. effect of inlet total pressure

The effect of inlet total pressure is obtained by comparing the results for the tests performed on nozzle of Barschdorff with total temperature $T_0$ = 388.44K, and different pressure at 75974 Pa, 78323 Pa and 80673 Pa. Proper surface tension ratios are used according to the correlation developed in the previous section. The inlet total pressure like the inlet total temperature in general does not affect the nucleation rate. It is observed from Figures 6.71, 6.72 and 6.73 that lower inlet total pressure delays the onset of spontaneous condensation and therefore decreases Wilson pressure and mean droplet size and provides a relatively smaller variation in the droplet radius. The effect is similar to that of higher inlet total temperature. However, the results are more sensitive to the change of inlet total pressure than to the change of inlet total temperature.

D. effect of expansion rate

In the previous sections, the effects of parameters are considered for the same nozzle with different inlet total conditions and/or different surface tension ratio. The expansion rate is determined by the nozzle geometry. Hence, in this section we shall consider the effects of different expansion rates (thus different nozzle geometries) with the same inlet total conditions and surface tension ratio. The results obtained for the three nozzles designed in the next chapter are used i.e. Nozzle NZ11 with expansion rate 2500 1/sec, NZ12 with expansion rate 5000 1/sec and NZ13 with expansion rate 10000 1/sec. The inlet condition, total temperature 500 K and total pressure 1.7 MPa is used.

In Figure 6.74 we can see that for higher expansion rate the larger area ratio causes smaller pressure ratio and the onset of condensation takes place earlier. The higher expansion rate generates higher nucleation rate and narrower nucleation zone. Although the total amount of pressure rise, thus the total amount of heat transfer, is about the same for different expansion rate,

the pressure rise is steeper for the higher expansion rate case since heat transfer takes place faster due to more nuclei available. The mean radius of lower expansion rate nozzle is smaller compared with the higher expansion rate nozzle due to delay of the onset of condensation. However, when spontaneous condensation occurs later, with the same amount of total heat transfer and less droplets, more heat transfer takes place for each individual droplet in the lower expansion rate case. As a result, the mean radius of lower expansion rate nozzle eventually outgrows the one of higher expansion rate nozzle.

Figure 6.75 shows the droplet sizes at the end of the expansion through the nozzle and we can observe that the higher expansion rate nozzle NZ13 yields smaller mean radius $\simeq$ .1 $\mu$m as compared to .25 $\mu$m for the nozzle of an expansion rate 2500 $sec^{-1}$. The variation in the droplet radius is also smaller for the higher expansion rate (Figure 6.76).

From the preceding discussions, we can conclude that the droplet size distribution and the droplet mean radius is a function of the inlet total pressure and temperature and the nozzle expansion rate. It is also sensitive to the value selected of the surface tension ratio. However, the variations (fluctuations) in the droplet radius are relatively insensitive to these parameters.

The variations in the droplet radius, for most of the cases studied, were within ± 0.01 μm. This indicates that the droplet sizes stay relatively monodisperse for various values of the parameters. A summary of the mean radius at the end of computation for the sixteen cases is provided in Table 6.1. The droplet radius varies from 0.003 μm to 0.074 μm depending upon the inlet total condition and the expansion rate. We can thus see the importance of manipulating the parameters to design a nozzle which can provide monodisperse droplets of desired radius.

## 6.2 Two Component Results

There are very few experimental data available for two component (one condensing vapor and one noncondensing vapor) spontaneous condensation. The vapor temperatures of the two available experiments both go well below the sublimation line [6.02], [6.03]. The uncertainties on the free surface energy, the spontaneous crystallization rate, the thermodynamic properties of supercooled liquid and ice nuclei, and the validity of the nucleation theories etc. makes the comparison between the theoretical numerical result and experimental data hardly meaningful. However, in order to investigate the effect of

initial vapor content on the spontaneous condensation, the nozzle of Barschdorff No. 7 is used in the numerical computations.

### 6.2.1 Effect of some important variables on the results

According to gasdynamics, we know that isentropic pressure ratio is not only function of area ratio (i.e. nozzle geometry), but also function of ratio of specific heat $\gamma$. For a two component vapor, the ratio of specific heat $\gamma$ depends on the initial vapor content. As a result, the pressure ratios for different initial vapor content for the same inlet condition shown in Figure 6.77 are different. Some other typical results for different initial vapor contents are shown in Figure 6.78 to 6.94. Comparing the results for w0=1 with single component result shown in Figure 6.50 to 6.56, we find that the results are identical. This can be seen as a validation of the theory and the numerical program.

### 6.2.2 Effect of initial vapor content

The effect of initial vapor content has a basic difference from those parameters presented in the single component case. From Figure 6.77 we notice that smaller initial vapor content gives a

smaller pressure rise. This is because smaller heat transfer due to phase change occurs due to less condensing vapor available. In single component case, all the parameters studied basically has no effect on the total amount of heat transfer. Smaller initial vapor content also delays the onset of the spontaneous condensation indicated by pressure rise and in turn the Wilson pressure. However, contrary to higher surface tension ratio and lower expansion rate in single component case, smaller initial vapor content gives higher nucleation rate and narrower nucleation zone. With smaller total amount of heat transfer and more nuclei, less heat transfer takes place on each individual droplet. Therefore, smaller mean radius (Figure 6.78), better monodispersion of droplet size (Figure 6.79), and less variation on supercooling (Figure 6.80 to 6.82) were found in smaller initial vapor content case. This in turn makes the mean radius growth rate slow (Figure 6.78) and generates less condensate and therefore, results in decreases in the wetness (Figure 6.89 to 6.91).

From Figure 6.83 to 6.85 we can also observe that while Pr tends to be smaller for the smaller initial vapor content, it still remains in the range of 0.9 to 1.0. On the other hand, Kn changes substantially with changes in initial vapor contents. The smaller the initial vapor content the larger Kn would be. Consequently,

the flow tends to behave as a free molecular flow (Kn > 3). Another interesting phenomena found from Figure 6.86 to 6.88 is that the order of magnitude of the two components of nucleation flux of Deich's nucleation theory are closer in the case of small initial vapor content. This shows that the stable nuclei initially formed are so small in the low initial vapor content case that the unsteady effect (represented by the second component of Deich's theory) plays a stronger role. Figure 6.92 to 6.94 show that with decreasing initial vapor content, the actual velocity as well as the isentropic expansion rate decrease.

# CHAPTER 7 NOZZLE DESIGN FOR OBTAINING MONODISPERSE DROPLETS

The objective of nozzle geometry design is to obtain proper $A/A^{*}(x)$ such that the desired droplet mean radius can be generated for certain inlet total conditions. In the preceding chapter, we have discussed the effects of different parameters $T_0$, $p_0$, and $\dot{p}$ on the mean radius of the droplets. We have also discussed the correlation between $\sigma/\sigma_0$ and the inlet total condition. These results form the basis of nozzle geometry design.

## 7.1 Equations

The relation among $T_0$, $p/p_0(x)$, $\dot{p}(x)$, $\gamma(T(x))$, and $c_p(T(x))$ can be expressed as [1.09] :

$$\ln\left[\frac{1+\sqrt{1-\left(\frac{p}{p_0}\right)^{(\gamma-1)/\gamma}}}{1+\sqrt{(\gamma-1)/(\gamma+1)}}\right]-\frac{1}{2}\ln\left[\frac{\left(\frac{p}{p_0}\right)^{(\gamma-1)/\gamma}}{2/(\gamma+1)}\right]$$

$$-\sqrt{1-\left(\frac{p}{p_0}\right)^{(\gamma-1)/\gamma}}+\sqrt{\frac{\gamma-1}{\gamma+1}}=\frac{\gamma-1}{2\gamma}\frac{\dot{p}}{\sqrt{2c_pT_0}}(x-x^*) \qquad (7.1)$$

where

$$\dot{p}=\frac{1}{p}\frac{dp}{dt}=\frac{C}{p}\frac{dp}{dx}$$

in which $p/p_0(x)$ is directly related to $A/A^*(x)$ and $\gamma(T(x))$ by

$$\frac{A}{A^*}=\left(\frac{2}{\gamma-1}\right)^{1/(\gamma-1)}\sqrt{\frac{\gamma-1}{\gamma+1}}\left(\frac{p}{p_0}\right)^{-1/\gamma}\sqrt{1-\left(\frac{p}{p_0}\right)^{(\gamma-1)/\gamma}} \qquad (7.2)$$

Since $T(x)$ is not known *a priori*, the coupling among the variables in the above equations is rather complicated. In most cases, however, $\gamma$ and $c_p$ are constant in the temperature range of interest. Thus for given $T_0$ and $\dot{p}(x)$, we can derive $p/p_0(x)$ from Equation (7.1), and then derive $A/A^*(x)$ from Equation (7.2). A convenient way which does not violate the generality is to further assume a constant expansion rate. With the above

assumption, Equation (7.1) can be solved for $p/p_0(x)$ easily using Newton's Method.

## 7.2 Design Procedure

The following procedure is based on constant $\gamma$ and $c_p$, and utilizes constant expansion rate and $T_0$ as design parameters. This procedure will lead to a preliminary nozzle profile.

Step 1 : Choose certain $T_0$ and $\dot{p}$, solve for $p/p_0(x)$ from Equation (7.1) and then solve for $A/A^*(x)$ from Equation (7.2).

Step 2 : By changing $p_0$ ( $p_0 \leq p_{0limit}$ ), we can obtain different droplet mean radius :

$$p_0 \uparrow \longrightarrow r_m \uparrow$$

$$p_0 \downarrow \longrightarrow r_m \downarrow$$

$p_{0limit}$ is the highest pressure allowable for maintaining as gaseous phase at the chosen $T_0$ in Step 1. $p_0$ greater than $p_{0limit}$ is not allowed. Two options are available in this step:

(a) If $r_m$ is too small, follow Step 3;

(b) If $r_m$ is too large, follow Step 5.

Step 3 : There are two options in this step:

(a) Start all over from Step 1, use the nozzle with the same $T_0$ and lower $\dot{p}$ to obtain $p/p_0(x)$ and $A/A^*(x)$;

(b) Start all over from Step 1, use the nozzle with the same $\dot{p}$ and higher $T_0$ to obtain $p/p_0(x)$ and $A/A^*(x)$.

Although both options lead to larger $r_m$, there are some differences between the two options. Using option (a) one does not have to increase $p_0$ substantially higher to achieve the same increase in $r_m$ compared to option (b). However, low expansion rate nozzles are relatively more difficult to fabricate due to the smaller variation in area ratio. With option (b), depending on the type of expanding vapor and the mean droplet size desired, one may have to raise $p_0$ to an extremely high level which may be difficult to implement experimentally.

Step 4 : Repeat Step 2 until the desired $r_m$ is obtained.

Step 5 : The two options exactly opposite to Step 3 are as follows:

(a) Start all over from Step 1, use the nozzle with the same $T_0$ and higher $\dot{p}$ to obtain $p/p_0(x)$ and $A/A^*(x)$;

(b) Start all over from Step 1, use the nozzle with the same $\dot{p}$ and lower $T_0$ to obtain $p/p_0(x)$ and $A/A^*(x)$.

Step 6 : Repeat Step 2 until the desired $r_m$ is obtained.

Variable expansion rate can be easily implemented without technical difficulties by the same procedure if the resulting profile is not satisfactory. The experience, trial and error, and state of art selection of $\dot{p}(x)$ will then have to come into the play. Even in the cases where $\gamma$ and $c_p$ vary substantially with temperature change, this preliminary nozzle profile can be used as the prototype for further modifications. An iterative design procedure can be adopted to perform the modification to satisfaction. First run the numerical test on the preliminary nozzle profile to obtain temperature T(x). Incorporate this T(x) into Equation (7.1) and (7.2), we can then solve for $p/p_0(x)$ and the new nozzle profile $A/A^*(x)$ and proceed with the design steps described above. Thus iteratively we can modify the design to our

satisfaction.

## 7.3 Some Examples Of Nozzle Geometry Design

With combinations of different total temperature and expansion rate, figure 7.1, 7.2 and 7.3 show the area ratio of a few sample nozzles designed for steam. By comparing the figures, we can see that for the same expansion rate, higher total temperature would give flatter nozzle shape. The same is true for the same total temperature with lower expansion rate. It is noted that the result of these nozzles are used to show the effect of expansion rate on some important variables in the previous chapter.

Using different total pressure, the mean radius at the exit of each nozzle is calculated and summarized in table 7.1. Such a table can serve as a design guideline and would be very useful to generate the geometry of the nozzle that could give the desired mean droplet radius. For example, if a mean radius of 0.16 μm is wanted, by looking at the table we could immediately find that for such nozzle, $T_0$ falls between 500 K and 425 K, expansion rate falls between 2500 1/sec and 10000 1/sec. Or one may use nozzle

NZ12 and fine tune the inlet total pressure between 1.7 MPa and .87 MPa to obtain the desired mean radius.

Although different nozzles may all be able to achieve the same goal with proper inlet total pressure and/or proper length, not all the implementations are feasible. Two determining factors are the degree of slanting of the physical nozzle shape and the exit pressure ratio of the nozzle. Highly slanted nozzle would have strong boundary layer effect, multidimensional effect and flow separation problems. Flat shaped nozzle presents less boundary layer effect and less flow separation problem, however creates more difficulties in precision and fabricating the nozzle. High exit pressure ratio would require either extremely high inlet pressure or the extremely high exit vacuum which are in general difficult to establish. With such extremely high pressure ratio, the strength of the nozzle material will also be a limiting factor. Thus a compromise between all the limiting factors has to be reached for a feasible design.

# CHAPTER 8 CONCLUSIONS

An analytical model to study spontaneous condensation of single component and two component (condensible vapor and noncondensible gas mixture) was developed. Two nucleation theories one based upon classical theory (Volmer and Frenkel), another Deich's theory were used. The following conclusions result from this study.

1. Computer codes to solve the models for both single component flow and two component (one condensing vapor and one noncondensing vapor) flow in a condensing nozzle were developed and validated using available experimental results. The comparison between experimental and numerical results was good. The code provides the mean droplet size and number density, pressure ratio and quality as a function of nozzle geometry and nozzle inlet conditions.

2. The pressure ratio obtained from both classical theory and Deich's theory compared favorably with the experimental data, however, the results of Deich's theory have slightly smaller standard deviation. In designing nozzles for obtaining relatively

monodisperse droplets, Deich's theory should be used based on the following reasons: (a) No acceptable correlation for surface tension ratio can be established for classical theory; (b) Classical theory tends to overestimate the mean droplet radius; and (c) Deich's theory is expected to perform better on high expansion rate nozzles than classical theory because it also accounts for the nozzle expansion rate, which plays an important role in the spontaneous condensation, in the nucleation process.

3. Surface tension ratio can be correlated with inlet total entropy for use with Deich's theory. A correlation for steam flow was developed and used successfully.

4. Lower inlet total pressure and higher inlet total temperature lead to a delay in pressure rise, smaller mean radius of the droplets after spontaneous condensation, and smaller variation in droplet sizes.

5. Higher expansion rate will generate higher nucleation rate and have steeper and earlier pressure rise. It also results in smaller mean radius and better monodispersion.

6. The influence of all parameters on monodispersion is rather small indicating that the spontaneous condensation process will

always result in relatively monodisperse droplets.

7. The influence of noncondensing vapor was investigated using the two component flow model. Low initial condensing vapor content results in a later and flatter pressure rise, smaller mean radius, larger number of droplets and better monodispersion. It also results in higher Kn Number so that the flow always falls into the free molecular flow regime.

8. A nozzle design procedure is developed to generate the nozzle geometry based upon given inlet total conditions that will produce droplets of the desired size. With constant expansion rate, higher total temperature and lower expansion rate would give flatter nozzle shape. Although different designs (nozzle geometry and inlet total conditions) can all reach the same goal, a state-of-art choice has to take into account of the boundary layer effect, multi-dimensional effect, precision of fabrication, strength of nozzle material etc. into consideration. Temperature dependence and variable expansion rate design can be implemented iteratively with the current proposed design procedure.

## 8.1 Recommendations

To accurately solve the problem involving condensing flow, further investigations on the following subjects are recommanded:

A. surface tension of small liquid droplet or surface free energy of small solid crystal with 10 to 100 molecules;

B. an accurate nucleation theory and experiments which can accurately verify the calculated result of the theory;

C. the state of the condensate below sublimation or triple line (solid or liquid);

D. an accurate theory for rate of crystallization;

E. values of thermodynamic properties such as enthalpy, density, specific heat etc. at all range of temperature and pressure.

It is also suggested that experiments of test nozzle be conducted with nozzle design procedure described in the previous chapter to confirm the numerical computation presented in this work.

REFERENCES


1.01 Turner, J.R., Kodas, T. and Friedlander, S.K., "Monodisperse Particle Production by Vapor Condensation in Nozzles", J. Chem. Phys., Vol. 8, No. 1, pp. 457 - 465, 1988.

1.02 Hunter, W.W., Jr., Nichols, C.E., Jr., "Wind Tunnel Seeding Systems for Laser Velocimeters", NASA Conference Publication 2393, Hampton Virginia, March 19 - 29, 1986.

1.03 Edwards, R.V. (editor), Report on Statistical Particle Bias Problems in Laer Anemometry, J. of Fluids Eng., Vol. 109, pp. 89 - 93, 1987.

1.04 Moore, M.J., and sieverding, C.H., "Two-Phase Steam Flow in Turbines and Separators", Chapter 3, Hemisphere Publishing Corporation, Washington, 1976.

1.05 Young, J.B., " The Spontaneous Condensation of Steam in Supersonic Nozzles", PhysicoChem. Hydrodynamics, Vol. 3, No. 1, pp. 57 -82, 1982.

1.06 Kirillov, I.I. and Yablonik, R.M., "Fundamentals of The Theory of Turbines Operating on Wet Steam", NASA TT F-611; translation of "Osnovy teorii viazhnoparovykh turbin", Mashinostroyeniye Press, Leningrad, 1963.

1.07 Wegener, P.P., and Mack, L.M., "Condensation in Supersonic and Hypersonic Wind Tunnels", Advances in Applied Mechanics, Vol. V, Academic Press, 1958.

1.08 Daum, F.L., and Gyarmathy, G., "Condensation of Air and Nitrogen in Hypersonic Wind Tunnels", AIAA J., Vol. 6, No. 3, pp.458 - 465, 1968.

1.09 Wagner, B., and Doker, M., "Prediction of Condensation Onset and Growth in the European Transonic Wind Tunnel ETW", 1984.

1.10 Lewis, J.W.L., and Williams, W.D., "Argon Condensation in Free-Jet Expansions", Arnold Eng. Dvlp. Center, Arnold Air Force Station Technical Report, July 1974.

1.11 Barschdorff, D., "Verlauf der Zustandsgroszen und

Gasdynamische Zusammenhange bei der Spontanen Kondensation reinen Wasserdampfes in Lavaludusen", Forsch. Ing.-Wes., Vol. 37, No. 5, pp. 146 - 157, 1971.

1.12 Binnie, A.M. and Woods, M.W., "The Pressure Distribution in a Convergent-Divergent Steam Nozzle", Proc. Instn. Mech. Engrs., Vol. 138, pp. 229 - 266, 1938.

1.13 Gyarmathy, G. and Meyer, H., "Spontanen Kondensation", VDI-For-schungshett 508, VDI-Verlag, Dusseldolf, 1965.

1.14 Kadambi, J.R. and Whirlow, D.K., "Steam Turbine Condensation-Shock Wave Interaction", EPRI Report, CS-3251, Nov. 1983.

1.15 Deich, M.E., et al., "A Study of the Structure of Two-Phase Flow Behind a Condensation Shock in Supersonic Nozzles", Heat Transfer - Soviet Research, Vol. 1, No. 5, pp. 95 -105, Sep. 1969.

1.16 Moore, M.J., Walters, P.T., Crane, R.I. and Davidson, B.J., "Predicting the Fog-Drop Size in Wet-Steam Turbines, Conference on Heat and Fluid Flow in Steam and Gas Turbine Plant, Instn. Mech. Engrs., pp. 101 - 109, 1973.

1.17 Saltanov, G.A., Seleznev, L.I. and Tsiklauri, G.V., "Generation and Growth of Condensed Phase in High Velocity Flows", Int. J. Heat and Mass Transfer, Vol. 16, pp. 1577 - 1587, 1973.

1.18 Wegener, P.P. (editor), "Non-Equilibrium Flows, Part I, New York, 1969. (Chapter 4 by Wegener)

1.19 Hill, P.G., "Condensation of Water Vapour During Supersonic Expansion in Nozzles", J. Fluid Mech., Vol. 25, Part 3, pp. 593 - 620, 1966.

1.20 Zettlemoyer, A.C., "Nucleation Phenomena", Elsevier, 1977.

3.01 Feder, J., Russell, K.C., Lothe, J. and Pound, G.M., "Homogeneous Nucleation and Growth of Droplets in Vapours", Adv. Phys. (Suppl. Phil. Mag.), Vol. 15, No. 57, pp. 111 - 178, 1966.

3.02 Volmer, M., "Kinetik der Phasenbildung", Steinkopff, Dresden and Leipzig, 1939.

3.03 Frenkel, J., "Kinetic Theory of Liquids", Oxford Univ. Press, New York, 1946.

3.04 Volmer, M. and Weber, A., Z. Phys. Chem., Vol. 119, p. 277, 1926.

3.05 Farkas, L., Z. Phys. Chem., Vol. 125, p. 236, 1927.

3.06 Lothe, J. and Pound, G.M., "Reconsiderations of Nucleation Theory", J. Chem. Phys., Vol. 36, p. 2080, 1962.

3.07 Deich, M.E., Stepanchuk, V.F. and Saltanov, G.A., "Calculation of the Rate of Formation of Condensation Centers in Supersaturated Vapor", heat Transfer - Soviet Research, Vol. 1, No. 2, pp. 106 - 111, 1969.

3.08 Lai, D.S. and Kadambi, J.R., "Monodisperse Seeder for Laser Anemonetry Using Condensation Technique: Part I - Single Component Two-Phase Flow Results", Report 3-831-1, submitted to NASA LeRC, Cleveland, Ohio, 1989.

3.09 Oriani, R.A. and Sundquist, B.E., "Amendations to Nucleation Theory and the Homogeneous Nucleation of Water from the Vapor", J. Chem. Phys., Vol. 38, No. 9, pp. 2082 - 2089, 1963.

3.10 Abraham, F.F., "Further Considerations on the Surface Free Energy of Embryonic Droplets in the Nucleation of a Liquid from the Vapor", J. Chem. Phys., Vol. 50, No. 9, pp. 3977 - 3985, 1969.

3.11 Kirkwood, J.G. and Buff, E.P., "The Statistical Mechanical Theory of Surface Tension", J. Chem. Phys., Vol. 17, pp. 338 - 343, 1949.

3.12 Tolman, R.C., "The Effect of Drop Size on Surface Tension", J. Chem. Phys., Vol. 17, No. 3, pp. 333 - 337, 1949.

3.13 Bension, G.C. and Shuttleworth, R., "The Surface Energy of Small Nuclei", J. Chem. Phys., Vol. 19, No. 1, pp. 130 - 131, 1951.

3.14 Leinhard, J.H., "A Heat Transfer Textbook", Prentice Hall Inc., p. 393, 1981.

4.01 Burmeister, L.C., "Convective Heat Transfer", John Wiley & Sons, 1983.

4.02 John, J.E.A., "Gas Dynamics", Allyn and Bacon, 1984.

4.03 Holman, J.P., "Heat Transfer", McGraw Hill, p. 254, 1976.

4.04 Gyarmathy, G., "Grundlagen einer Theorie der Nassdampfturbine", Dissertation ETH, Zurich, Juris-Verlag, 1962. see also CEGB Translation 3017.

4.05 Kang, S.W., "Analysis of Condensation Droplet Growth in Rarefied and Continuum Environments", AIAA J., Vol. 5, No. 7, pp. 1288 - 1295, 1967.

4.06 Fuchs, N.A., "Evaporation and Droplet Growth inGaseous Media", Translated by Pratt, J.M., Pergamon Press, 1959.

4.07 Schrage, R.W., "A Theoretical Study of Interphase Mass Transfer", Columbia U. Press, New York, 1953.

4.08 Mills, A.F., Seban, R.A., "The Condensation Coefficient of Water", Int. J. Heat Mass Transfer, Vol. 10, pp. 1815 - 1827, 1967.

4.09 Cambell, B.A., Bakhtar, F., "Condensation Phemomena in High Speed Flow of Steam", Proc. Instn. Mech. Engrs., Vol. 182, pp. 395 - 405, D147 - 157, 1971.

4.10 Stein, G., "Condensation of Ice Clusters by Homogeneous Nucleation from the Vapor Phase", Ph.D. Thesis, Uale U., New Haven, Conn., 1967.

4.11 Wu, B., "A Study on Vapor Condensation by Homogeneous Nucleation", Ph.D. Thesis, Yale U., New Haven, Conn., 1972.

4.12 Oswatitsch, K., "Kondensationserscheinungen in Ueberschalldusen", Z. Angew. Math. Mech., Vol. 22, No. 1, pp. 1 -14, 1942.

4.13 Buckle, E.R., and Pouring, A.A., "Effects of Seeding on the Condensation of Atmospheric Moisture in Nozzles", Nature, Vol. 208, p. 367, 1965.

5.01 Meyer, C.A., McClintock, R.B., Silvestri, G.J., and Spencer, R.C., Jr., "1967 ASME Steam Table", 2nd Ed., p. 55, 1968.

5.02 Ozisik, M.N., "Basic Heat Transfer", McGraw-Hill, 1977.

5.03 Kakac, S., "Boilers Evaporators & Condensers", John Wiley & Sons Inc., pp. 817 - 818, 1991.

5.04 Reynolds, W.C., "Thermodynamic Properties in SI", Dept. of Mech. Eng., Stanford U., p. 154, 1979.

5.05 Michaelides, E.E., and Plazaola, Z.J., "Singularities in Two-Phase flow Equations — Critical Flow in Nozzles", Numerical Methods For Multiphase Flows, ASME, FED-Vol. 91, pp. 83 - 89, 1990.

5.06 Bilicki, Z., Kestin, J., and Mikielewicz, J., "Two-Phase Downflow in a Vertical Pipe and the Phenomenon of Choking; Homogeneous Diffusion Model", Int. J. Heat and Mass Transfer, Vol. 30, pp. 1427 - 1434, 1987.

5.07 Bilicki, Z., Dafermos, C., Kestin, J., Majda, G., and Zeng, D.L., "Trajectories and Singular Points in Steady-State Models of Two-Phase", Int. J. Mult. Flow, Vol. 13, pp. 511 - 533, 1987.

5.08 Wu, B.J.C., "Computer Programs for Calculating Condensation Rate in Steady, Adiabatic Expansions in Supersonic Nozzles", Office of Naval Research, Techical Report AD-775 257, 1974.

6.01 Bartell, L.S., "On Tolman's Equation For The Surface Tension Of Microdrops: Implication In Cluster Formation", J. Chem. Phys., Vol. 91, No. 23, pp. 5985 - 5986, 1987.

6.02 Wegener P.P. and Pouring A.A., "Experiments on Condensation of Water Vapor by Homogeneous Nucleation in Nozzles", The Phys. of Fluids, Vol. 7, No. 3, pp. 352 - 361, 1964.

6.03 Jaeger H.L., Willson E.J. and Hill P.G., "Nucleation of Supersaturated Vapors in Nozzles. I. $H_2O$ and $NH_3$", J. of Chem. Phys., Vol. 51, No. 12, pp. 5380 - 5388, 1969.

A.01 Reynolds, W.C., and Perkins, H.C., "Engineering Thermodynamics", McGraw-Hill, 1977.

G.01 Devore, J.L., "Probability and Statistics for Engineering and the Sciences", Brooks/Cole Publishing Company, 1982.

## APPENDIX A

## DERIVATION OF DEICH'S NUCLEATION THEORY

The nucleation rate consists of two components which we will derive separately as follows.

1. First component $J_1$

This component is arised from the collision of many single molecules which happen to form the droplet of critical size. The number of molecules to make the critical size per unit mass and per unit time $I_1$ can be expressed as:

$$I_1 = - 4\pi r_{cr}^2 \beta \left( N \frac{\partial z}{\partial n} \right)_{cr} \qquad (A.1)$$

where $\beta$ = number of molecules bombarding at a unit surface per unit time

$N$ = the equilibrium number distribution of the droplet

$z$ = f/N is a non-dimensional number distribution where f is a non-equilibrium number distribution

$n$ = number of molecules in each droplet

The expression for $\beta$ is well known and can be found in any gas kinetic theory book to be

$$\beta = \frac{p}{\sqrt{2\pi m k T}} \tag{A.2}$$

where $m$ = mass of molecule = $\frac{1}{\bar{N}}$

$k$ = Boltzmann's constant = $mR = R/\bar{N}$

$\bar{N}$ = number of molecules per unit mass of the condensing vapor

The physical meaning of Equation (A.1) may be interpreted as follows: $4\pi r_{cr}^2 \beta$ represents the number of molecules reaching the surface of a droplet of critical size per unit time. N is the number of droplets with critical size. The product of the two would be the total number of molecules impinging on all the droplets with critical size. In other words, this product represents the number of molecules condensing on the nuclei of critical radius per unit time. $n_{cr}$ is the number of molecules in a droplet with critical size. $-\left(\frac{\partial z}{\partial n}\right)_{cr}$ represents the change of the non-dimensional number distribution from the droplet with $n_{cr} - 1$ molecules to the droplet with $n_{cr}$ molecules. Thus the product of these three terms gives the net molecule number flux growing from $n_{cr} - 1$ molecules to $n_{cr}$ molecules, i.e. the nucleation rate.

According to Wegener [1.18], equilibrium number distribution N can be expressed as

$$N = \bar{N} \exp \left( \frac{nkT\Lambda - 4\pi r^2 \sigma}{kT} \right) \tag{A.3}$$

where the Gibb's enthalpy change associated with the formation of the droplet against the pressure difference $(p - p_\infty)$ to obtain the drop initially at $p_\infty$ at the actual vapor pressure p was neglected, and the ideal gas assumption was used. If we use R and $\bar{N}$ instead of m and k in Equation (A.2) and (A.3), also noting that the number of molecules n in a droplet with radius r can be expressed as:

$$n = \frac{4}{3} \pi r^3 \rho_f \bar{N} \tag{A.4}$$

Equation (A.2) and (A.3) can then alternatively be expressed as:

$$\beta = \frac{p\bar{N}}{\sqrt{2\pi R T_g}} \tag{A.5}$$

$$N = \bar{N} \exp \left( \frac{\frac{4}{3}\pi r^3 \rho_f \bar{N} R T_g \Lambda - 4\pi \bar{N} r^2 \sigma}{R T_g} \right) \tag{A.6}$$

If we assume that

1. The vapor has an equilibrium distribution before the expansion,
2. The expansion is so rapid such that the number distribution of the droplet does not have enough time to adjust, thus remains at the initial equilibrium distribution,

the non-equilibrium number distribution f would be the same as the initial equilibrium distribution $N_0$ :

$$f = N_0 = \bar{N} \exp\left( \frac{\frac{4}{3}\pi r^3 \rho_f \bar{N} R T_0 \Lambda_0 - 4\pi \bar{N} r^2 \sigma}{R T_0} \right) \qquad (A.7)$$

With Equation (A.6) and (A.7), the non-dimensional number distribution z can now be expressed as:

$$z = \frac{f}{N} = \frac{N_0}{N} = \exp\left( \frac{R T_0 \Lambda_0 \frac{4}{3}\pi r^3 \rho_f \bar{N} - 4\pi \bar{N}\, r^2 \sigma_0}{R T_0} \right.$$

$$\left. - \frac{R T \Lambda \frac{4}{3}\pi r^3 \rho_f \bar{N} - 4\pi \bar{N}\, r^2 \sigma}{R T} \right) \qquad (A.8)$$

The derivative $\frac{\partial z}{\partial n}$ can now be derived by chain rule,

$$\frac{\partial z}{\partial n} = \frac{\partial z}{\partial r}\frac{\partial r}{\partial n} \tag{A.9}$$

From Equation (A.4), we have

$$\frac{\partial n}{\partial r} = 4\pi r^2 \rho_f \bar{N} \tag{A.10}$$

therefore,

$$\frac{\partial r}{\partial n} = \frac{1}{4\pi r^2 \rho_f \bar{N}} \tag{A.11}$$

Differentiate Equation (A.8) with respect to r gives

$$\frac{\partial z}{\partial r} = \left( \frac{RT_0\Lambda_0 4\pi r^2 \rho_f \bar{N} - 8\pi\bar{N}r\sigma_0}{RT_0} - \frac{RT\Lambda 4\pi r^2 \rho_f \bar{N} - 8\pi\bar{N}r\sigma}{RT} \right)$$

$$\exp\left( \frac{RT_0\Lambda_0 \frac{4}{3}\pi r^3 \rho_f \bar{N} - 4\pi\bar{N}r^2\sigma_0}{RT_0} \right.$$

$$\left. - \frac{RT\Lambda \frac{4}{3}\pi r^3 \rho_f \bar{N} - 4\pi\bar{N}r^2\sigma}{RT} \right) \tag{A.12}$$

Now, substitute Equation (A.5), (A.6), (A.9), (A.11) and (A.12) into Equation (A.1) we get

$$I_1 = \frac{p\bar{N}}{\sqrt{2\pi RT}\,\rho_f}\left(\frac{RT_0\Lambda_0 4\pi r_{cr}^2\,\rho_f\bar{N} - 8\pi\bar{N}r_{cr}\sigma_0}{RT_0} - \right.$$

$$\left.\frac{RT\Lambda 4\pi r_{cr}^2\,\rho_f\bar{N} - 8\pi\bar{N}r_{cr}\sigma}{RT}\right)\exp\left(\frac{RT_0\Lambda_0\frac{4}{3}\pi r_{cr}^3\,\rho_f\bar{N} - 4\pi\bar{N}r_{cr}^2\,\sigma_0}{RT_0}\right.$$

$$\left. - \frac{RT\Lambda\frac{4}{3}\pi r_{cr}^3\,\rho_f\bar{N} - 4\pi\bar{N}r_{cr}^2\,\sigma}{RT}\right) \qquad (A.13)$$

The number of nuclei with critical size generated per unit time per unit mass of condensing vapor can be computed by:

$$J_1 = \frac{I_1}{n_{cr}} \qquad (A.14)$$

where

$$n_{cr} = \frac{4}{3}\pi r_{cr}^2\,\rho_f\bar{N} \qquad (A.15)$$

Substituting Equation (A.13) and (A.15) into Equation (A.14) and with $r_{cr}$ expressed as

$$r_{cr} = \frac{2\sigma}{\rho_f RT\Lambda} \qquad (A.16)$$

we can now obtain the final expression of the first component nucleation rate as

$$J_1 = \frac{3\Lambda\bar{N}p\sqrt{RT_g}}{\sqrt{8\pi}\,\sigma}\left(\frac{T_g\Lambda\sigma_0/\sigma - T_0\Lambda_0}{T_0}\right)\exp\left[-\frac{Z_1^2}{\Lambda^2}\,\frac{3T\Lambda\sigma_0/\sigma - 2(T\Lambda)_0}{T_0\Lambda}\right] \tag{A.17}$$

where

$$Z_1^2 = \frac{16\pi\bar{N}\sigma^3}{3\rho_f^2(RT_g)^3}$$

2. Second component $J_2$

From chapter 2 we know that the droplets with mean radius smaller than critical radius is unstable and will evaporated provided that the vapor condition (e.g. temperature and pressure) remains unchanged. However, during the expansion, the vapor condition will change and so does the critical radius. We have shown that the critical radius is decreasing during the nucleation zone. Thus some of the droplets with subcritical size formed upstream would not have enough time to evaporate when they are transported to a downstream region, where they become supercritical. Consequently, these droplets would then become stable and serve as the nuclei for further condensation. This constitutes the second component of Deich's nucleation theory, which is not taken into account in the classical and Lothe-Pound nucleation theories.

It is obvious that the higher the expansion rate is, the faster will the rate of decrease of the critical radius be. And the faster the rate of decrease of the critical radius, the larger the number of droplets would become supercritical from subcritical. Also changing of critical radius $r_{cr}$ is the same as changing the number of molecules in a critical droplet $n_{cr}$. Therefore, if the same two assumptions used in deriving the first component nucleation rate are made as well, the number of molecules that would make critical size droplet per unit time per unit mass of the condensing vapor $I_2$ can be computed as:

$$I_2 = - N_0 \frac{dn_{cr}}{dt} \tag{A.18}$$

Using chain rule $I_2$ can be further expressed as:

$$I_2 = - N_0 \frac{dn_{cr}}{dr_{cr}} \frac{dr_{cr}}{d\Delta T} \frac{d\Delta T}{dt} \tag{A.19}$$

Differentiate Equation (A.15) we get

$$\frac{dn_{cr}}{dr_{cr}} = 4\pi r_{cr}^2 \rho_f \bar{N} \tag{A.20}$$

In addition to Equation (A.16), $r_{cr}$ can also be expressed as [1.06]:

$$r_{cr} = \frac{2\sigma}{\rho_f h_{fg} \ln\left(\frac{T_s}{T_g}\right)} \qquad (A.21)$$

With $\Delta T = T_s - T_g$, $r_{cr}$ would look like

$$r_{cr} = \frac{2\sigma}{\rho_f h_{fg} \ln\left(1 + \frac{\Delta T}{T_g}\right)} \qquad (A.22)$$

By differentiating Equation (A.22) with respect to $\Delta T$ we would have

$$\frac{dr_{cr}}{d\Delta T} = \frac{-r_{cr}}{T_g \ln\left(\frac{T_s}{T_g}\right)} \qquad (A.23)$$

Substitute Equation (A.7), (A.20) and (A.23) into Equation (A.19) and utilize the expression of $r_{cr}$ with Equation (A.16) will give

$$I_2 = \frac{4\pi r_{cr}^3 \rho_f \bar{N}^2}{T_g \ln\left(\frac{T_s}{T_g}\right)} \frac{d\Delta T}{dt} \exp\left(\frac{4}{3}\pi r_{cr}^3 \rho_f \bar{N} \Lambda_0 - \frac{4\pi \bar{N} r_{cr}^2 \sigma_0}{R T_0}\right) \qquad (A.24)$$

Similar to Equation (A.14), $J_2$ can be expressed as

$$J_2 = \frac{I_2}{n_{cr}} \tag{A.25}$$

By substituting Equation (A.16) into Equation (A.15) and (A.24), the second component of Deich's nucleation theory $J_2$ can be computed as:

$$J_2 = \frac{3\,\bar{N}}{T_g \ln\left(\frac{T_s}{T_g}\right)} \frac{d\Delta T}{dt} \exp\left[ - \frac{Z_1^2}{\Lambda^2} \frac{3T\sigma_0}{T_0\sigma} \right] \tag{A.26}$$

The total nucleation rate J is the sum of the two components

$$J = J_1 + J_2 \tag{A.27}$$

## APPENDIX B

## RELATION BETWEEN SUPERCOOLING RATE $d\Delta T/dt$ AND EXPANSION RATE $\dot{p}$

As shown in Appendix A, the second component of the Deich's nucleation rate depends on the supercooling rate $d\Delta T/dt$, which can be shown to be related to the expansion rate as follows.

By definition $\Delta T = T_s - T_g$, thus

$$\frac{d\Delta T}{dt} = \frac{dT_s}{dt} - \frac{dT_g}{dt} \tag{B.1}$$

Assume isentropic expansion, we have

$$p = T_g \frac{\gamma}{\gamma - 1} \cdot \text{constant} \tag{B.2}$$

$$\dot{p} = -\frac{1}{p}\frac{dp}{dt} = \frac{-\gamma}{\gamma - 1}\frac{1}{T_g}\frac{dT_g}{dt} \tag{B.3}$$

thus

$$\frac{dT_g}{dt} = -T_g \frac{\gamma - 1}{\gamma}\dot{p} \tag{B.4}$$

Also from Clausius-Clapeyron equation we have

$$\frac{dp}{dT_s} = \frac{h_{fg}}{v_{sg} T_s} \tag{B.5}$$

where $v_{sg}$ is the specific volume of saturated vapor at pressure p. With Equation (B.3), this gives

$$\frac{dT_s}{dt} = \frac{v_{sg} T_s}{h_{fg}} \frac{dp}{dt} = -\dot{p} \frac{p v_{sg} T_s}{h_{fg}} \tag{B.6}$$

Hence, substituting Equation (B.4) and (B.6) back into Equation (B.1) we have

$$\frac{d\Delta T}{dt} = \left( T_g \frac{\gamma - 1}{\gamma} - \frac{p v_{sg} T_s}{h_{fg}} \right) \dot{p} \tag{B.7}$$

which shows that the supercooling rate $d\Delta T/dt$ is directly proportional to the expansion rate $\dot{p}$.

## APPENDIX C

## DERIVATIVE OF TOTAL WETNESS

To solve the equation of velocity, the expression of the derivative of total wetness dw/dx is required. Two ways we can derive this equation, mathematically or physically. Both methods give exactly the same expression.

1. Mathematically

dw/x can be obtained by directly differentiating w Equation (4.26)

$$\frac{dw}{dx}(x) = \frac{d}{dx}\int_{x_i=0}^{x} w_i(x_i;\ x)\ dx_i \qquad (C.1)$$

Assume

$$w_i(x_i;\ x) = \frac{\partial g}{\partial x_i}(x_i;\ x) \qquad (C.2)$$

Substitute Equation (C.2) into (C.1), we have

$$\frac{dw}{dx}(x) = \frac{d}{dx}\int_{x_i=0}^{x} w_i(x_i;\ x)\ dx_i$$

$$= \frac{d}{dx}\int_{x_i=0}^{x} \frac{\partial g}{\partial x_i}(x_i;\ x)\ dx_i$$

$$= \frac{d}{dx}\left[g(x;x) - g(0;x)\right]$$

$$= \left[\frac{\partial g}{\partial x_i}(x;x)\ \frac{dx}{dx} + \frac{\partial g}{\partial x}(x;x)\ \frac{dx}{dx}\right] - \left[\frac{\partial g}{\partial x_i}(0;x)\ \frac{d0}{dx} + \frac{\partial g}{\partial x}(0;x)\ \frac{dx}{dx}\right]$$

$$= \frac{\partial g}{\partial x_i}(x;x) + \frac{\partial g}{\partial x}(x;x) - \frac{\partial g}{\partial x}(0;x)$$

$$= w_i(x;x) + \frac{\partial g}{\partial x}(x;x) - \frac{\partial g}{\partial x}(0;x) \qquad (C.3)$$

Also from Equation (C.2) we know that

$$\frac{\partial w_i}{\partial x}(x_i;\ x) = \frac{\partial}{\partial x}\left[\frac{\partial g}{\partial x_i}(x_i;\ x)\right] = \frac{\partial}{\partial x_i}\left[\frac{\partial g}{\partial x}(x_i;\ x)\right] \qquad (C.4)$$

Thus

$$\int_{x_i=0}^{x} \frac{\partial w_i}{\partial x}(x_i;\ x)\ dx_i = \int_{x_i=0}^{x} \frac{\partial}{\partial x_i}\left[\frac{\partial g}{\partial x}(x_i;\ x)\right] dx_i$$

$$= \frac{\partial g}{\partial x}(x;x) - \frac{\partial g}{\partial x}(0;x) \qquad (C.5)$$

From Equation (C.5) and (C.3), we have

$$\frac{dw}{dx}(x) = \frac{d}{dx}\int_{x_i=0}^{x} w_i(x_i;\ x)\ dx_i$$

$$= w_i(x;x) + \int_{x_i=0}^{x} \frac{\partial w_i}{\partial x}(x_i;\ x)\ dx_i \qquad (C.6)$$

Differentiate Equation (4.24) with respect to x and utilize Equation (4.2), we have

$$\frac{dw}{dx}(x) = \frac{1}{c(x)}\ \frac{4}{3}\ \pi r_{cr}^{3}(x)\ \rho_f\ J(x)$$

$$+ \frac{4\pi}{c(x)} \int_{x_i=0}^{x} \frac{r_i^2(x_i;\ x)\ \alpha_i(x_i;\ x)\ J(x_i)\ [T_{f,i}(x_i;\ x) - T_g(x)]dx_i}{[h_g(T_g(x)) - h_f(T_{f,i}(x_i;\ x))]\ c(x_i)} \qquad (5.3)$$

2. Physically

The increase of the total wetness can be attributed to two parts:

(1) the birth of a new group of droplet, and (2) the growth of all the groups of the old droplets. The mass of the new born droplets per unit mass of the mixture is

$$(dw)_{new} = \rho_f \frac{4}{3}\pi r_{cr}^3(x)\ J(x)\ dt \tag{C.7}$$

The increase of mass of the group born at $x_i$ currently located at x will be

$$(dw)_{old} = \rho_f 4\pi r_i^2(x_i;\ x)\ dr_i\ J(x_i)\ dt_i \tag{C.8}$$

The increase of total wetness can then be calculated by

$$dw = (dw)_{new} + \int_{x_i=0}^{x} (dw)_{old} \tag{C.9}$$

Note that

$$dt = \frac{dx}{c(x)} \tag{C.10}$$

Thus we have

$$\frac{dw}{dx}(x) = \rho_f \frac{4}{3}\pi r_{cr}^3(x)\ \frac{J(x)}{c(x)} + \int_{x_i=0}^{x} \rho_f 4\pi r_i^2(x_i;\ x)\ \frac{dr_i}{dx}\ \frac{J(x_i)}{c(x_i)}\ dx_i$$

(C.11)

Also from Equation (4.2) we have

$$\rho_f 4\pi r_i^2(x_i;\, x)\ \frac{dr_i}{dx}(x_i;\, x)$$

$$= \frac{4\pi r_i^2(x_i;\, x)\ \alpha_i(x_i;\, x)[T_{f,i}(x_i;\, x) - T_g(x)]}{[h_g(T_g(x)) - h_f(T_{f,i}(x_i;\, x))]\ c(x)} \qquad (C.12)$$

Hence, substitute Equation (C.12) into (C.11) we obtain

$$\frac{dw}{dx}(x) = \frac{1}{c(x)}\ \frac{4}{3}\ \pi r_{cr}^3(x)\ \rho_f\ J(x)$$

$$+ \frac{4\pi}{c(x)} \int_{x_i=0}^{x} \frac{r_i^2(x_i;\, x)\ \alpha_i(x_i;\, x)\ J(x_i)\ [T_{f,i}(x_i;\, x) - T_g(x)]dx_i}{[h_g(T_g(x)) - h_f(T_{f,i}(x_i;\, x))]\ c(x_i)}$$

(5.3)

## APPENDIX D

## DERIVATION OF EQUATION OF VELOCITY

The equation of velocity can be derived from the differential form of continuity equation, momentum equation, energy equation, and the equation of state. These equations are listed as follows.

continuity equation

$$\frac{d\rho}{\rho} + \frac{dc}{c} + \frac{dA}{A} + \frac{dw}{1 - w} = 0 \qquad (D.1)$$

momentum equation

$$cdc + \frac{1 - w}{\rho} dp = 0 \qquad (D.2)$$

energy equation

$$cdc + (1 - w)c_p dT_g + wc_f dT_f = h'_{fg} dw \qquad (D.3)$$

equation of state

$$p = \rho R T_g \qquad (D.4)$$

First, differentiate equation of state Equation (D.4) gives

$$dT_g = \frac{1}{R}\left(\frac{1}{\rho}\,dp - \frac{d\rho}{\rho}\,RT_g\right) \qquad (D.5)$$

Use Equation (D.2) for $\frac{1}{\rho}\,dp$ , and Equation (D.1) for $\frac{d\rho}{\rho}$ in Equation (D.5) we get

$$dT_g = \frac{1}{R}\left[\frac{-cdc}{1-w} + \left(\frac{dc}{c} + \frac{dA}{A} + \frac{dw}{1-w}\right)RT_g\right] \qquad (D.6)$$

Substitute Equation (D.6) into Equation (D.3) gives

$$cdc + (1-w)c_p\,\frac{1}{R}\left[\frac{-cdc}{1-w} + \left(\frac{dc}{c} + \frac{dA}{A} + \frac{dw}{1-w}\right)RT_g\right] + wc_f dT_f = h'_{fg}dw \qquad (D.7)$$

Group all the terms with dc together and divide the whole equation with $(1-w)c_pT_g$ we have

$$\frac{dc}{c}\left[\frac{c^2(1 - c_p/R)}{(1-w)c_pT_g} - 1\right] = \frac{dA}{A} + \frac{dw}{1-w} + \frac{wc_f dT_f - h'_{fg}dw}{(1-w)c_pT_g} \qquad (D.8)$$

Note that for ideal gas $R = c_p - c_v$ , thus Equation (D.8) will be

$$\frac{dc}{c}\left[\frac{c^2}{(1-w)\gamma RT_g} - 1\right] = \frac{dA}{A} + \frac{dw}{1-w} + \frac{wc_f dT_f - h'_{fg}dw}{(1-w)c_pT_g} \qquad (D.9)$$

From the definition of Mach number

$$M^2 = \frac{c^2}{\gamma RT} \tag{D.10}$$

we can now obtain the equation of velocity

$$\frac{dc}{dx} = \frac{c}{\left(\frac{M^2}{1-w} - 1\right)} \left[\frac{dA}{dx}\frac{1}{A} + \frac{wc_f}{(1-w)c_{p,g}T_g}\frac{dT_f}{dx} + \frac{c_{p,g}T_g - h'_{f,g}}{(1-w)c_{p,g}T_g}\frac{dw}{dx}\right] \tag{5.2}$$

Utilizing the differential form of the two component continuity equation, momentum equation, energy equation, and the equation of state, with exactly the same procedure, we can also yield the equation of velocity for two component model. The arithmetic for such derivation is straight forward and lengthy, thus will not be presented here.

## APPENDIX E

## DERIVATION OF MEAN MOLECULAR WEIGHT AND DENSITY

1. Mean Molecular Weight

The initial mass fraction of the condensing vapor $w_0$ is defined as

$$w_0 = \frac{m_{v0}}{m} = \frac{m_{v0}}{m_{v0} + m_n} \tag{E.1}$$

where

$m_{v0}$ = initial mass of condensing vapor

$m_n$ = mass of noncondensing inert gas

$m$ = total mass of the mixture

wetness $w$, the mass fraction of the condensate, can be evaluated as

$$w = \frac{m_c}{m} = \frac{m_{v0} - m_v}{m} \tag{E.2}$$

where

$m_c$ = mass of condensate

$m_v$ = remaining mass of condensing vapor after condensation

Since the number of moles of the mixture vapor is the sum of the moles of the condensing vapor and inert gas, the mean molecular weight for the vapor phase defined as the mass per mole of the mixture vapor can then be related to the molecular weight of the condensing vapor $M_v$ and inert gas $M_n$ by

$$\frac{m_v + m_n}{M_g} = \frac{m_v}{M_v} + \frac{m_n}{M_n} \tag{E.3}$$

From Equation (E.1) we have

$$\frac{m_n}{m} = 1 - w_0 \tag{E.4}$$

From Equation (E.1) and (E.2) we have

$$\frac{m_v}{m} = w_0 - w \tag{E.5}$$

$M_g$ can then be calculated from Equation (E.3) as

$$M_g = \frac{m_v + m_n}{\frac{m_v}{M_v} + \frac{m_n}{M_n}} = \frac{w_0 - w + 1 - w_0}{(w_0 - w)\frac{1}{M_v} + (1 - w_0)\frac{1}{M_n}}$$

$$= \frac{1 - w}{(w_0 - w)\frac{1}{M_v} + (1 - w_0)\frac{1}{M_n}} \qquad (E.6)$$

2. Vapor Density

Assume both condensing vapor and noncondensing inert gas are ideal gases and of the same temperature. From Dalton's rule [A.01]

$$p = p_v + p_n = \rho_v \frac{R}{M_v} T_g + \rho_n \frac{R}{M_n} T_g = \rho_g \frac{R}{M_g} T_g \qquad (E.7)$$

Thus we obtain

$$\frac{\rho_g}{M_g} = \frac{\rho_v}{M_v} + \frac{\rho_n}{M_n} \qquad (E.8)$$

where $M_g$ is expressed as Equation (E.6).

## APPENDIX F

## INPUT OF THE FORTRAN PROGRAM

1. Thermodynamic Properties

PSAT(T) : saturated pressure $P_{sat}(T)$ as a function of temperature T

TSAT(P) : saturated temperature $T_{sat}(P)$ as a function of pressure P

HG(T) : vapor enthalpy $h_g(T)$ as a function of temperature T

TVAP(HG) : vapor temperature $T_g(h_g)$ as a function of vapor enthalpy HG

CP(T) : constant pressure specific heat of vapor $c_p(T)$ as a function of temperature T, in some cases $c_p$ remains constant in the temperature range of interest

GMISEN : ratio of specific heat of vapor $c_p$ / $c_v$, in some cases it remains constant in the temperature range of interest

HF(T) : liquid enthalpy $h_f(T)$ as a function of temperature T

SF(T) : liquid entropy $s_f(T_f)$ as a function of temperature T

DF(T,P) : liquid density $\rho_f(T,P)$ as a function of temperature T and pressure P, in some cases $\rho_f$ remains constant

in the temperature and pressure range of interest

CF(T) : specific heat of liquid $c_f(T)$ as a function of temperature T, in some cases $c_f$ remains constant in the temperature range of interest

SIGMA0(T) : suface tension of flat surface $\sigma_0(T)$ expressed in the form of fitting polynomial NTERMS, SB(I), SC(I), SD(I)

MV : molecular weight M of the expanding vapor

2. Nozzle Geometry

AR(x) or PR(x) : area ratio or isentropic pressure ratio as a function of streamwise distance of nozzle expressed in the form of coefficients of fitting polynomials NTERMA, AB(I), AC(I), AD(I) or NTERMP, PB(I), PC(I), PD(I)

N : No. of grids

DIST : overall distance

X0 : starting location of the nozzle to the throat

3. Constants

R : universal gas constants

NA : Avagadra Number

PI : $\pi$

4. Initial Conditions

T0 : inlet total temperature $T_0$

P0 : inlet total pressure $P_0$

H0V : inlet total enthalpy $h_0$

S0V : inlet total entropy $s_0$

5. Iteration Parameters

NITER : maximum times of iteration

EPSM, EPS : convergence criteria of the relative deviation of the iteration of Mach No., and other variables such as velocity VEL, vapor temperature TVAP, pressure P, droplet radius RI

RELAX, RELAX2 : relaxation factor of the intermediate iteration result before and after the end of nucleation

6. Experimental Data

NEXP : No. of experimental data

PREXP : experimental pressure ratio

**UNITS USED IN THE PROGRAM**

1. Pressure : $N/m^2$
2. Temperature : K
3. Density : $Kg/m^3$
4. Velocity : m/s
5. Length : m
6. Enthalpy : J/Kg
7. Entropy : J/(Kg K)
8. Specific Heat : J/(Kg K)
9. Universal Gas Constant : J/(Kg mol K)
10. Molecular Weight : Kg/(Kg mol)
11. Surface Tension : N/m
12. Thermal Conductivity : J/(s m K)

## APPENDIX G

## DEFINITION OF THE CORRELATION COEFFICIENT

The correlation coefficient can be defined as follows. Given n pairs of observations $(x_i, y_i)$, the correlation coefficient r can be shown to be [G.01]:

$$r = \frac{n \sum x_i y_i - (\sum x_i)(\sum y_i)}{\sqrt{n \sum x_i^2 - (\sum x_i)^2}\ \sqrt{n \sum y_i^2 - (\sum y_i)^2}} \qquad (G.1)$$

r serves as a measure of the degree of linear relationship among variables. The value of r is between 1 and -1. The larger the |r| is, the stronger the linear correlation is.

Table 6.1 Summary of one component test case result

C: classical theory, D: Deich's theory
error (Pa): standard deviation of pressure comparison between theory and experiment
STD ($10^{-3}$ μm): standard deviation of droplet radius distribution

| Test Case | Nucl | $\sigma/\sigma_\infty$ | $T_0$ (K) | $P_c$ (Pa) | $P_w$ (Pa) | error | $r_m$ (μm) | STD |
|---|---|---|---|---|---|---|---|---|
| Barschdorff No. 4 | D | .805 | 376.9 | 78323 | 33246 | .0112 | .0241 | 3.65 |
| | C | 1.020 | | | 33447 | .0124 | .0262 | 4.29 |
| Barschdorff No. 7 | D | .810 | 388.4 | 78323 | 27367 | .0172 | .0156 | 3.03 |
| | C | .995 | | | 27650 | .0179 | .0168 | 3.51 |
| Barschdorff No. 10 | D | .840 | 399.8 | 78323 | 21941 | .0023 | .0091 | 2.45 |
| | C | 1.000 | | | 22086 | .0021 | .0098 | 3.39 |
| Binnie and Wood No. 92 | D | .865 | 411.9 | 146030 | 47309 | .0086 | .0251 | 3.95 |
| | C | 1.040 | | | 47483 | .0084 | .0251 | 4.67 |
| Binnie and Wood No. 93 | D | .850 | 410.6 | 145960 | 48684 | .0095 | .0221 | 3.68 |
| | C | 1.030 | | | 48711 | .0095 | .0222 | 4.74 |
| Deich | D | .835 | 403.2 | 99972 | 27531 | .0116 | .0039 | 1.44 |
| | C | .985 | | | 27898 | .0121 | .0044 | 1.56 |
| Gyarmathy and Meyer No. 102 | D | .875 | 420.7 | 206840 | 72633 | .0062 | .0634 | 7.80 |
| | C | 1.060 | | | 72892 | .0053 | .0702 | 8.54 |
| Gyarmathy and Meyer No. 108 | D | .830 | 392.3 | 62052 | 18346 | .0027 | .0154 | 3.30 |
| | C | .995 | | | 18511 | .0028 | .0164 | 3.70 |
| Gyarmathy and Meyer No. 107 | D | .805 | 389.8 | 62052 | 18148 | .0073 | .0057 | 2.42 |
| | C | .965 | | | 18394 | .0070 | .0068 | 1.96 |
| Gyarmathy and Meyer No. 112 | D | .770 | 388.7 | 37921 | 9281 | .0056 | .0030 | 1.32 |
| | C | .905 | | | 9398 | .0062 | .0035 | 1.15 |
| Gyarmathy and Meyer No. 119 | D | .960 | 442.1 | 492280 | 187080 | .0077 | .0636 | 7.07 |
| | C | 1.150 | | | 190690 | .0079 | .0740 | 7.36 |
| Gyarmathy and Meyer No. 91 | D | .880 | 445.1 | 232010 | 47295 | .0044 | .0128 | 2.62 |
| | C | .990 | | | 47330 | .0046 | .0130 | 3.29 |
| Kadambi No. 3 | D | .780 | 352.3 | 33508 | 13664 | .0283 | .0066 | 1.96 |
| | C | .995 | | | 13742 | .0290 | .0072 | 2.42 |
| Kadambi No. 4 | D | .750 | 368.2 | 39920 | 14550 | .0298 | .0060 | 2.20 |
| | C | .955 | | | 14327 | .0291 | .0068 | 2.82 |
| Kadambi No. 5 | D | .785 | 367.1 | 52882 | 21295 | .0495 | .0086 | 3.36 |
| | C | .985 | | | 21565 | .0500 | .0091 | 3.90 |
| Moore No. A | D | .735 | 354.6 | 24407 | 9297 | .0228 | .0079 | 3.41 |
| | C | .925 | | | 9316 | .0231 | .0094 | 2.57 |

TABLE 7.1 mean radius calculated at nozzle exit 18 cm downstream to the nozzle throat for nozzles of various design

STD ($10^{-3}$ $\mu$m): standard deviation of droplet radius distribution

| nozzle | $T_0$ (K) | $\dot{p}$ (1/sec) | $P_0$ (MPa) | $r_m$ ($\mu$m) | STD |
|---|---|---|---|---|---|
| NZ11 | 500 | 2500 | 1.7 | 0.2795 | 5.96 |
| NZ11 | 500 | 2500 | 0.87 | 0.0715 | 12.3 |
| NZ12 | 500 | 5000 | 1.7 | 0.2117 | 4.35 |
| NZ12 | 500 | 5000 | 0.87 | 0.0896 | 6.23 |
| NZ13 | 500 | 10000 | 1.7 | 0.1304 | 4.33 |
| NZ13 | 500 | 10000 | 0.87 | 0.0534 | 5.50 |
| NZ21 | 425 | 2500 | 0.33 | 0.1339 | 9.71 |
| NZ21 | 425 | 2500 | 0.17 | 0.0407 | 5.73 |
| NZ22 | 425 | 5000 | 0.33 | 0.0869 | 7.13 |
| NZ22 | 425 | 5000 | 0.17 | 0.0250 | 3.86 |
| NZ23 | 425 | 10000 | 0.33 | 0.0451 | 5.93 |
| NZ23 | 425 | 10000 | 0.17 | 0.0152 | 2.87 |
| NZ31 | 350 | 2500 | 0.027 | 0.0111 | 2.54 |
| NZ31 | 350 | 2500 | 0.013 | 0.0037 | 1.22 |
| NZ32 | 350 | 5000 | 0.027 | 0.0073 | 1.92 |
| NZ32 | 350 | 5000 | 0.013 | 0.0032 | .851 |
| NZ33 | 350 | 10000 | 0.027 | 0.0057 | 1.00 |
| NZ33 | 350 | 10000 | 0.013 | 0.0026 | .626 |

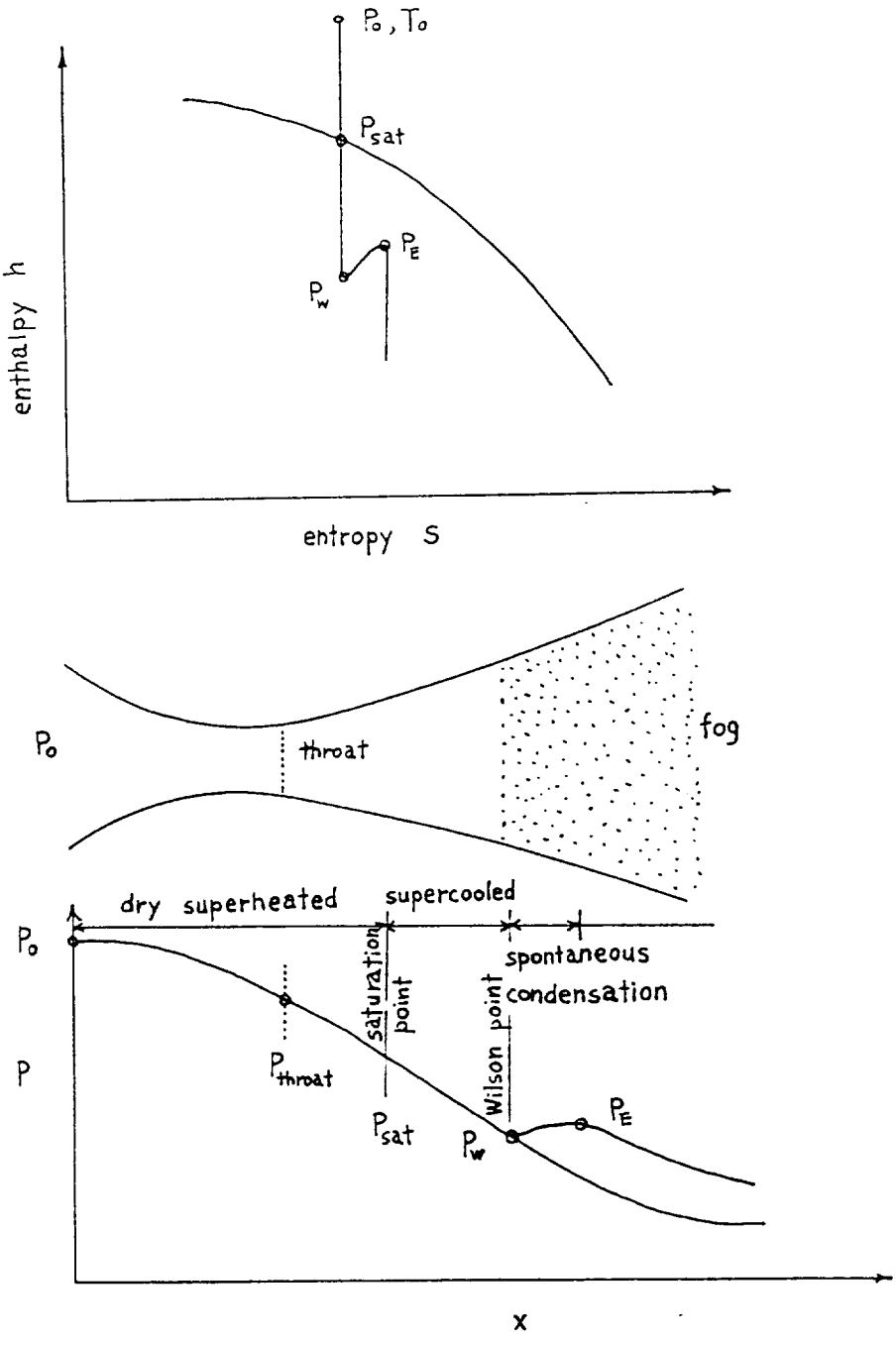


Figure 2.1 Spontaneous Condensation In A Laval Nozzle

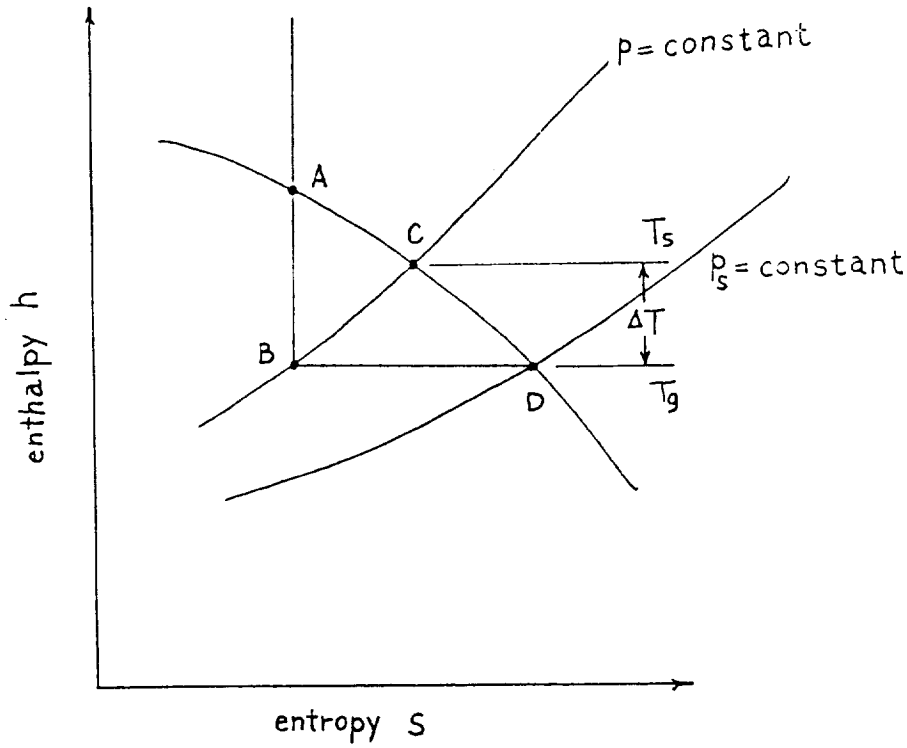


Figure 2.2 Spontaneous Condensation On Mollier Chart

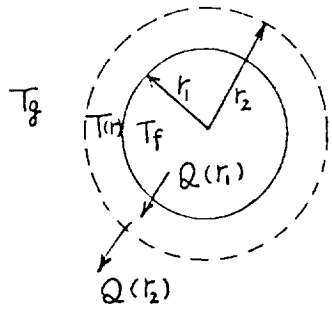


Figure 4.1 Heat Transfer Occured In The Vicinity Of A Droplet Submerged In Supercooled Vapor

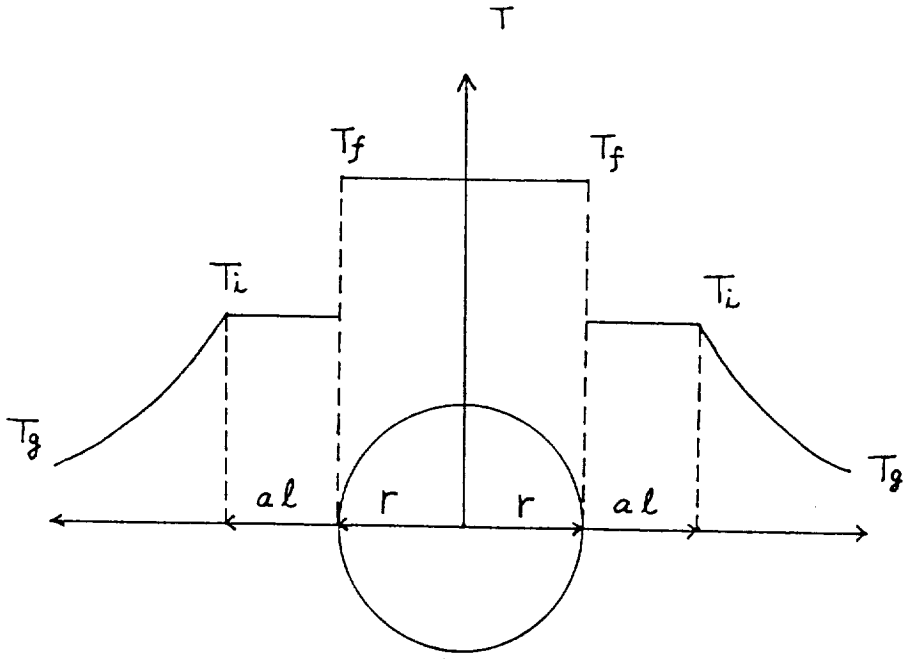


Figure 4.2 Temperature Field In The Vicinity Of A Droplet Submerged In Supercooled Vapor For Slip And Transient Flow Regime

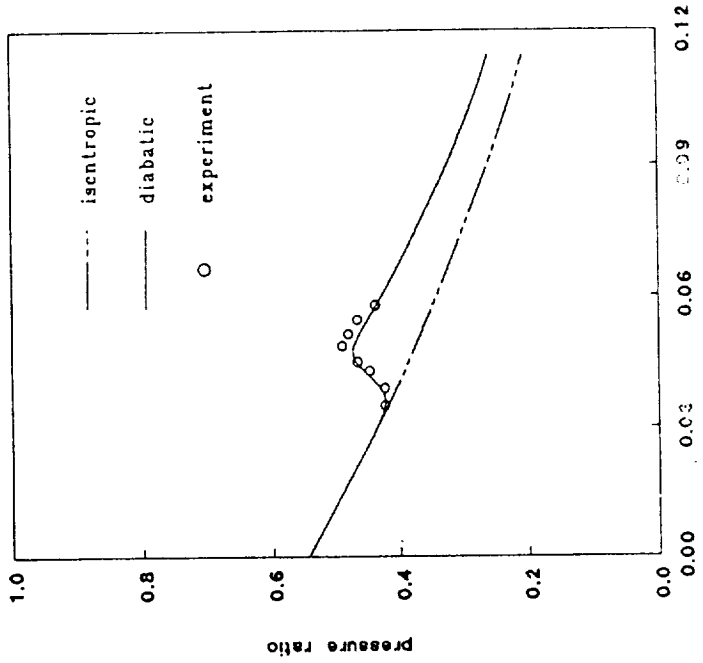


Figure 6.1 Pressure Ratio of Barschdorff No.4 For Classical Theory

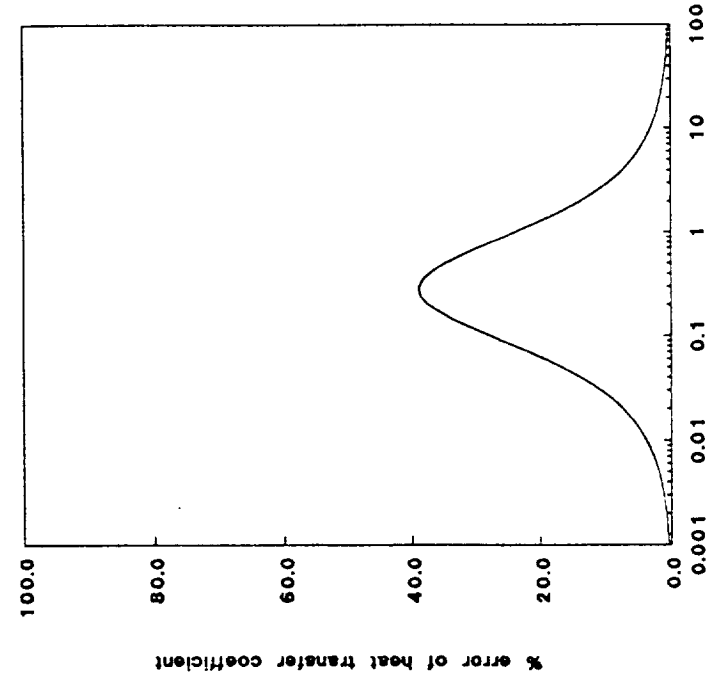


Figure 4.3 Difference Between Gyarmathy Model (a=0) And Transient Model (a=2)

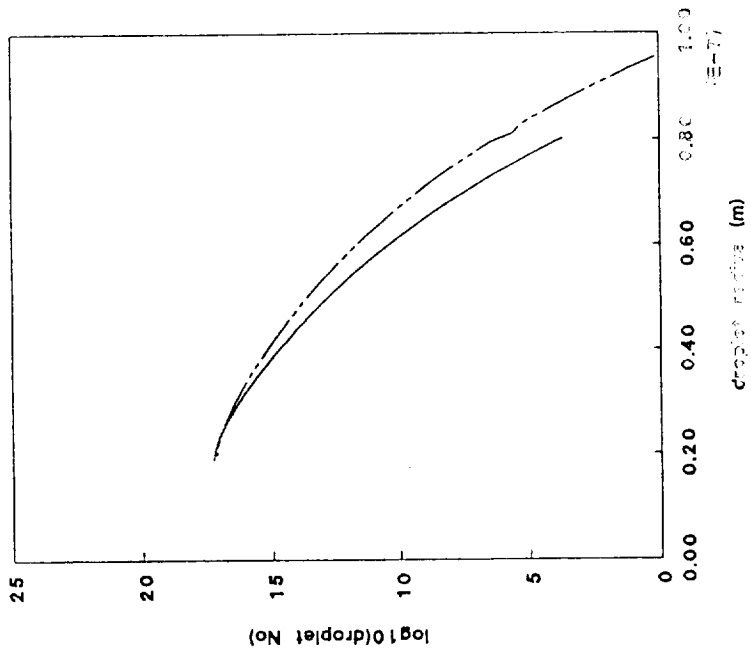


Figure 6.3 Droplet Size Distribution Of Barschdorff No. 4

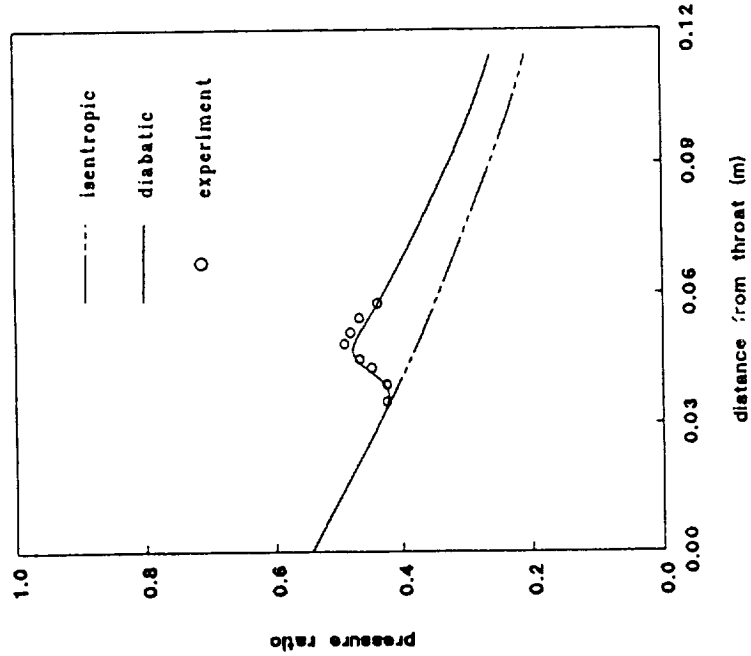


Figure 6.2 Pressure Ratio Of Barschdorff No. 4 For Deich's Theory

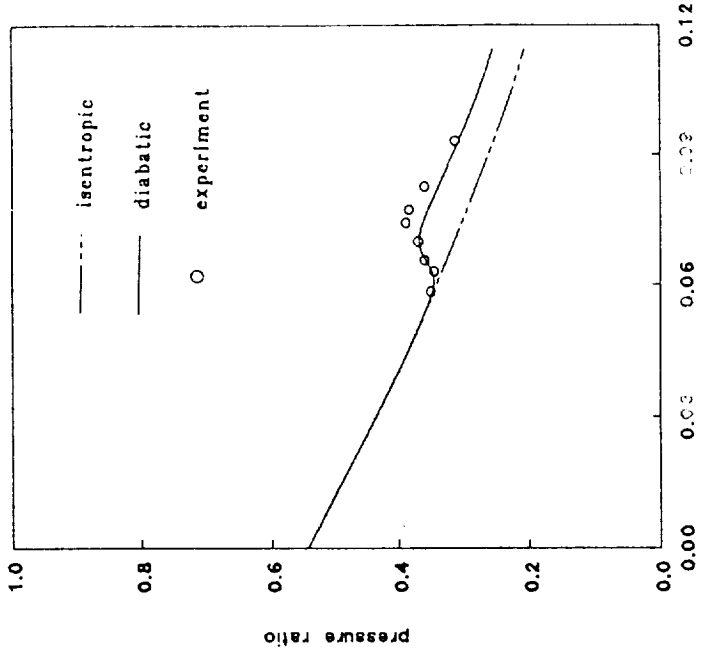


Figure 6.5 Pressure Ratio Of Barschdorff
No. 7 For Deich's Theory

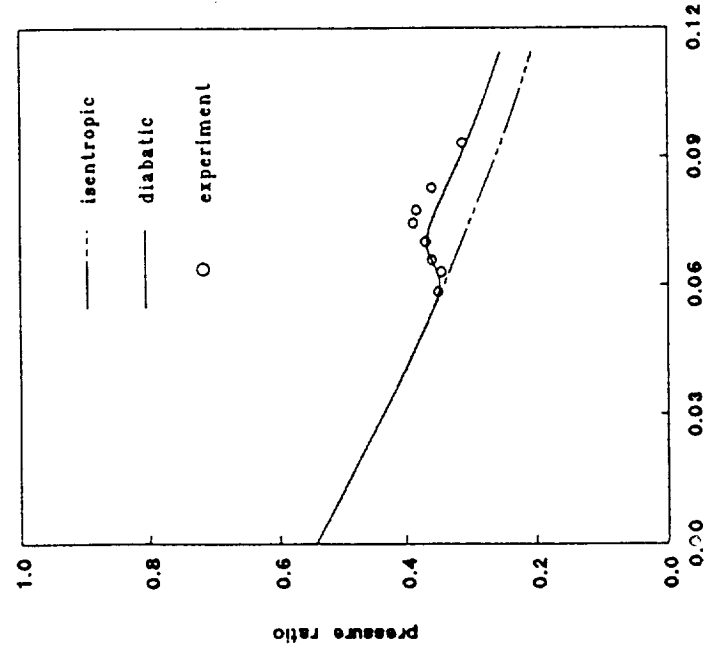


Figure 6.4 Pressure Ratio Of Barschdorff
No. 7 for Classical Theory

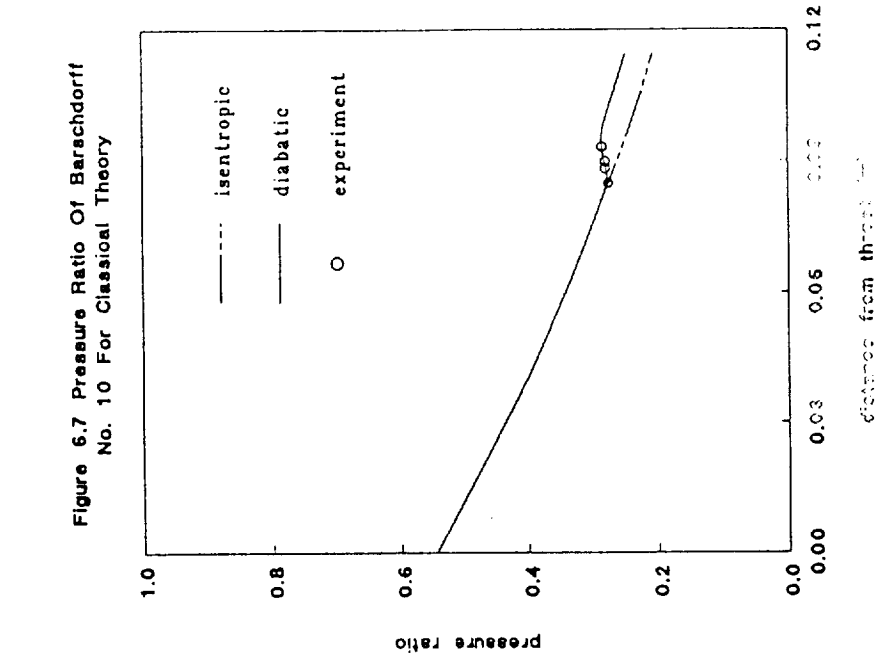


Figure 6.7 Pressure Ratio Of Barschdorff No. 10 For Classical Theory

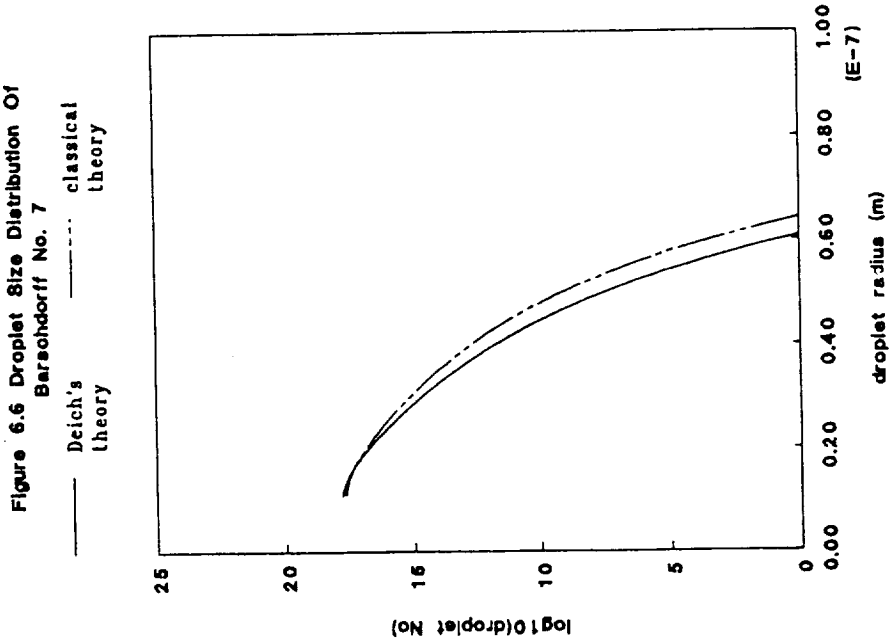


Figure 6.6 Droplet Size Distribution Of Barschdorff No. 7

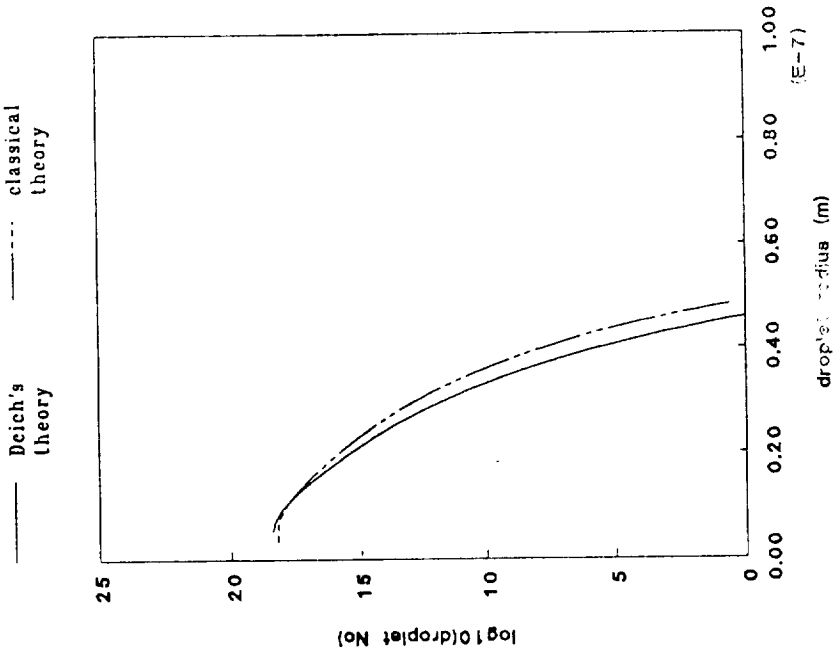


Figure 6.9 Droplet Size Distribution Of Barschdorff No. 10

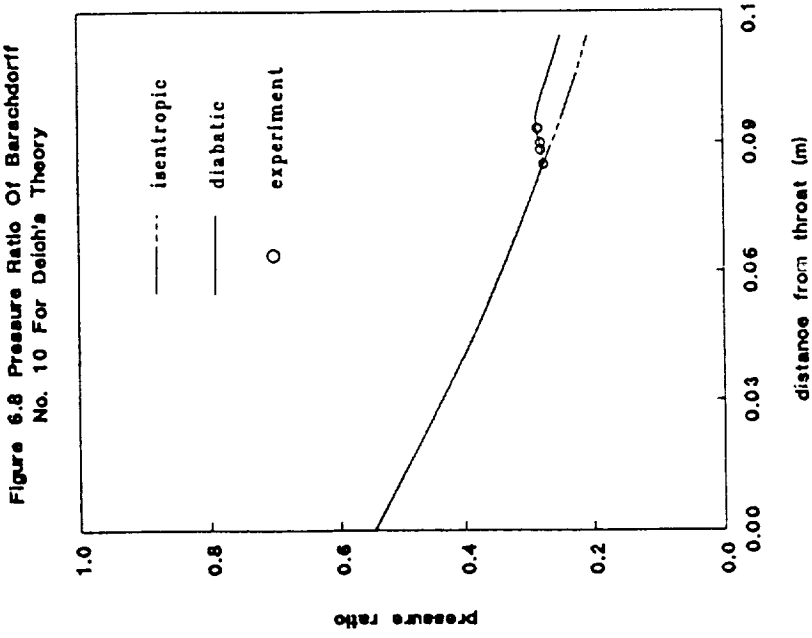


Figure 6.8 Pressure Ratio Of Barschdorff No. 10 For Deich's Theory

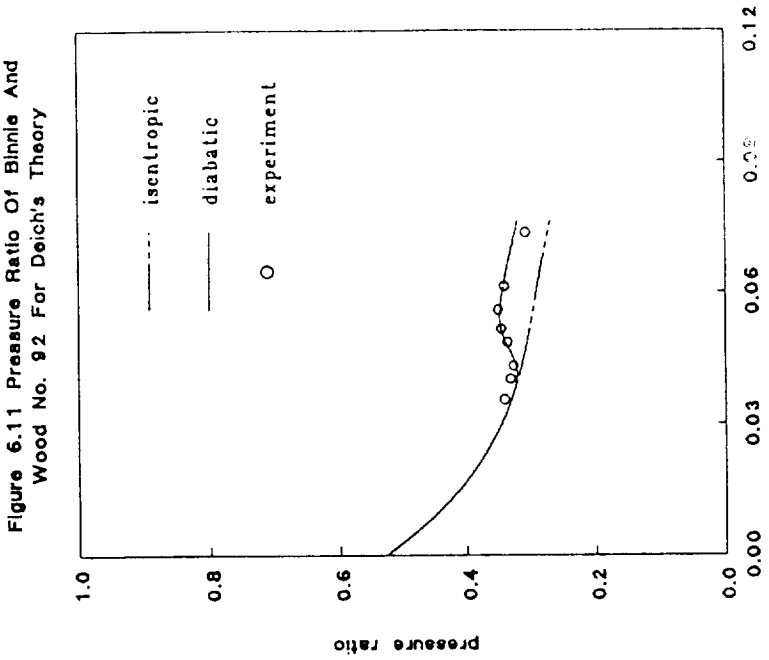


Figure 6.11 Pressure Ratio Of Binnie And Wood No. 92 For Deich's Theory

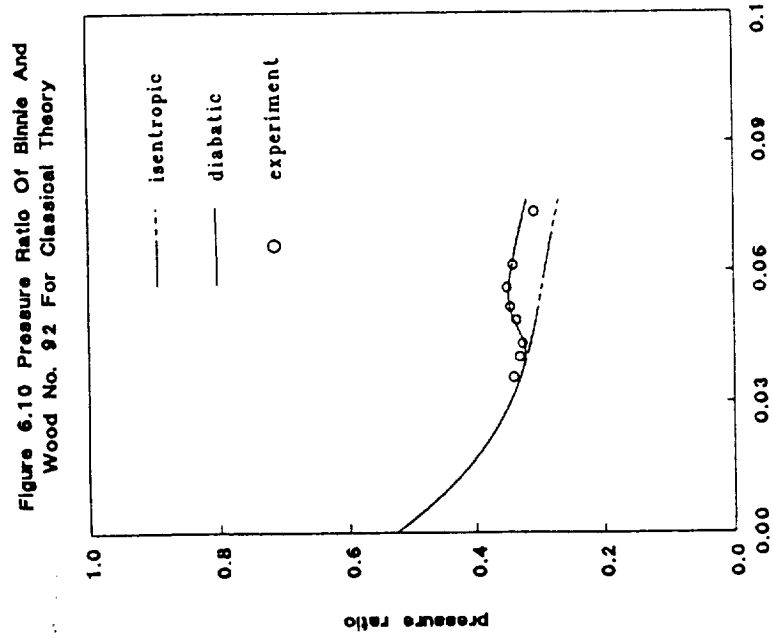


Figure 6.10 Pressure Ratio Of Binnie And Wood No. 92 For Classical Theory

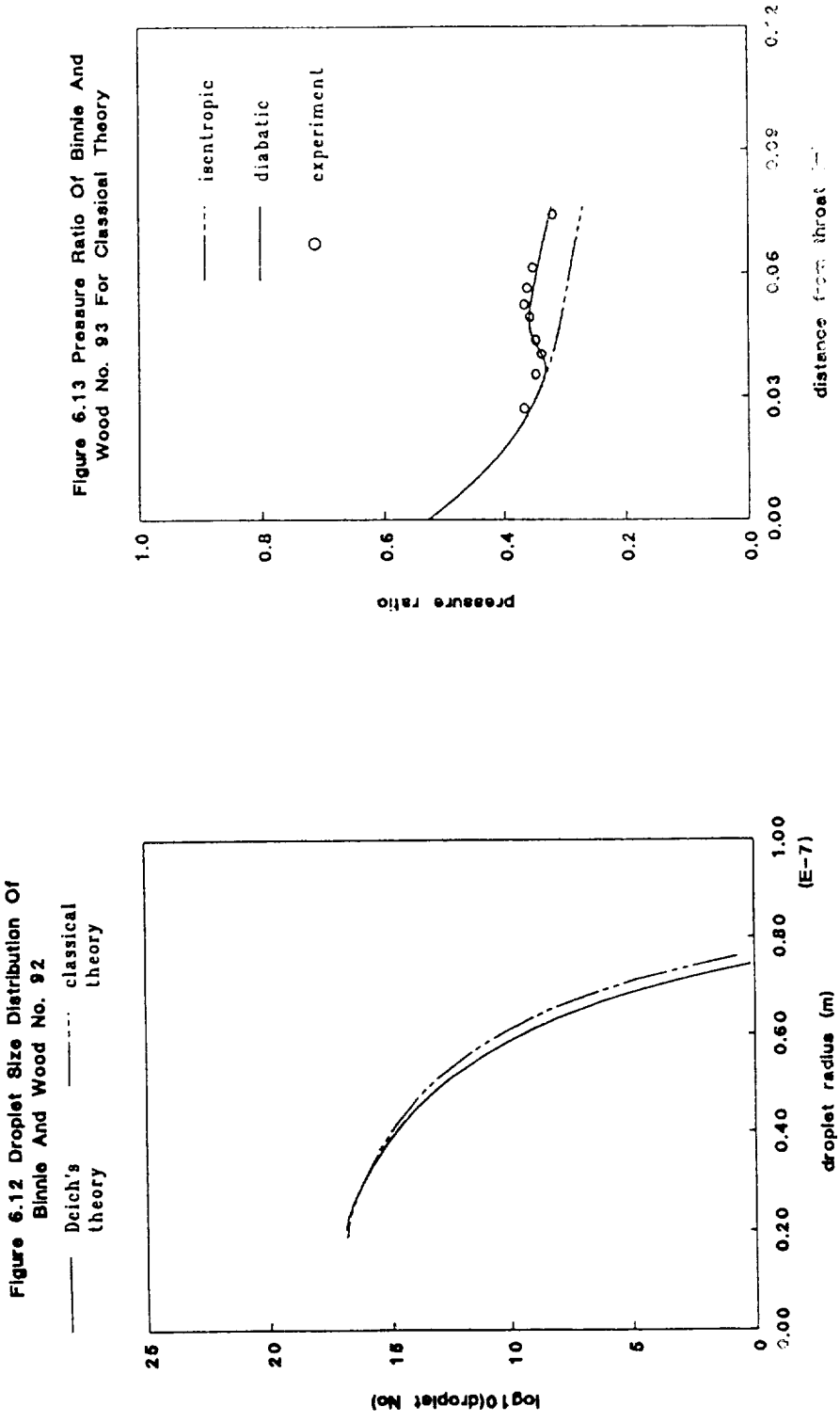
Figure 6.12 Droplet Size Distribution Of Binnie And Wood No. 92
Deich's theory
classical theory
log10(droplet No)
droplet radius (m)
(E-7)
0
5
10
15
20
25
0.00
0.20
0.40
0.60
0.80
1.00


Figure 6.13 Pressure Ratio Of Binnie And Wood No. 93 For Classical Theory
isentropic
diabatic
experiment
pressure ratio
distance from throat
0.0
0.2
0.4
0.6
0.8
1.0
0.00
0.03
0.06

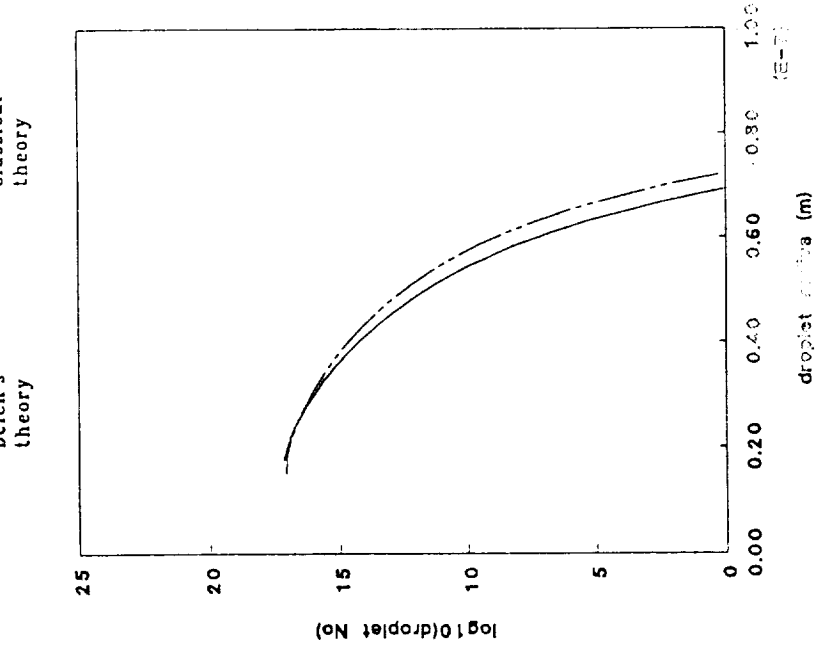


Figure 6.15 Droplet Size Distribution Of Binnie and Wood No. 93

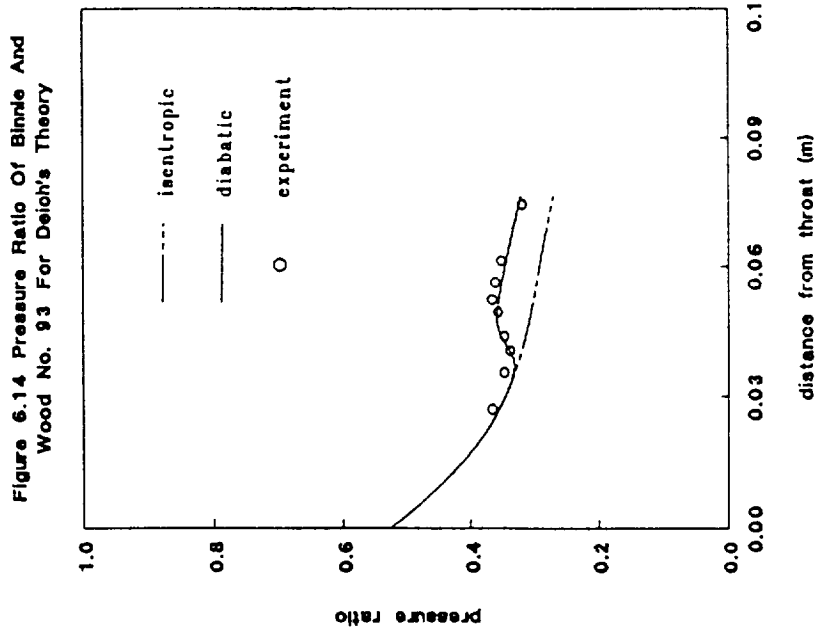


Figure 6.14 Pressure Ratio Of Binnie And Wood No. 93 For Deich's Theory

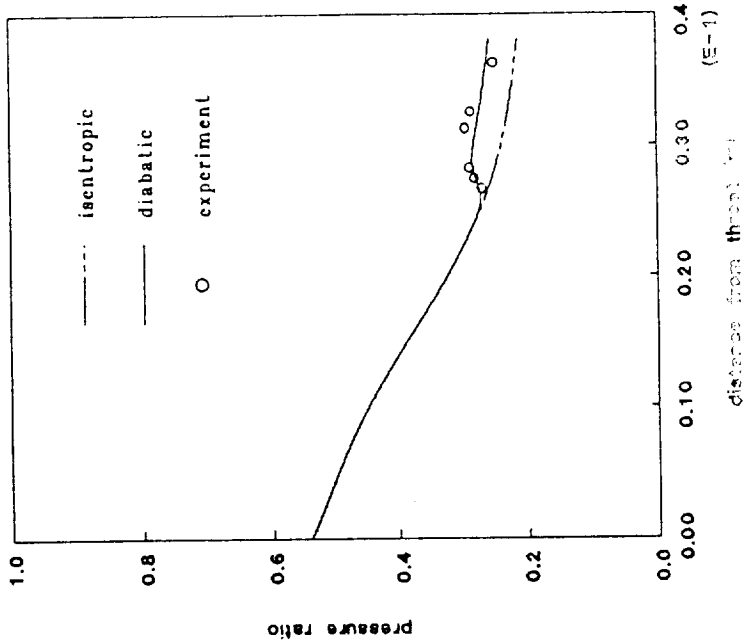


Figure 6.17 Pressure Ratio Of Deich For Deich's Theory

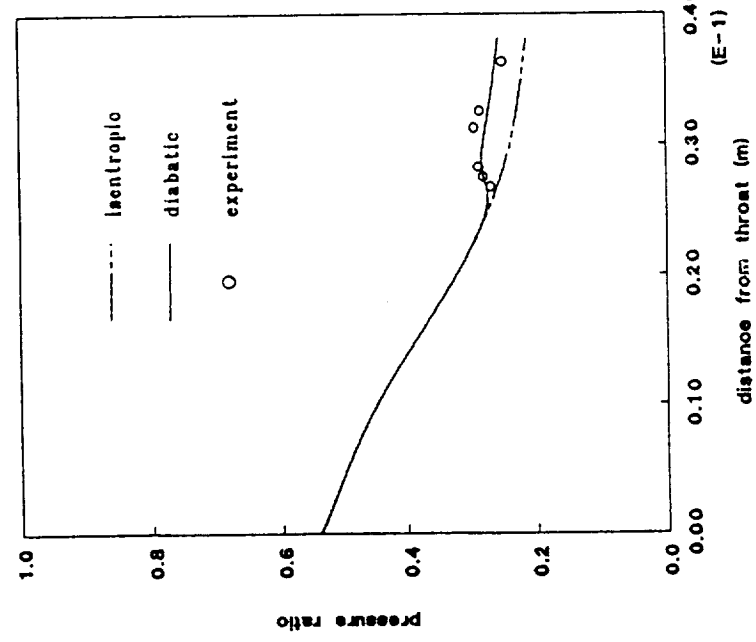


Figure 6.16 Pressure Ratio Of Deich For Classical Theory

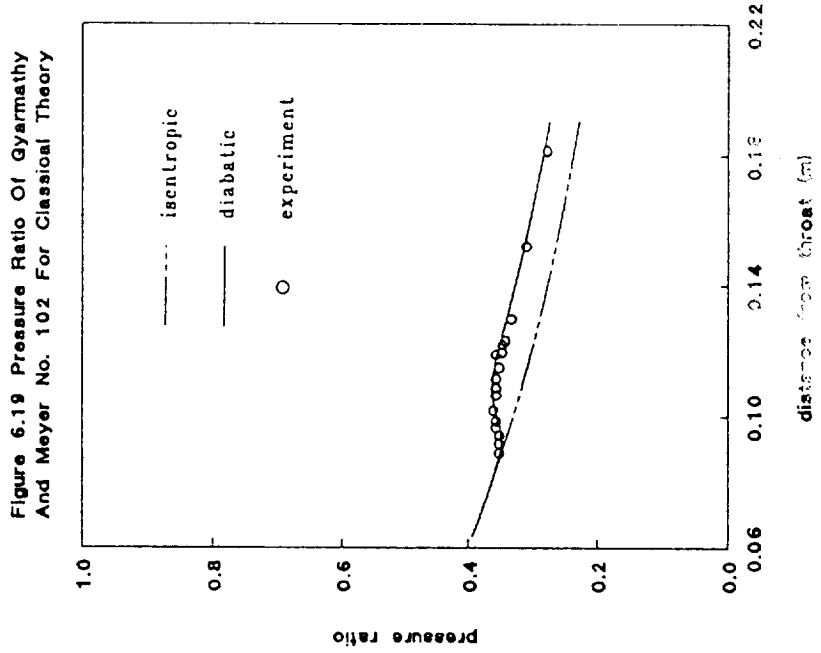


Figure 6.19 Pressure Ratio Of Gyarmathy And Meyer No. 102 For Classical Theory

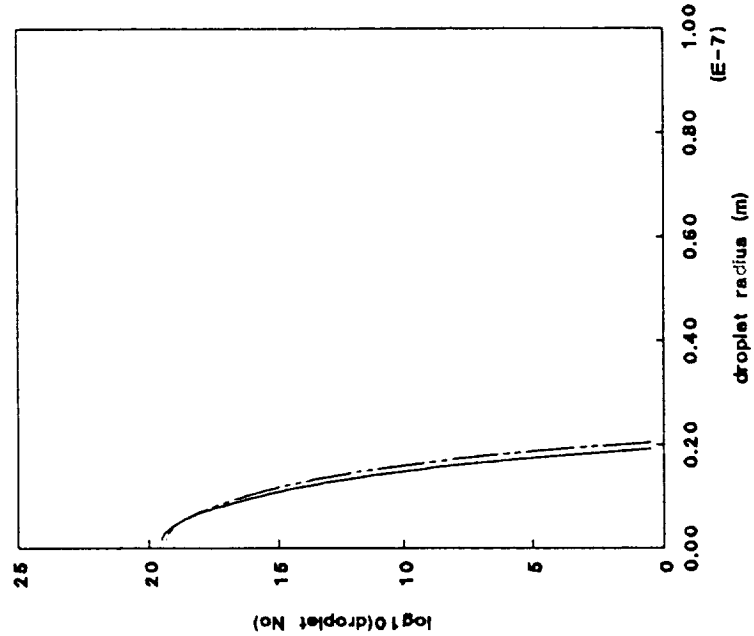


Figure 6.18 Droplet Size Distribution Of Deich

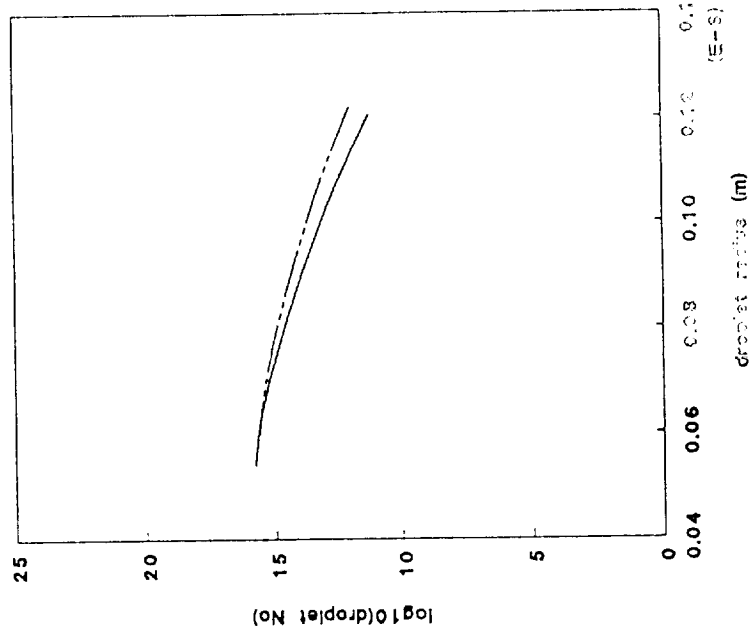


Figure 6.21 Droplet Size Distribution Of Gyarmathy And Meyer No. 112

—— Deich's theory  ——·—· classical theory

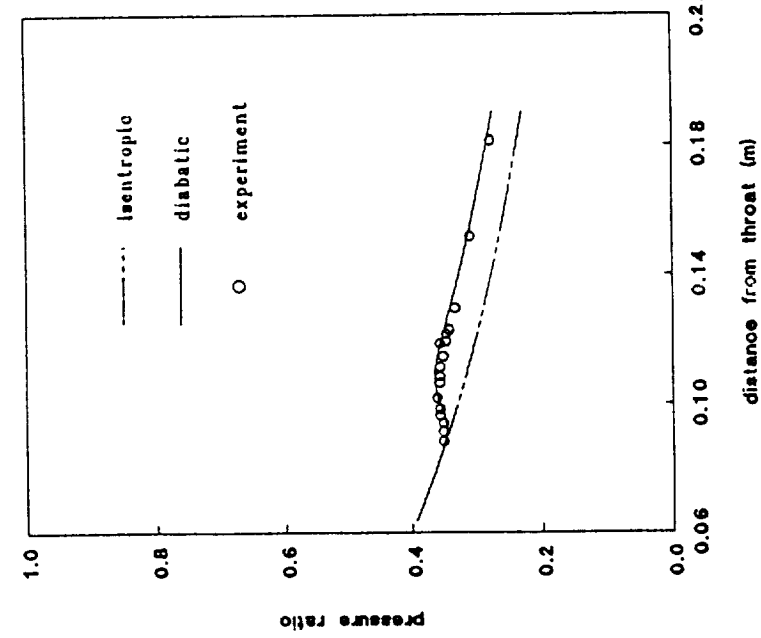


Figure 6.20 Pressure Ratio Of Gyarmathy And Meyer No. 102 For Deich's Theory

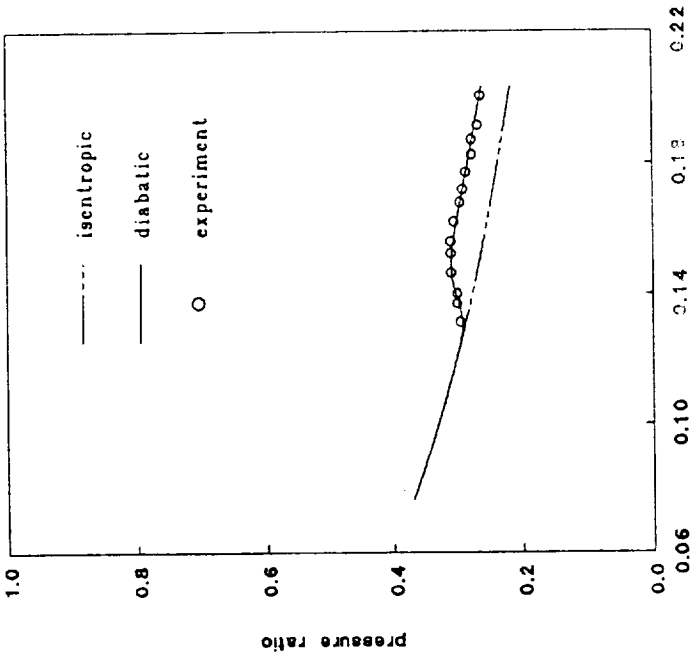


Figure 6.23 Pressure Ratio Of Gyarmathy And Meyer No. 108 For Deich's Theory

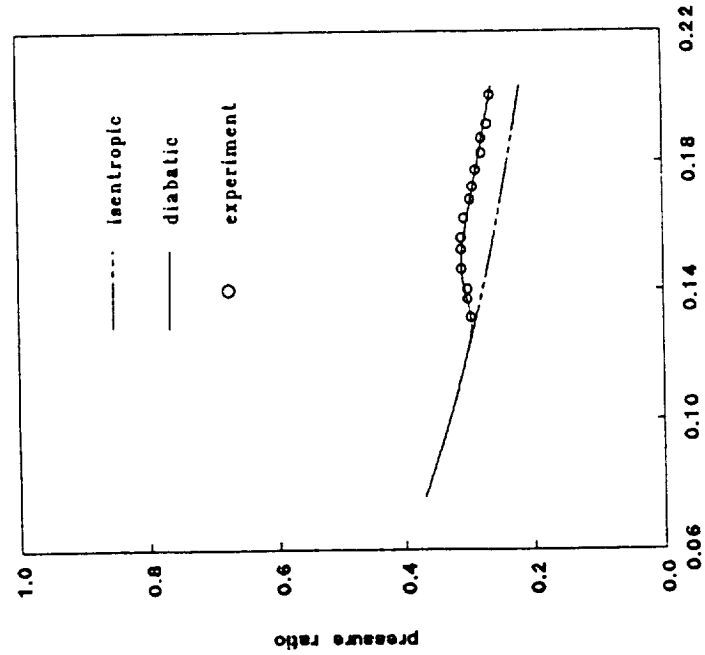


Figure 6.22 Pressure Ratio Of Gyarmathy And Meyer No. 108 For Classical Theory

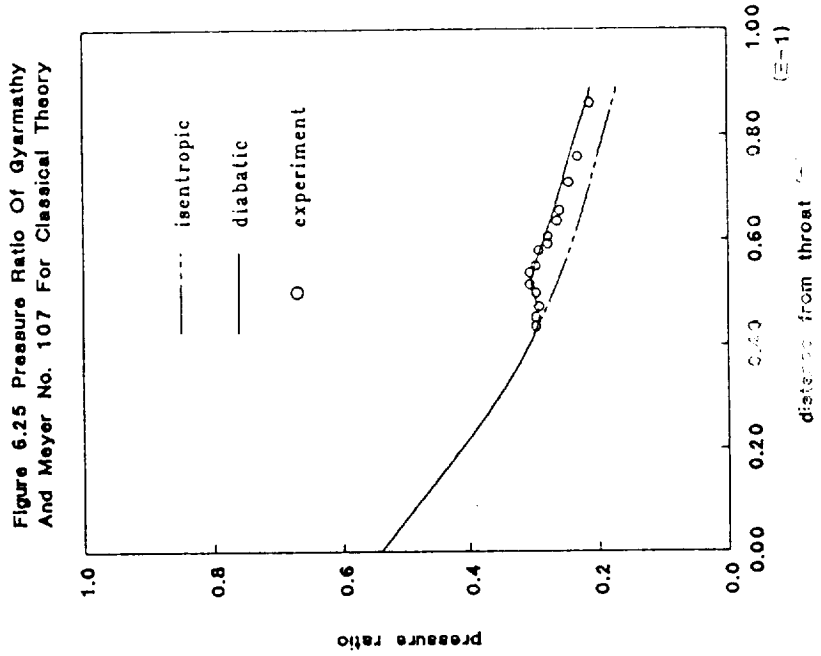


Figure 6.25 Preasure Ratio Of Gyarmathy And Meyer No. 107 For Classical Theory

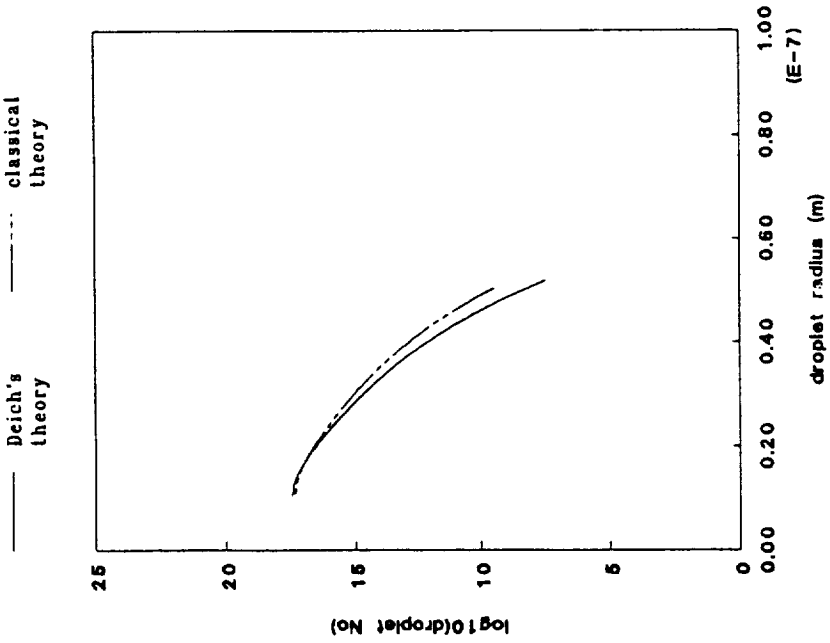


Figure 6.24 Droplet Size Distribution Of Gyarmathy And Meyer No. 108

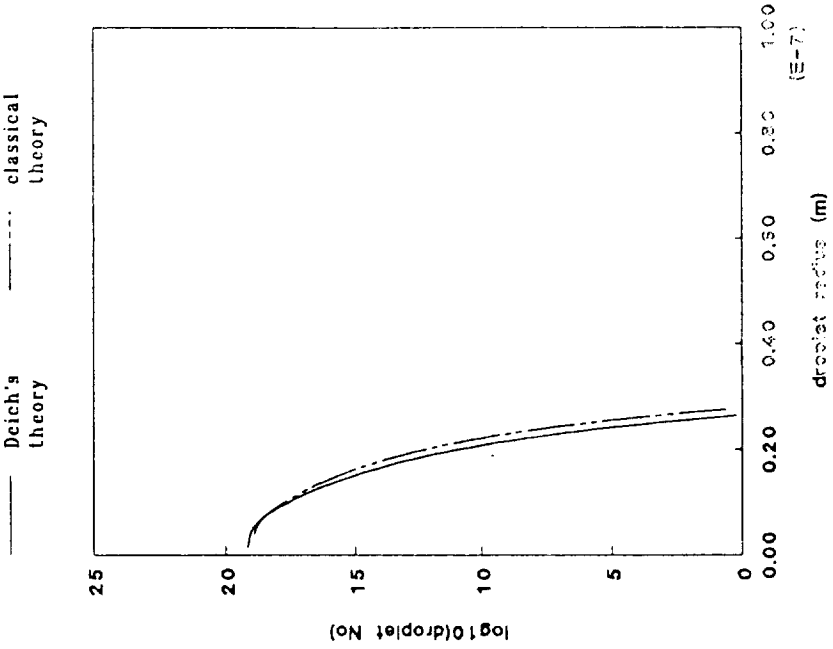


Figure 6.27 Droplet Size Distribution Of Gyarmathy And Meyer No. 107

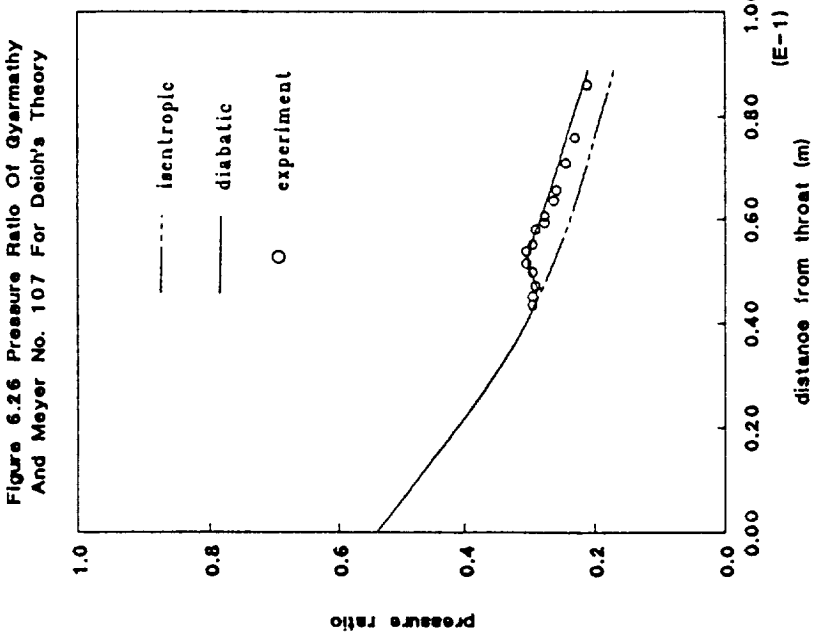


Figure 6.26 Pressure Ratio Of Gyarmathy And Meyer No. 107 For Deich's Theory

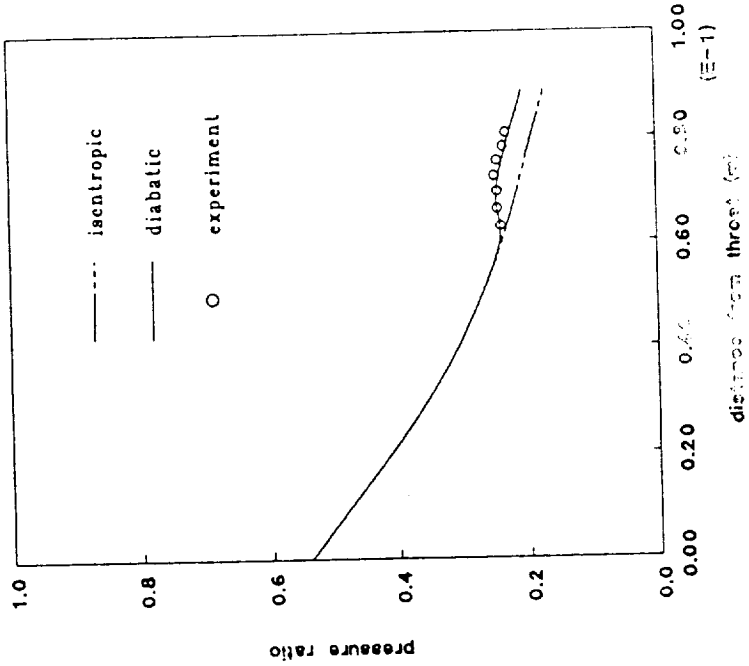


Figure 6.29 Pressure Ratio Of Gyarmathy And Meyer No. 112 For Deich's Theory

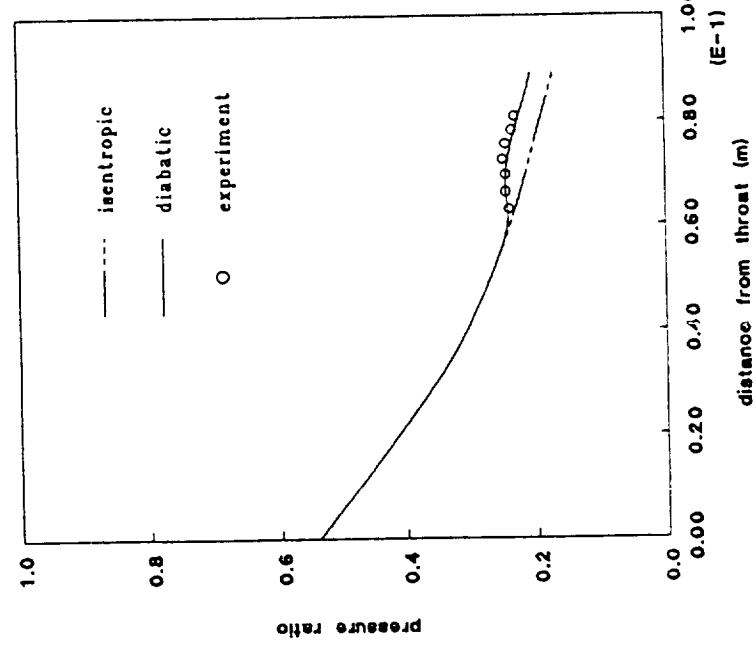


Figure 6.28 Pressure Ratio Of Gyarmathy And Meyer No. 112 For Classical Theory

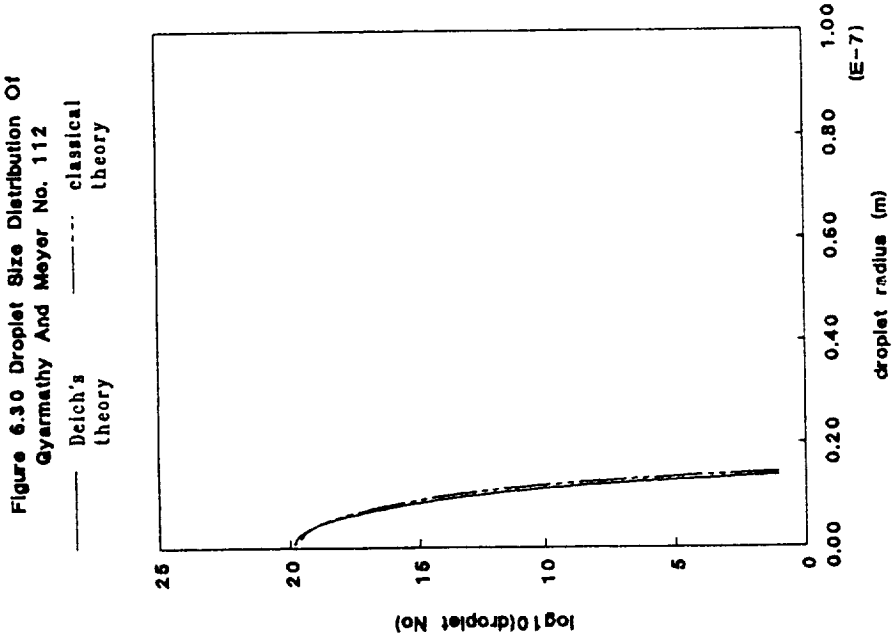


Figure 6.30 Droplet Size Distribution Of Gyarmathy And Meyer No. 112

—— Delch's theory ---- classical theory

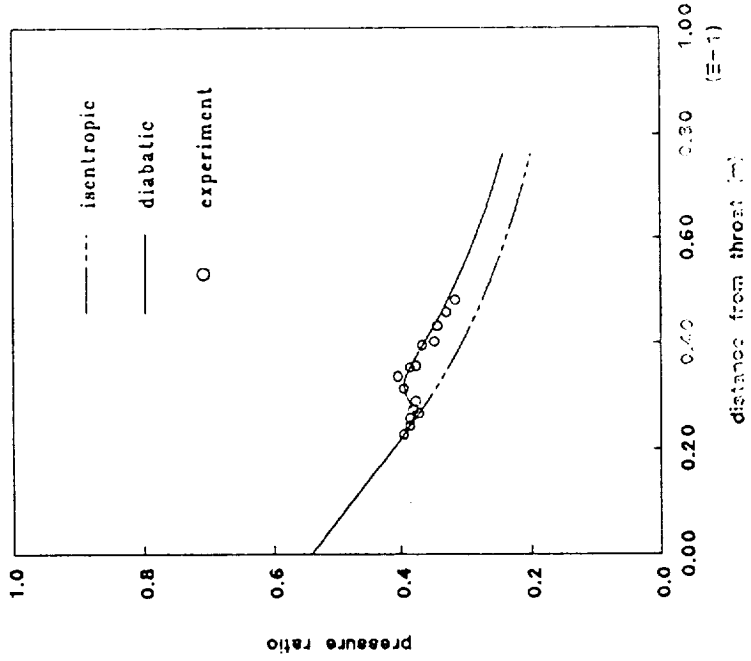


Figure 6.31 Pressure Ratio Of Gyarmathy And Meyer No. 119 For Classical Theory

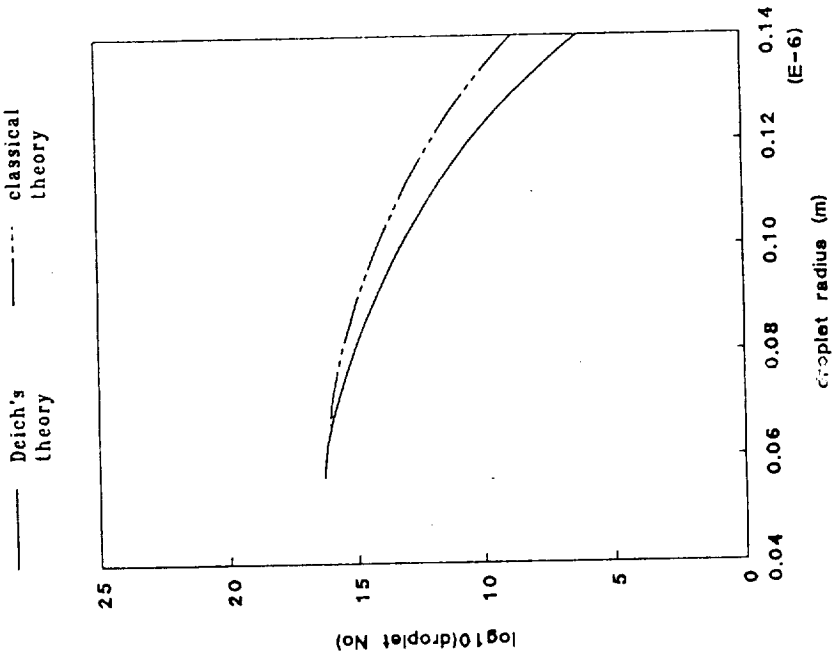


Figure 6.33 Droplet Size Distribution Of Gyarmathy And Meyer No. 119

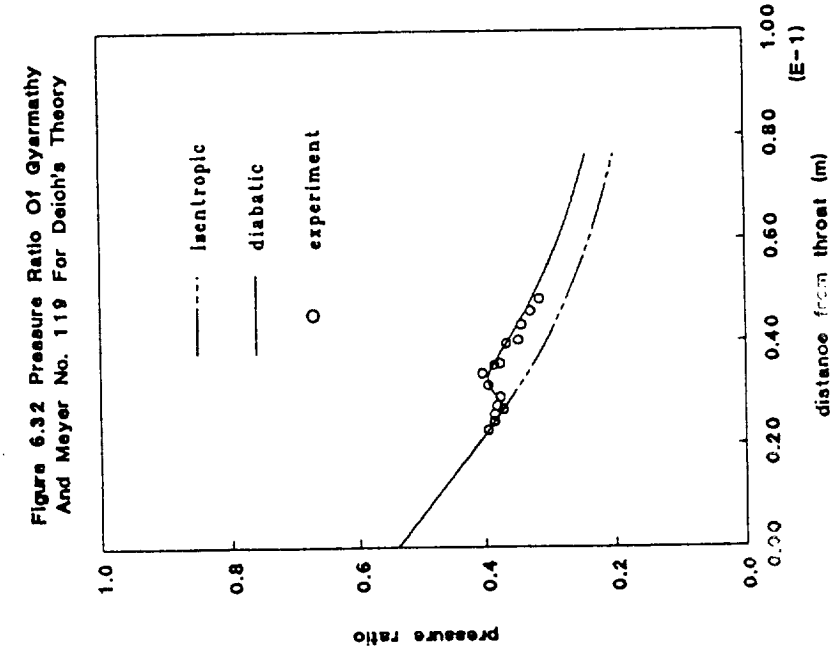


Figure 6.32 Pressure Ratio Of Gyarmathy And Meyer No. 119 For Deich's Theory

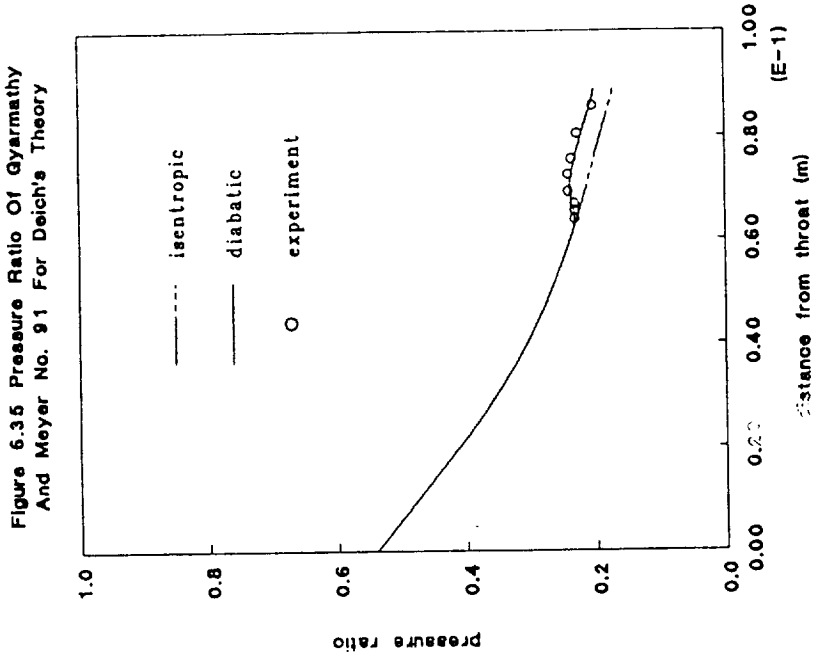


Figure 6.35 Pressure Ratio Of Gyarmathy And Meyer No. 91 For Deich's Theory

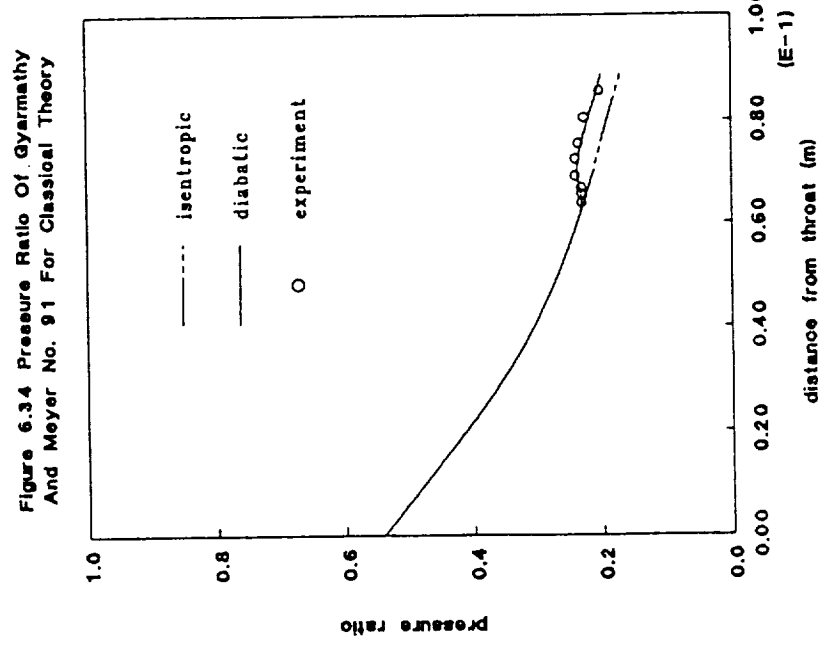


Figure 6.34 Pressure Ratio Of Gyarmathy And Meyer No. 91 For Classical Theory

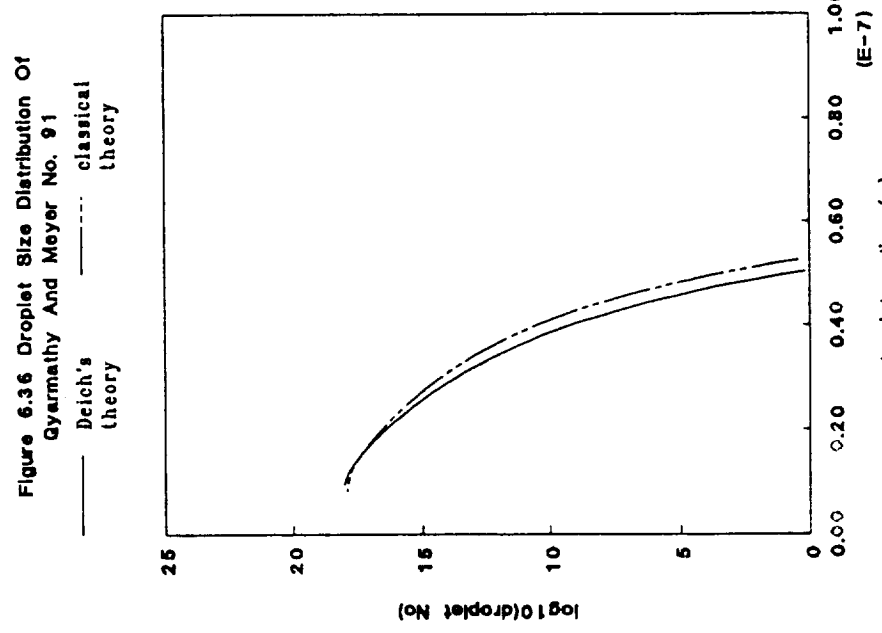
Figure 6.36 Droplet Size Distribution Of Qyarmathy And Meyer No. 91
Deich's theory
classical theory
log10(droplet No)
droplet radius (m)
(E-7)
25
20
15
10
5
0
0.00
0.20
0.40
0.60
0.80
1.00

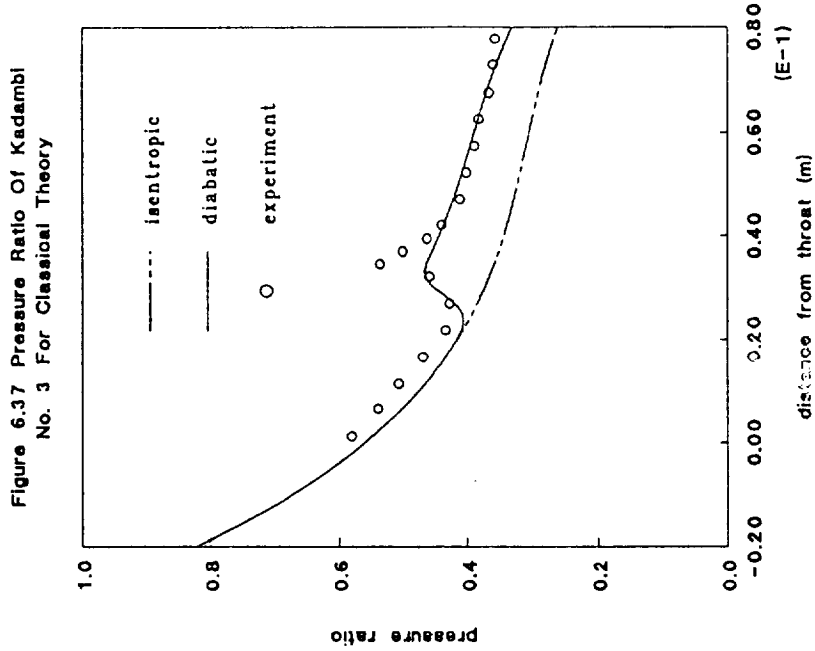
Figure 6.37 Pressure Ratio Of Kadambi No. 3 For Classical Theory
isentropic
diabatic
experiment
pressure ratio
distance from throat (m)
(E-1)
1.0
0.8
0.6
0.4
0.2
0.0
-0.20
0.00
0.20
0.40
0.60
0.80

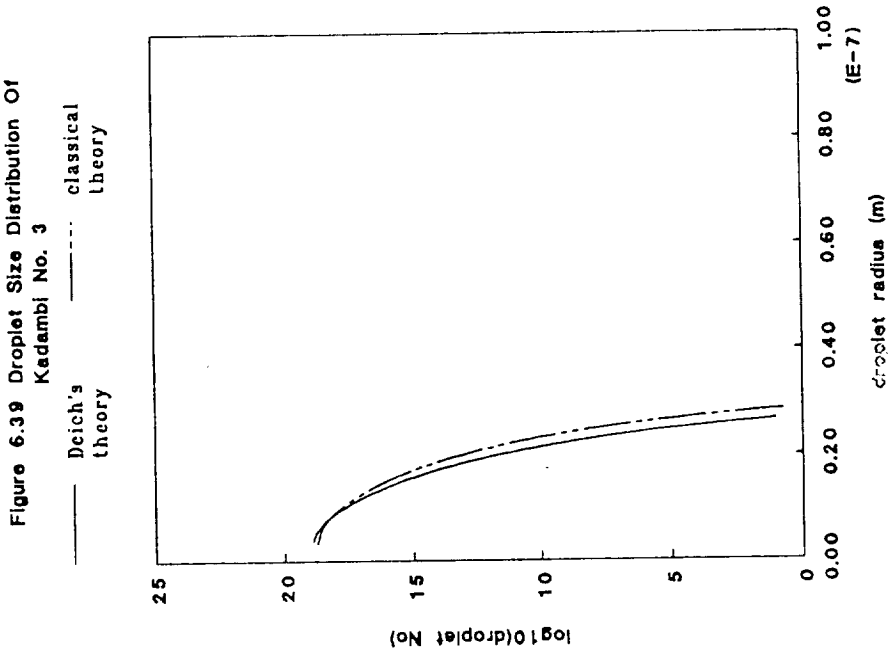


Figure 6.39 Droplet Size Distribution Of Kadambi No. 3

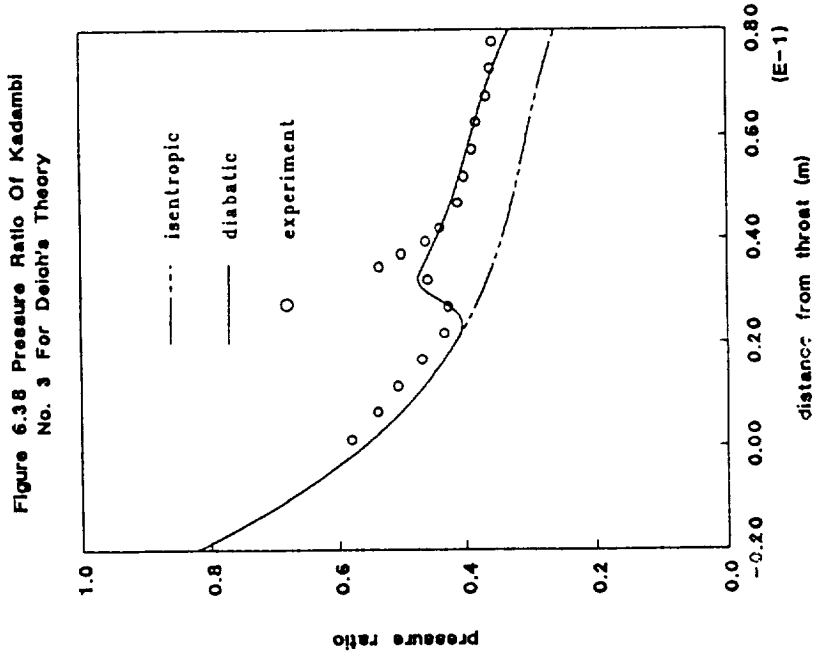


Figure 6.38 Pressure Ratio Of Kadambi No. 3 For Deich's Theory

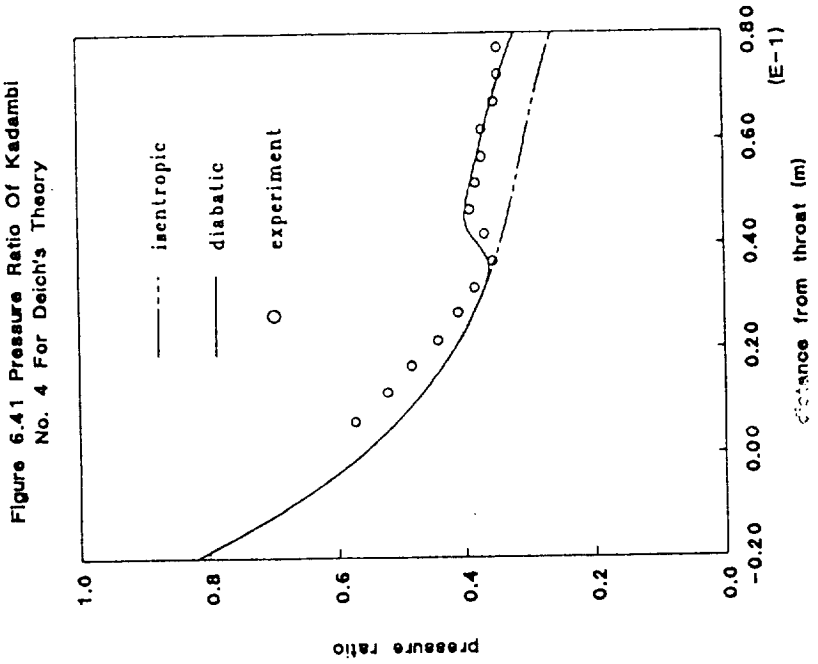


Figure 6.41 Pressure Ratio Of Kadambi
No. 4 For Deich's Theory

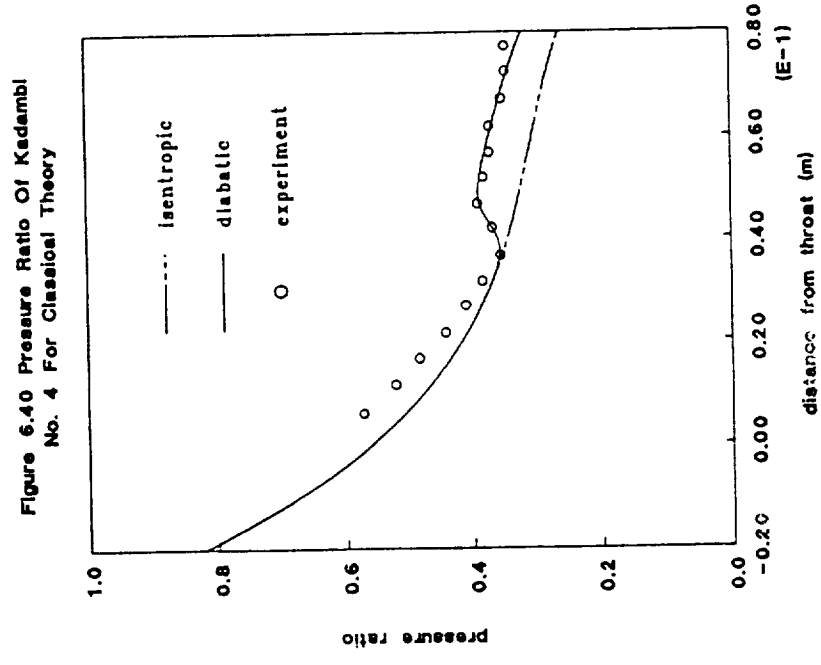


Figure 6.40 Pressure Ratio Of Kadambi
No. 4 For Classical Theory

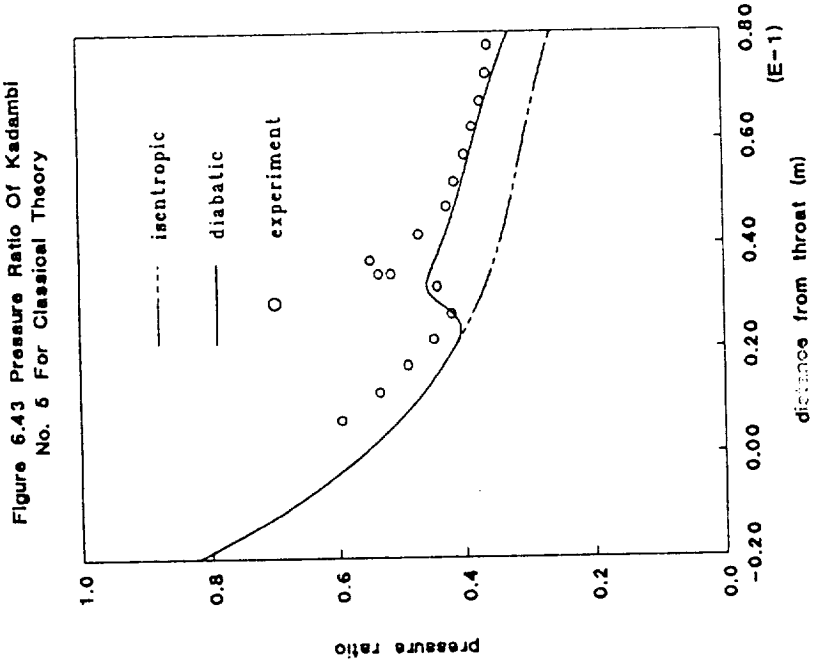


Figure 6.43 Pressure Ratio Of Kadambi No. 6 For Classical Theory

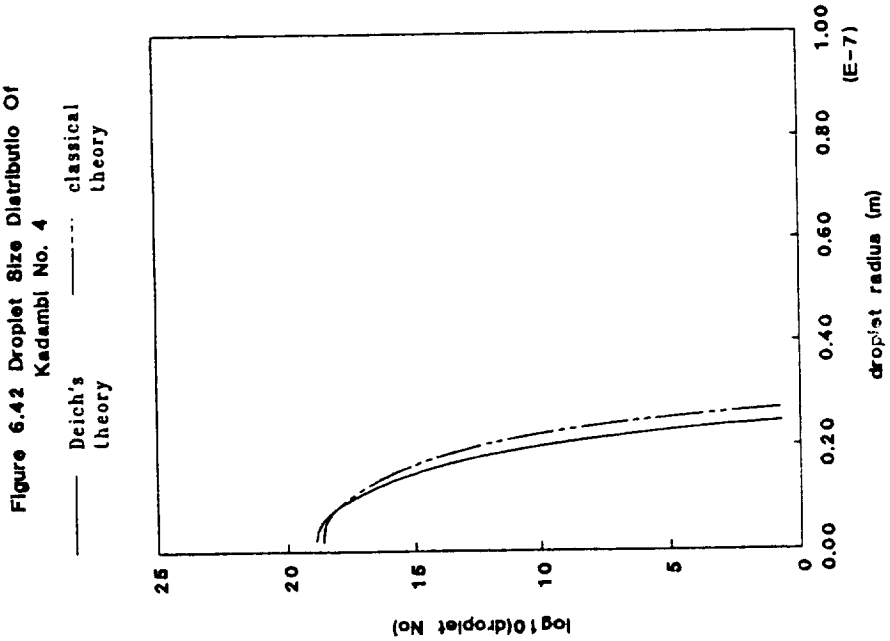


Figure 6.42 Droplet Size Distributio Of Kadambi No. 4

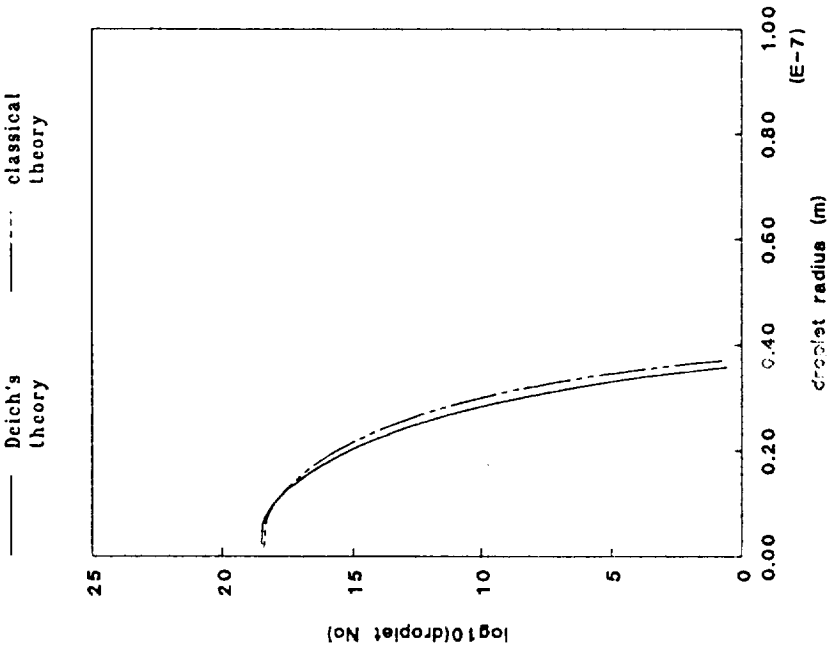


Figure 6.45 Droplet Size Distribution Of Kadambi No. 5

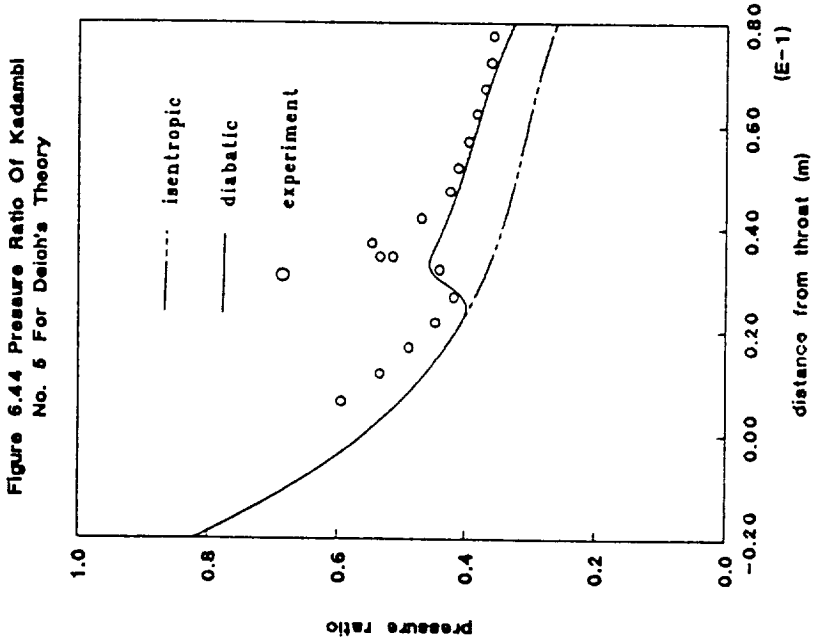


Figure 6.44 Pressure Ratio Of Kadambi No. 5 For Deich's Theory

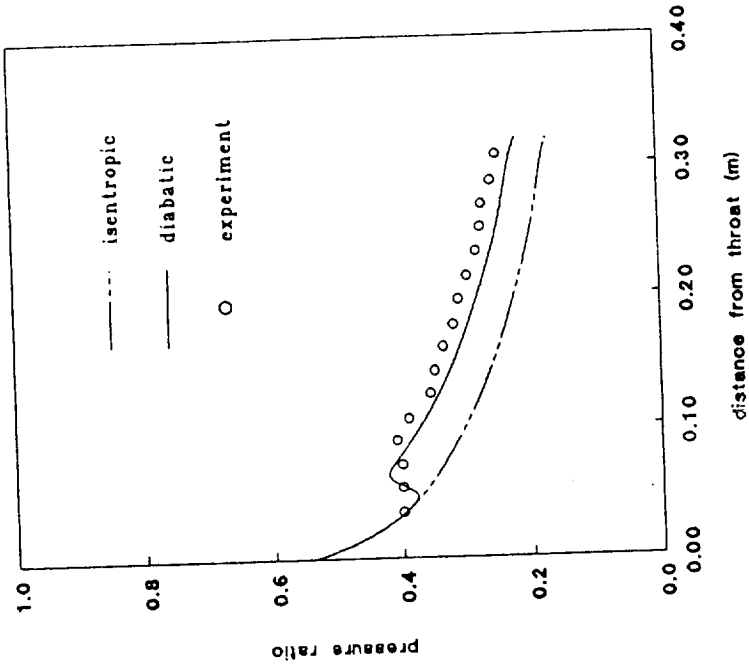


Figure 6.47 Pressure Ratio Of Moore No. A For Deich's Theory

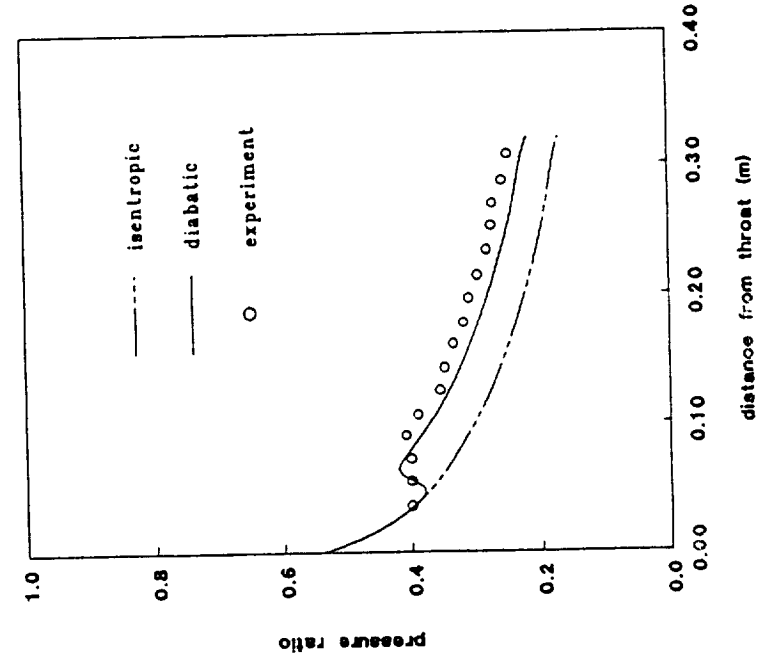


Figure 6.46 Pressure Ratio Of Moore No. A For Classical Theory

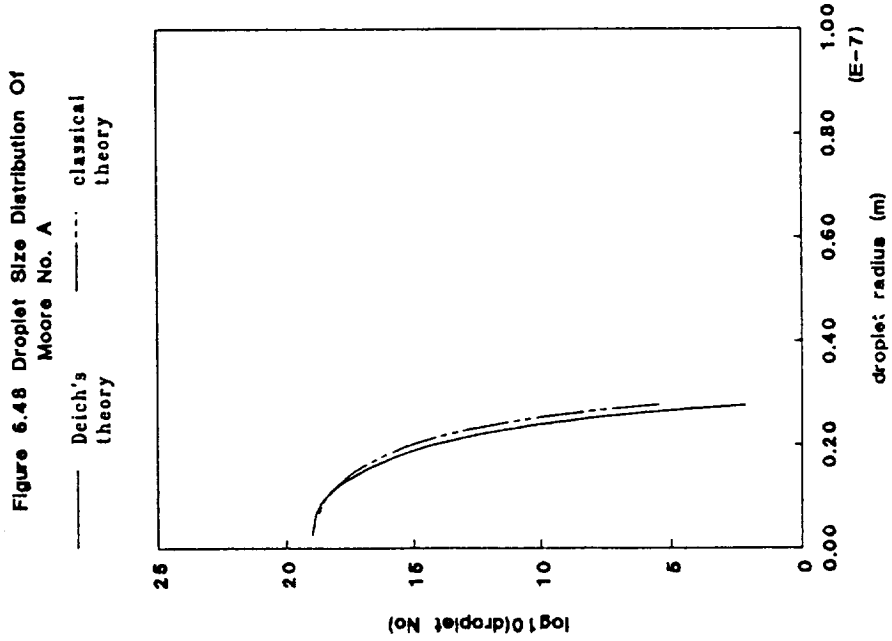
Figure 6.48 Droplet Size Distribution Of Moore No. A
Deich's theory
classical theory
log10(droplet No)
25
20
15
10
5
0
0.00
0.20
0.40
0.60
0.80
1.00
(E-7)
droplet radius (m)

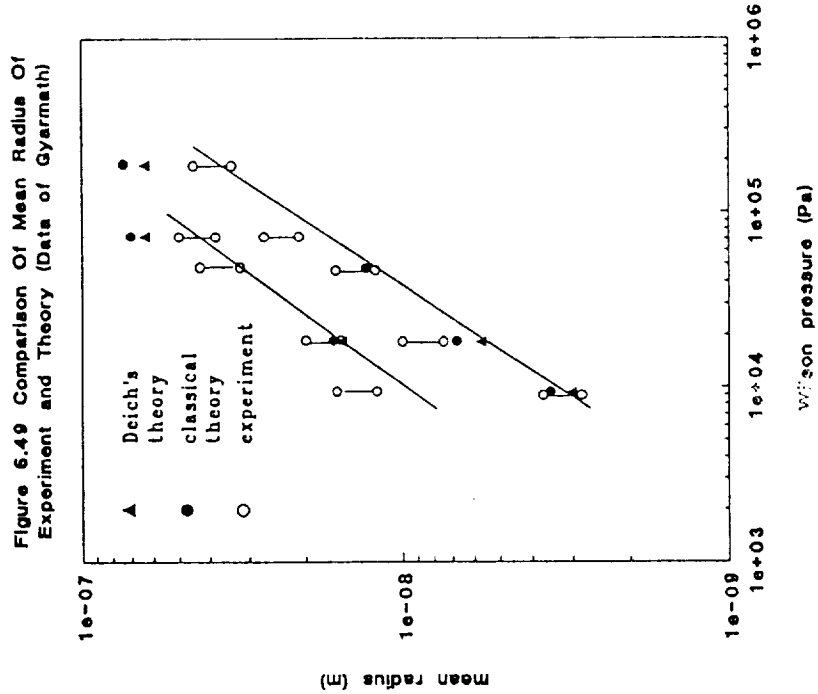
Figure 6.49 Comparison Of Mean Radius Of Experiment and Theory (Data of Gyarmath)
Deich's theory
classical theory
experiment
mean radius (m)
1e-07
1e-08
1e-09
1e+03
1e+04
1e+05
1e+06
Wilson pressure (Pa)

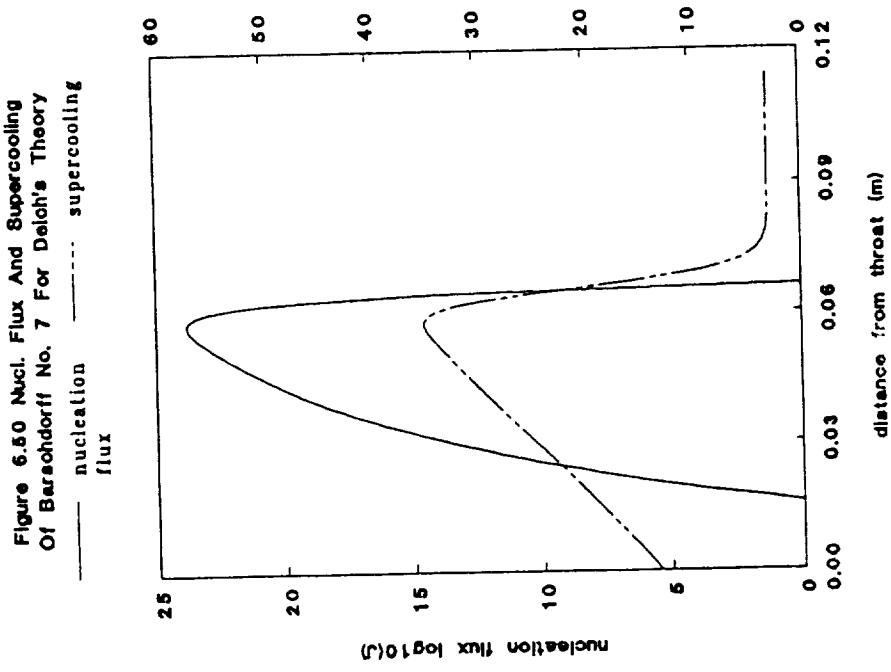


Figure 6.50 Nucl. Flux And Supercooling Of Barschdorff No. 7 For Delch's Theory

—— nucleation flux ——— supercooling

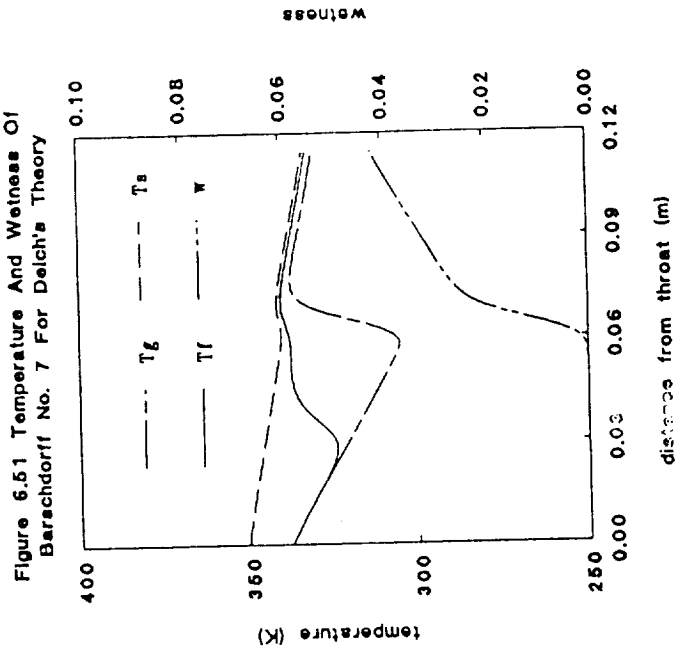


Figure 6.51 Temperature And Wetness Of Barschdorff No. 7 For Delch's Theory

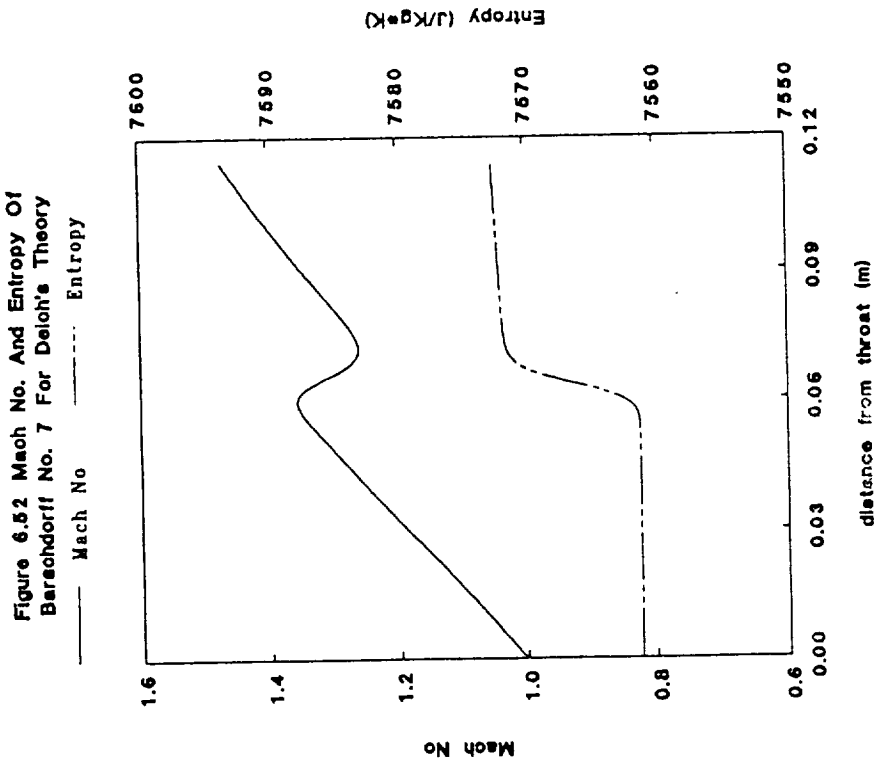


Figure 6.52 Mach No. And Entropy Of Barschdorff No. 7 For Deich's Theory

—— Mach No ——·—— Entropy

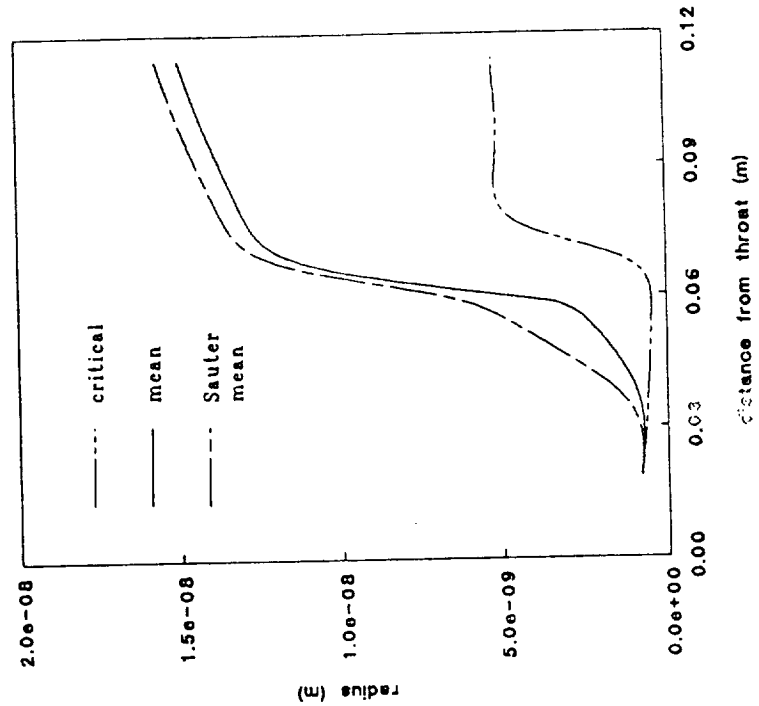


Figure 6.53 Critical And Mean Radius Of Barschdorff No. 7 For Deich's Theory

Figure 6.54 Velocity And Expansion Rate Of Barschdorff No. 7 For Deich's Theory

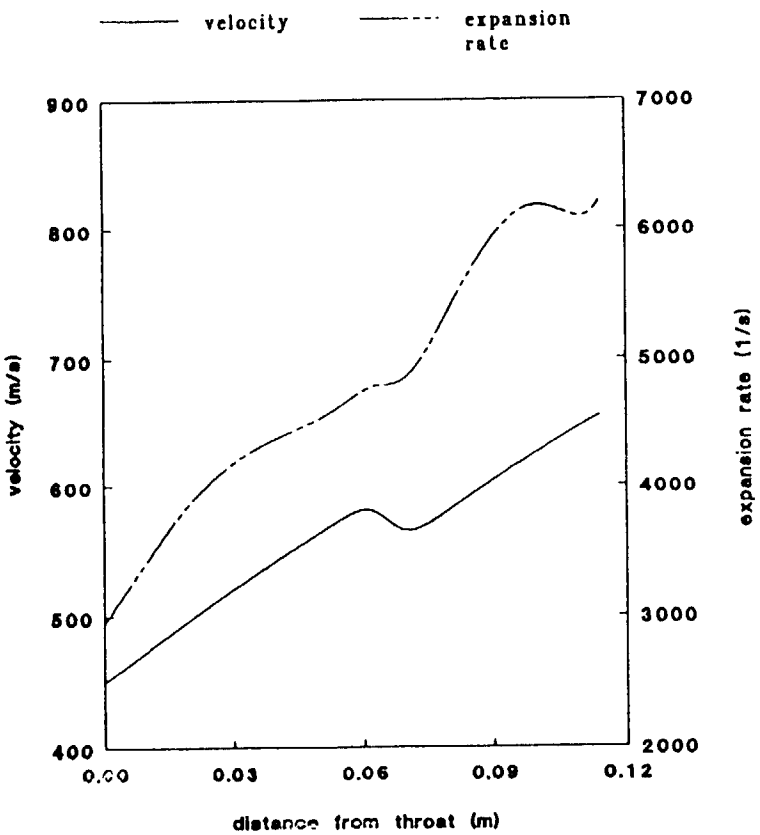


Figure 6.55 Knudsen No. And Prandtl No. Of Barsohdorff No. 7 For Deich's Theory

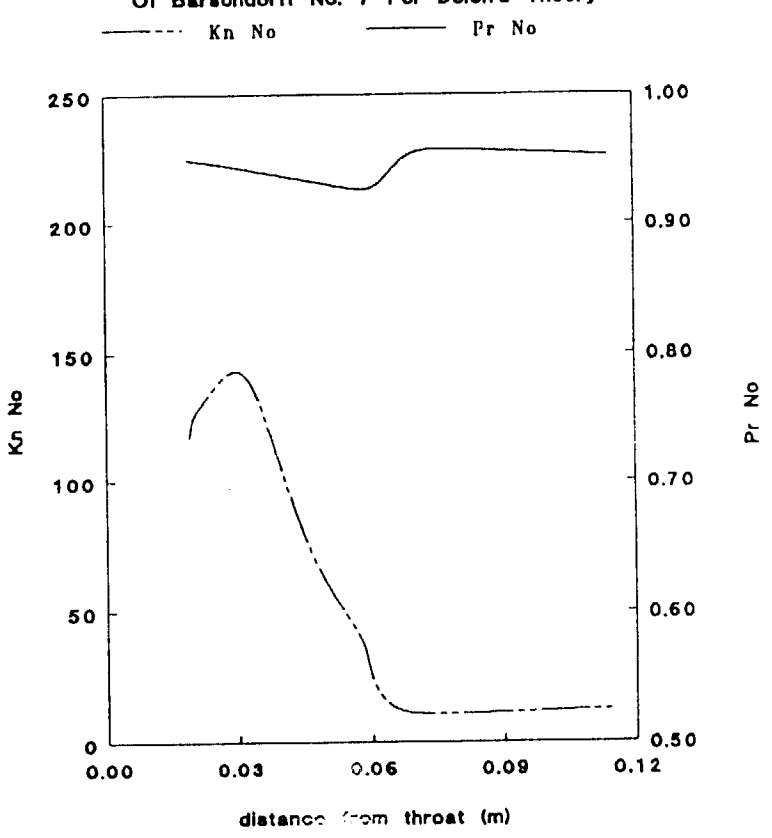

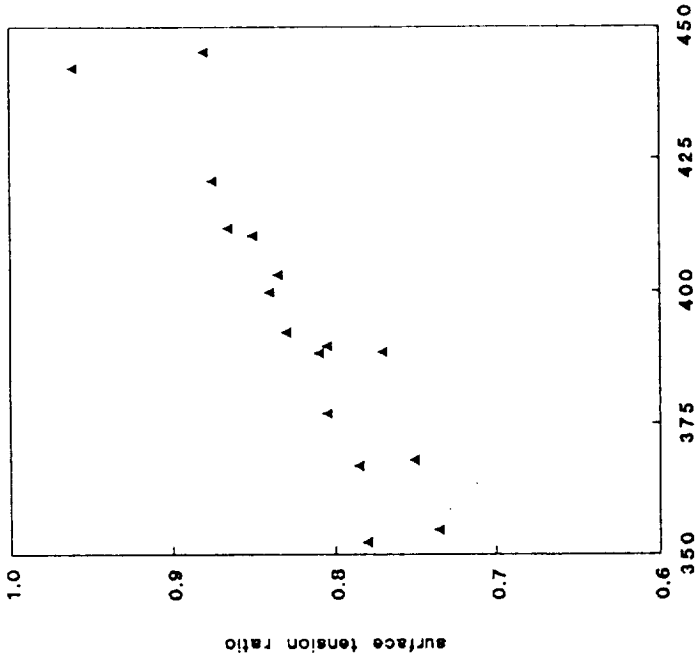


Figure 6.57 Surface Tension Ratio Versus Total Temperature For Deich's Theory

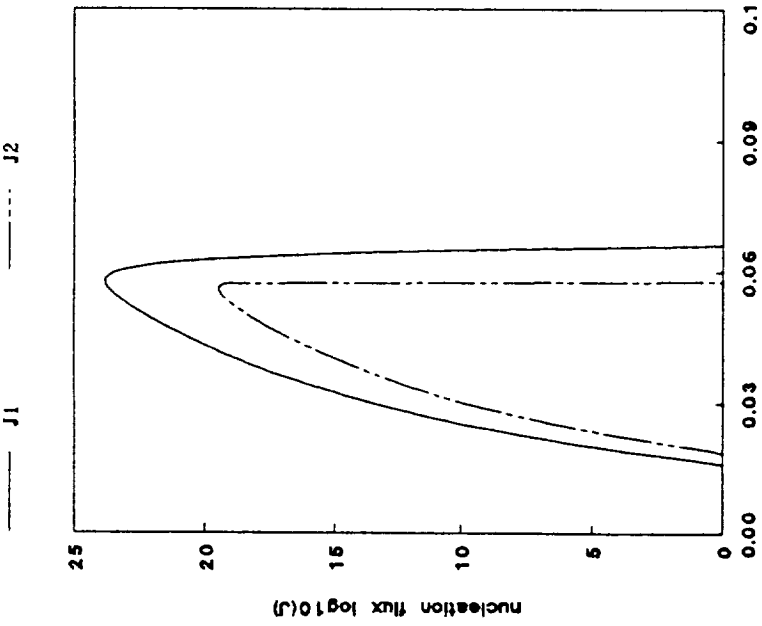


Figure 6.56 Two Components Of Nucl. Flux Of Barsohdorff No. 7 For Deich's Theory

—— J1 ——·—· J2

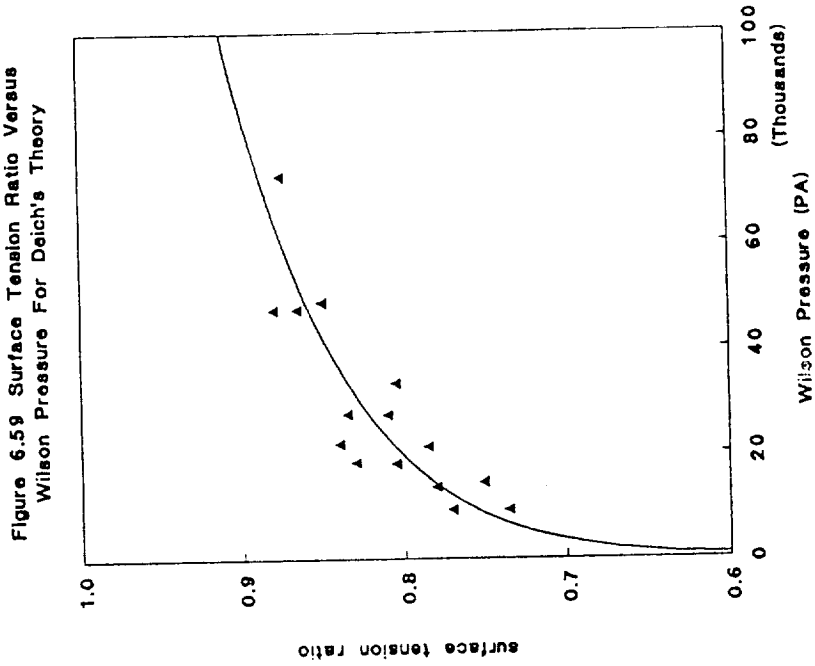
Figure 6.59 Surface Tension Ratio Versus
Wilson Pressure For Deich's Theory
surface tension ratio
1.0
0.9
0.8
0.7
0.6
0
20
40
60
80
100
Wilson Pressure (PA)
(Thousands)

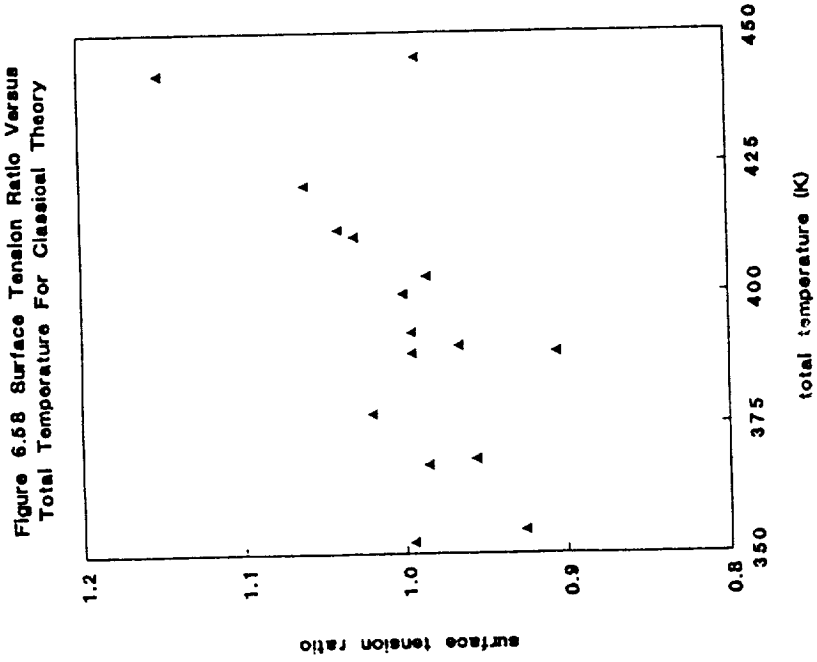
Figure 6.58 Surface Tension Ratio Versus
Total Temperature For Classical Theory
surface tension ratio
1.2
1.1
1.0
0.9
0.8
350
375
400
425
450
total temperature (K)

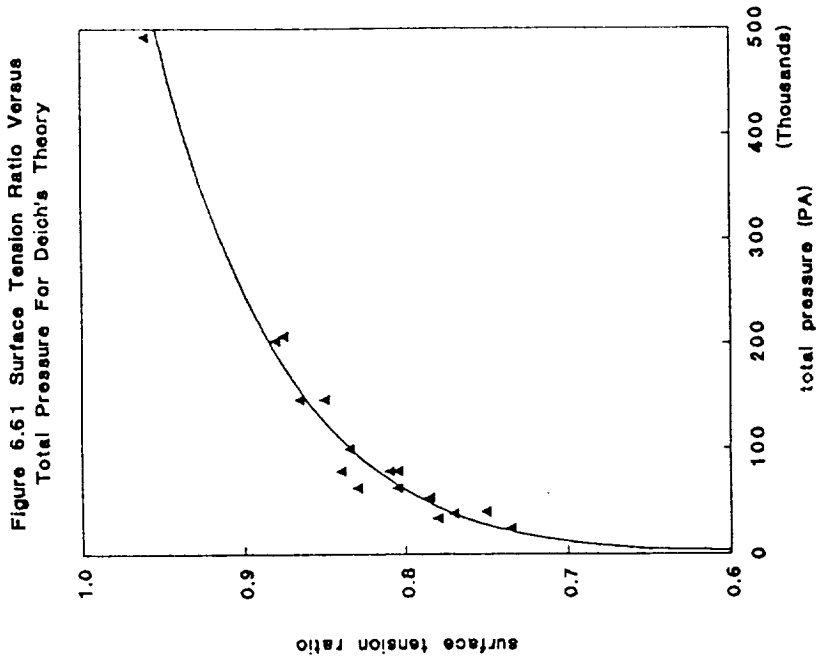


Figure 6.61 Surface Tension Ratio Versus
Total Pressure For Deich's Theory

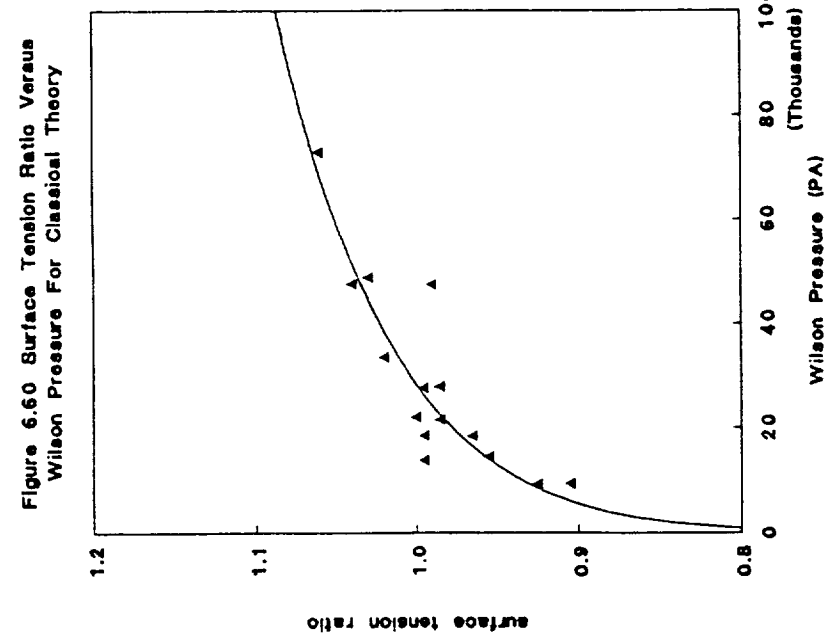


Figure 6.60 Surface Tension Ratio Versus
Wilson Pressure For Classical Theory

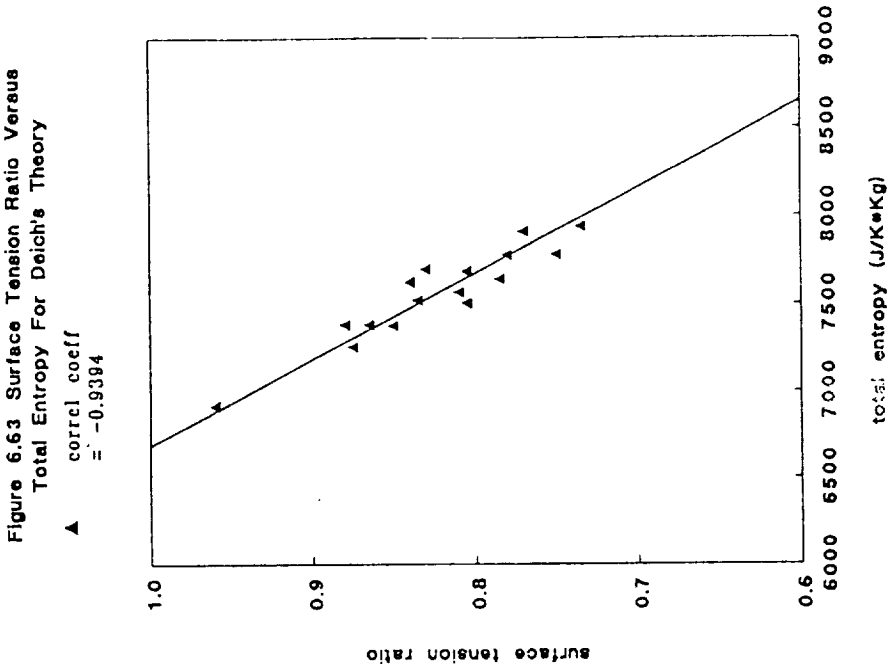
Figure 6.63 Surface Tension Ratio Versus
Total Entropy For Deichs Theory
correl coeff
= -0.9394
surface tension ratio
1.0
0.9
0.8
0.7
0.6
6000 6500 7000 7500 8000 8500 9000
total entropy (J/K*Kg)

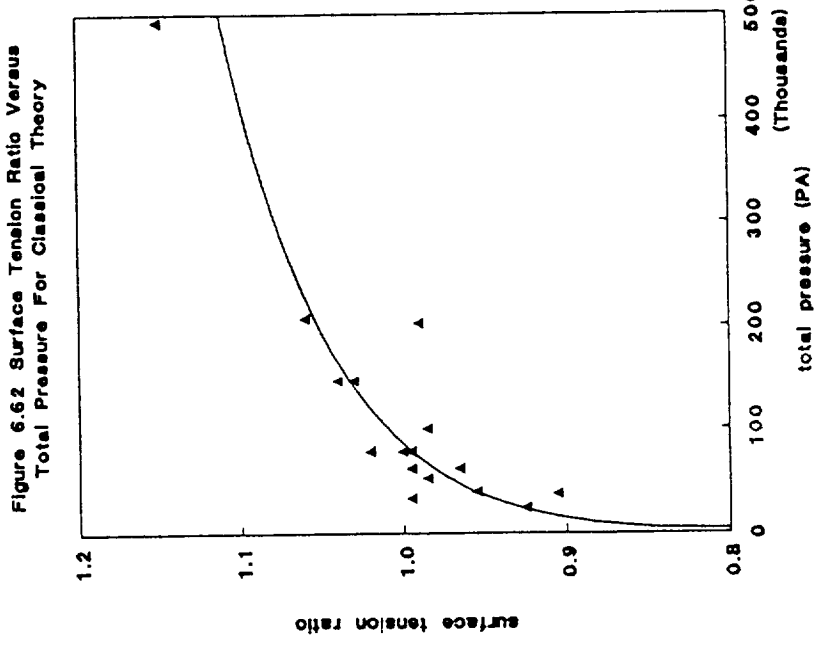
Figure 6.62 Surface Tension Ratio Versus
Total Pressure For Classical Theory
surface tension ratio
1.2
1.1
1.0
0.9
0.8
0 100 200 300 400 500
(Thousands)
total pressure (PA)

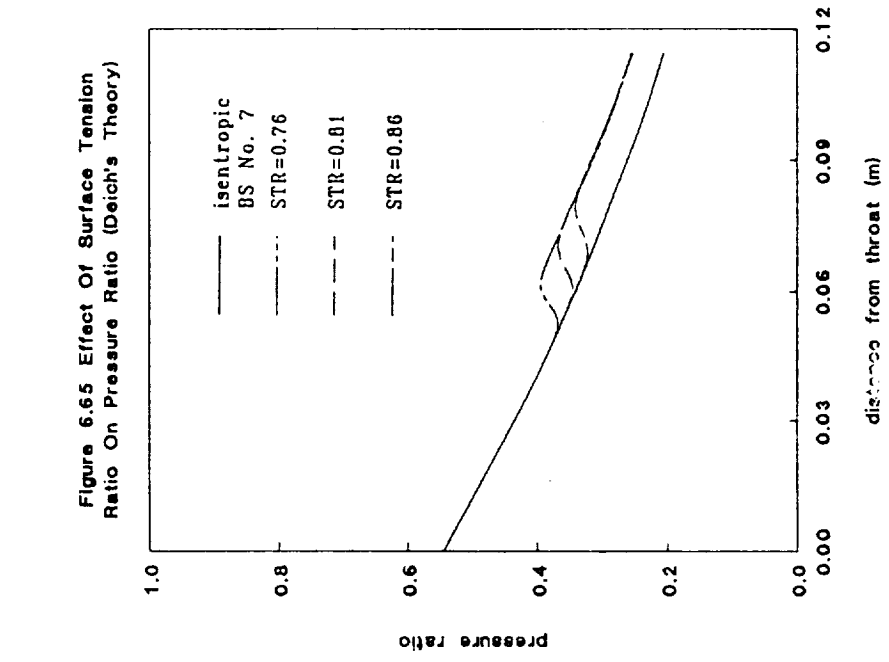
Figure 6.65 Effect Of Surface Tension
Ratio On Pressure Ratio (Deich's Theory)
isentropic
BS No. 7
STR=0.76
STR=0.81
STR=0.86
pressure ratio
1.0
0.8
0.6
0.4
0.2
0.0
0.00
0.03
0.06
0.09
0.12
distance from throat (m)

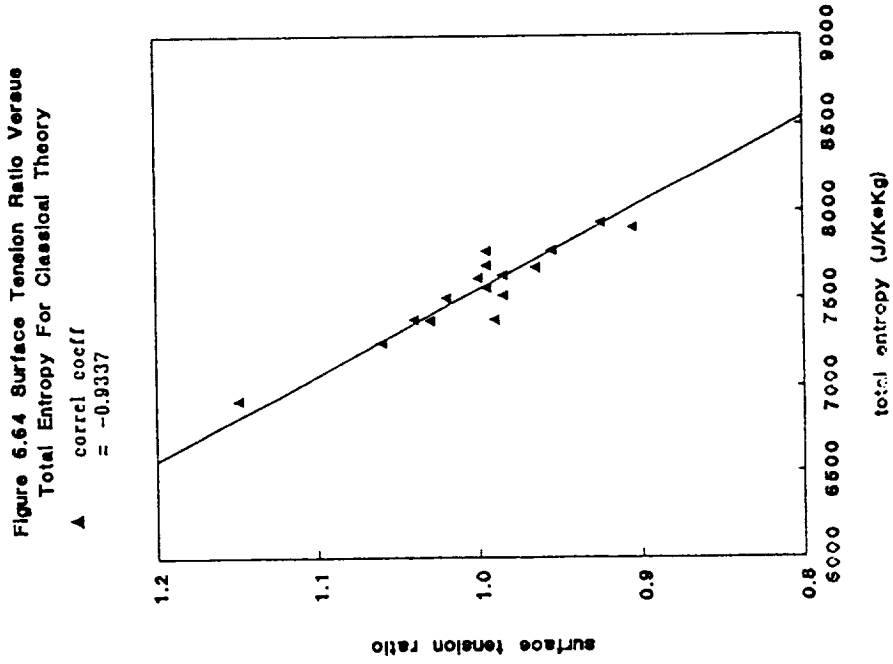
Figure 6.64 Surface Tension Ratio Versus
Total Entropy For Classical Theory
correl coeff
= -0.9337
surface tension ratio
1.2
1.1
1.0
0.9
0.8
6000
6500
7000
7500
8000
8500
9000
total entropy (J/K•Kg)

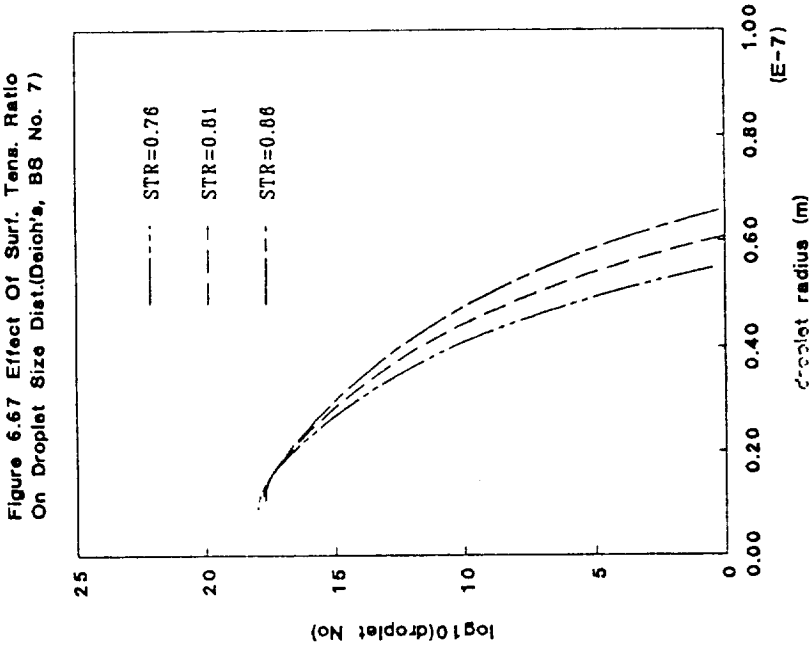


Figure 6.67 Effect Of Surf. Tens. Ratio On Droplet Size Dist.(Deich's, BS No. 7)

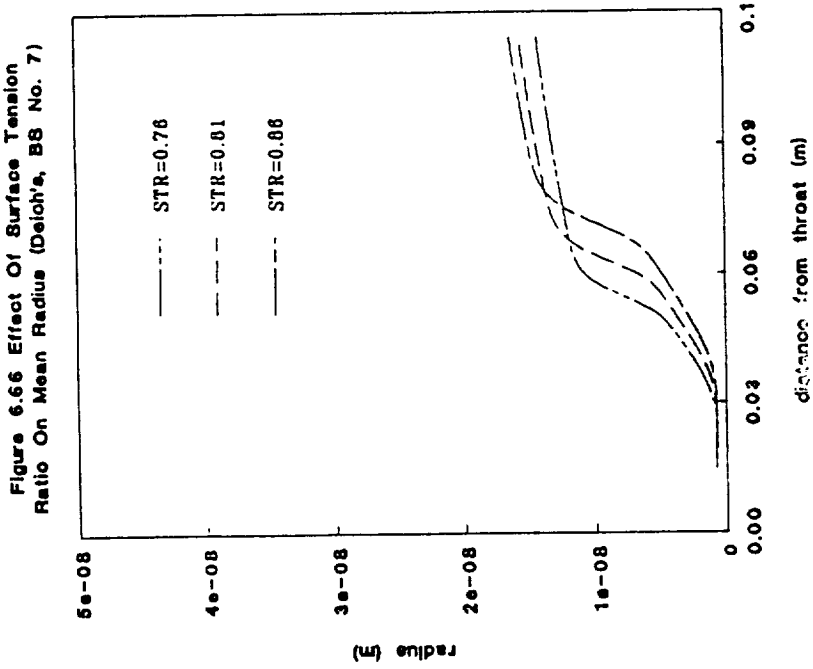


Figure 6.66 Effect Of Surface Tension Ratio On Mean Radius (Deich's, BS No. 7)

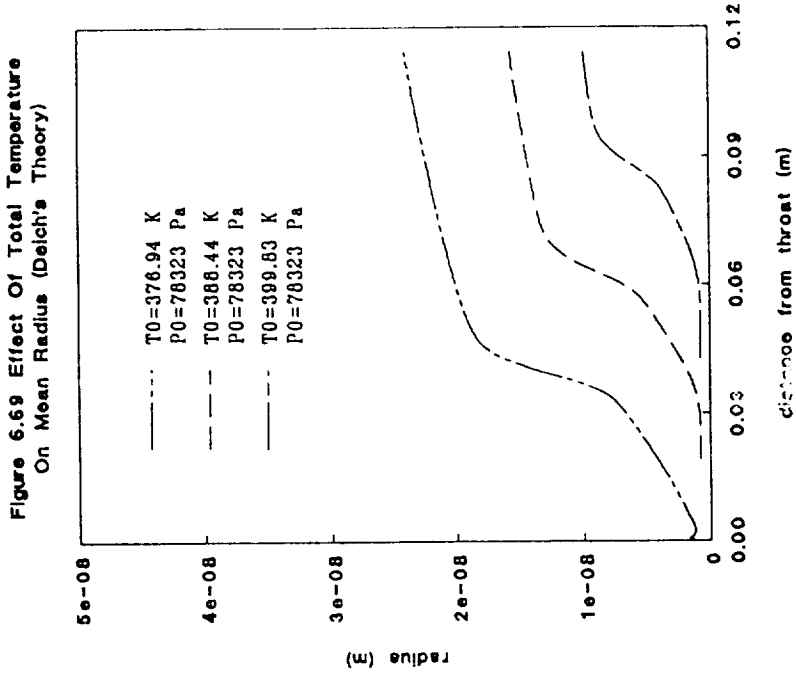
Figure 6.69 Effect Of Total Temperature
On Mean Radius (Delch's Theory)
T0=376.94 K
P0=70323 Pa
T0=388.44 K
P0=70323 Pa
T0=399.83 K
P0=70323 Pa
radius (m)
5e-08
4e-08
3e-08
2e-08
1e-08
0
0.00
0.03
0.06
0.09
0.12
distance from throat (m)

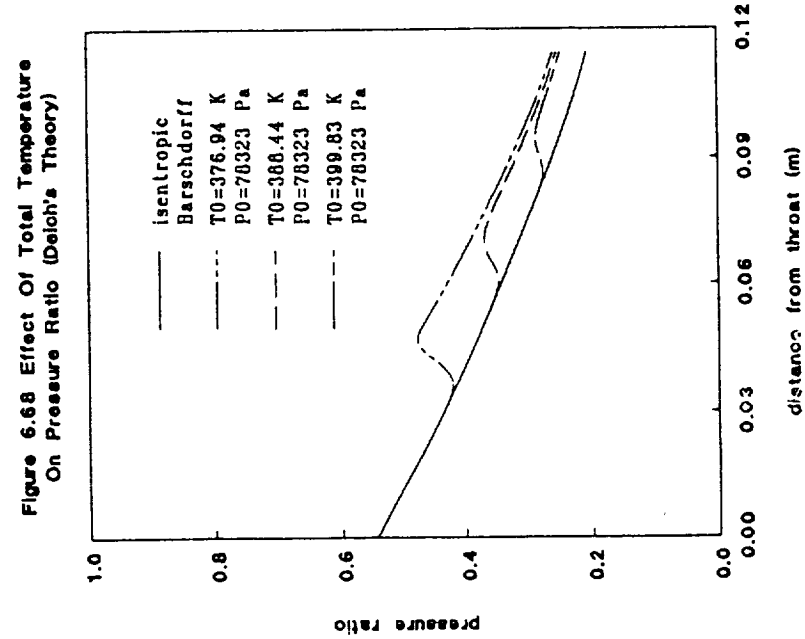
Figure 6.68 Effect Of Total Temperature
On Pressure Ratio (Delch's Theory)
isentropic
Barschdorff
T0=376.94 K
P0=70323 Pa
T0=388.44 K
P0=70323 Pa
T0=399.83 K
P0=70323 Pa
pressure ratio
1.0
0.8
0.6
0.4
0.2
0.0
0.00
0.03
0.06
0.09
0.12
distance from throat (m)

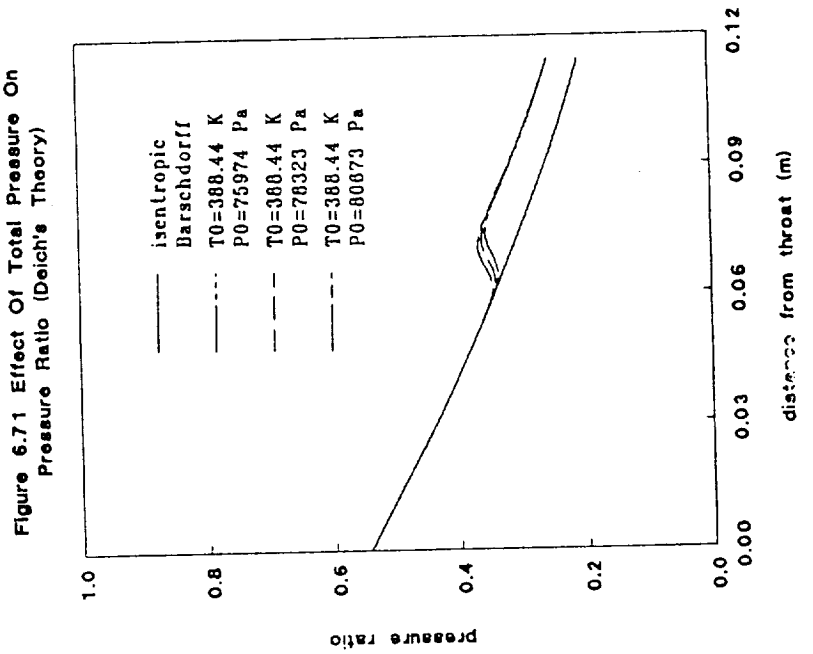


Figure 6.71 Effect Of Total Pressure On Pressure Ratio (Deich's Theory)

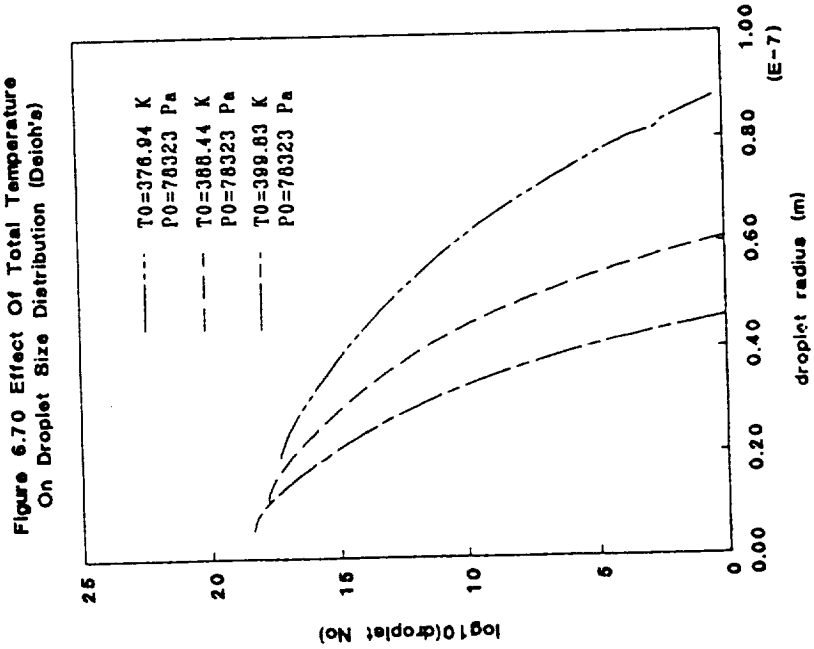


Figure 6.70 Effect Of Total Temperature On Droplet Size Distribution (Deich's)

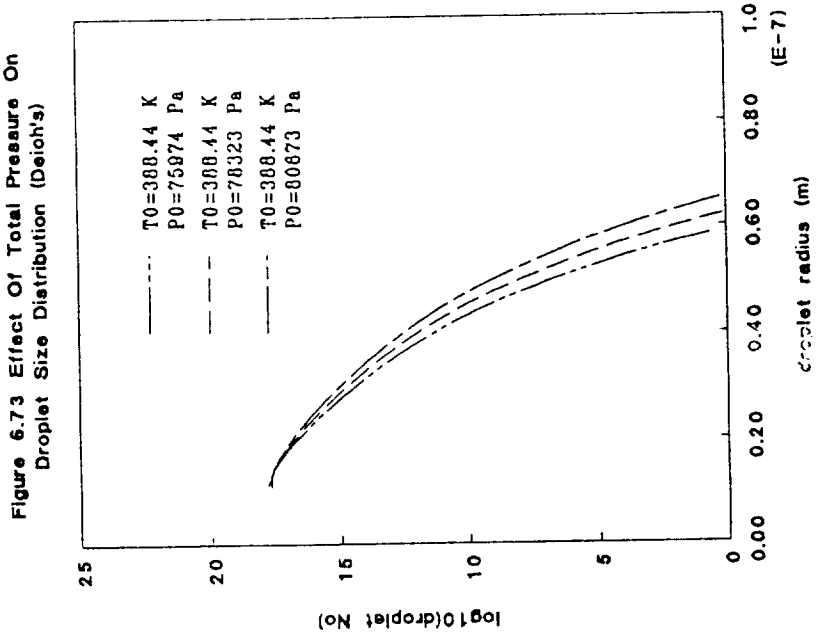
Figure 6.73 Effect Of Total Pressure On
Droplet Size Distribution (Deich's)
T0=388.44 K
P0=75974 Pa
T0=388.44 K
P0=78323 Pa
T0=388.44 K
P0=80873 Pa
log10(droplet No)
droplet radius (m)
(E-7)

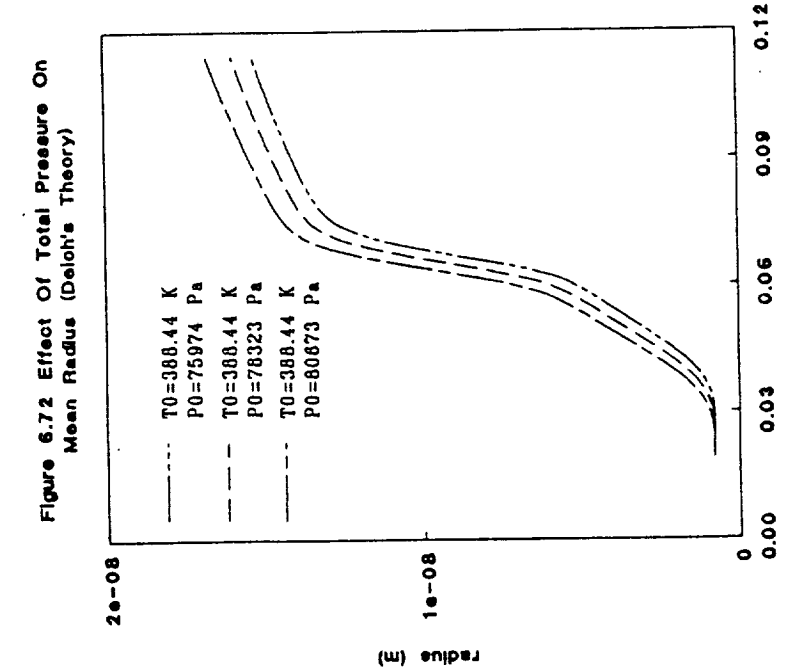
Figure 6.72 Effect Of Total Pressure On
Mean Radius (Deich's Theory)
T0=388.44 K
P0=75974 Pa
T0=388.44 K
P0=78323 Pa
T0=388.44 K
P0=80873 Pa
radius (m)
distance from throat (m)

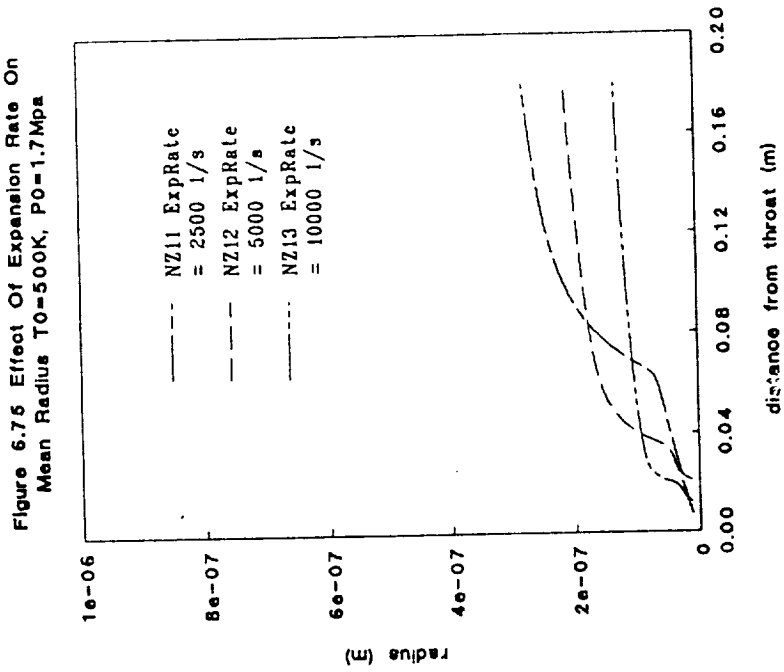
Figure 6.75 Effect Of Expansion Rate On
Mean Radius T0=500K, P0=1.7Mpa
NZ11 ExpRate
= 2500 1/s
NZ12 ExpRate
= 5000 1/s
NZ13 ExpRate
= 10000 1/s
radius (m)
1e-06
8e-07
6e-07
4e-07
2e-07
0
0.00
0.04
0.08
0.12
0.16
0.20
distance from throat (m)

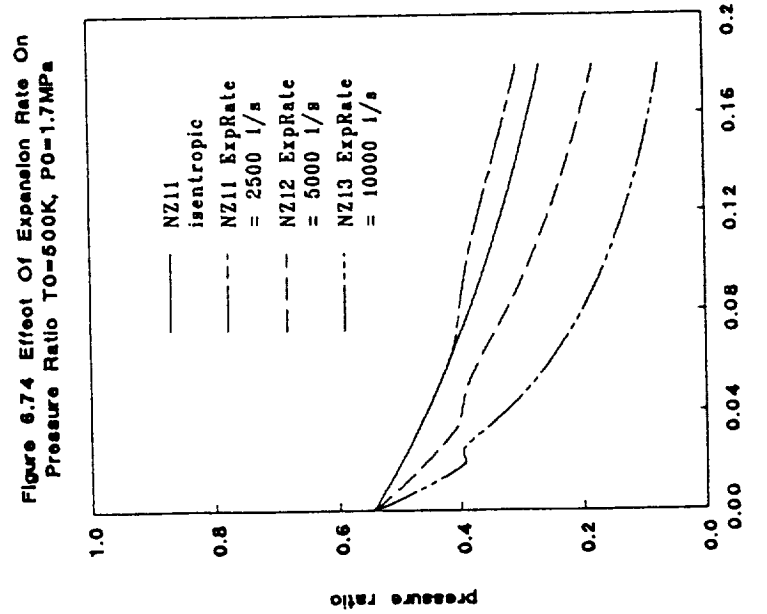
Figure 6.74 Effect Of Expansion Rate On
Pressure Ratio T0=500K, P0=1.7MPa
NZ11
isentropic
NZ11 ExpRate
= 2500 1/s
NZ12 ExpRate
= 5000 1/s
NZ13 ExpRate
= 10000 1/s
pressure ratio
1.0
0.8
0.6
0.4
0.2
0.0
0.00
0.04
0.08
0.12
0.16
0.20
distance from throat (m)

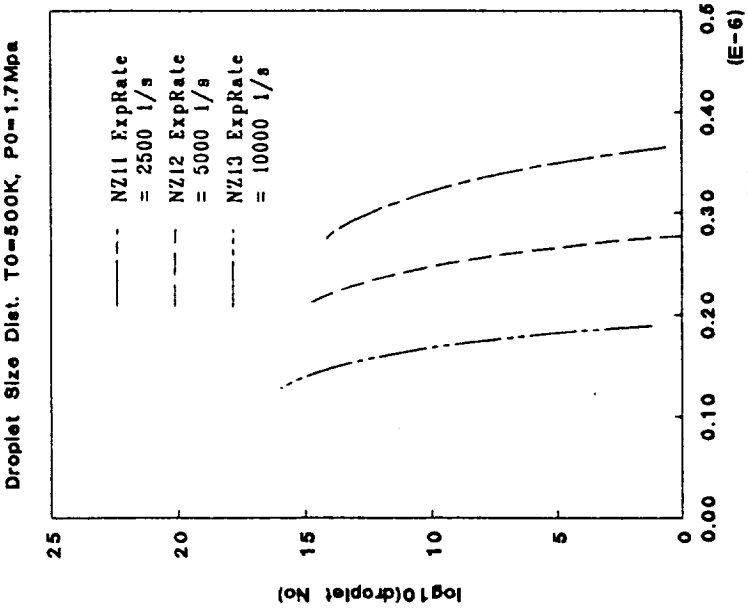


Figure 6.76 Effect Of Expansion Rate On Droplet Size Dist. T0=500K, P0=1.7Mpa

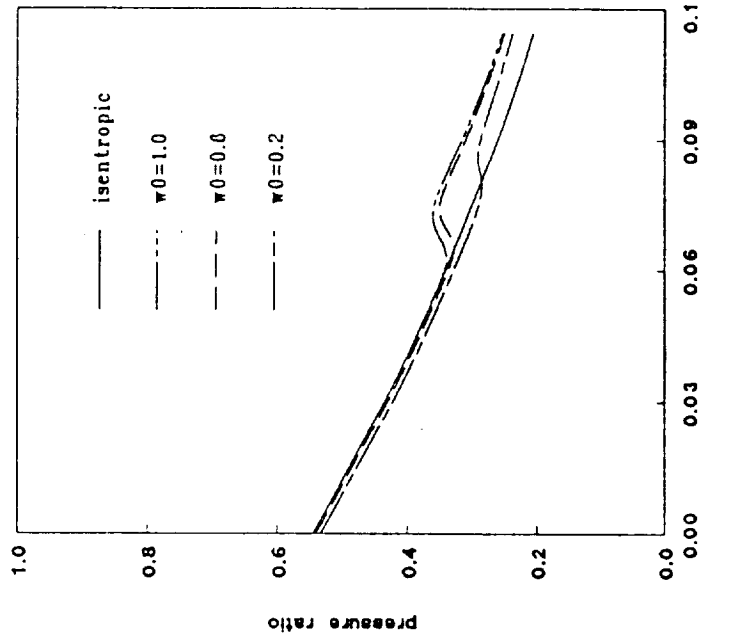


Figure 6.77 Press. Ratio Of Barschdorff No. 7 Using Two Component Vapor

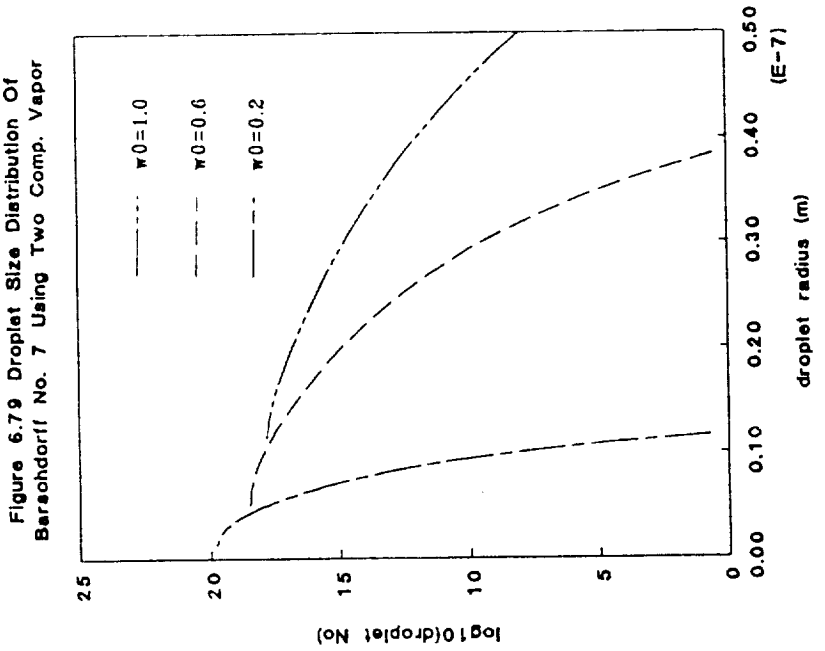
Figure 6.79 Droplet Size Distribution Of
Barschdorff No. 7 Using Two Comp. Vapor
w0=1.0
w0=0.6
w0=0.2
log10(droplet No)
25
20
15
10
5
0
0.00
0.10
0.20
0.30
0.40
0.50
(E-7)
droplet radius (m)

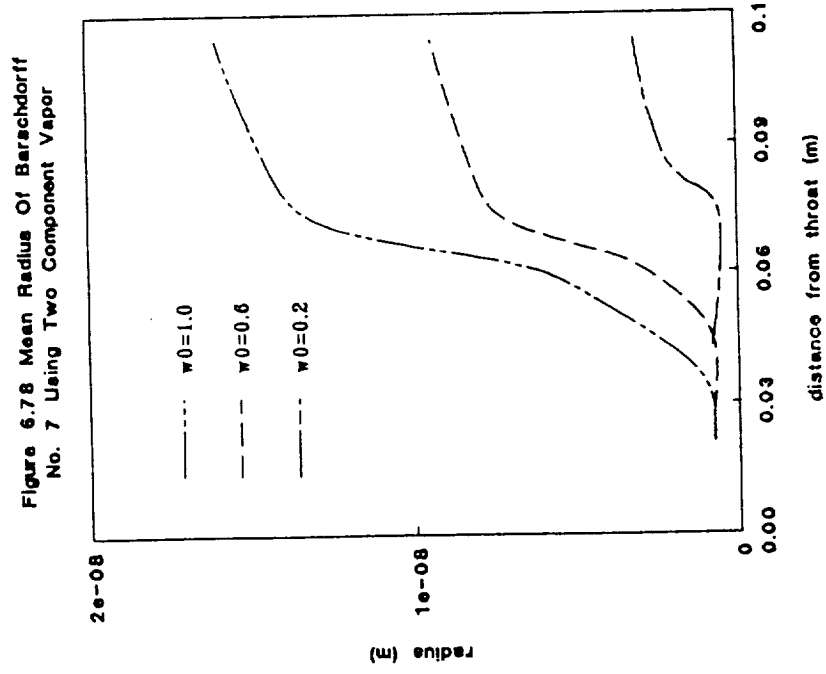
Figure 6.78 Mean Radius Of Barschdorff
No. 7 Using Two Component Vapor
w0=1.0
w0=0.6
w0=0.2
radius (m)
2e-08
1e-08
0
0.00
0.03
0.06
0.09
0.12
distance from throat (m)

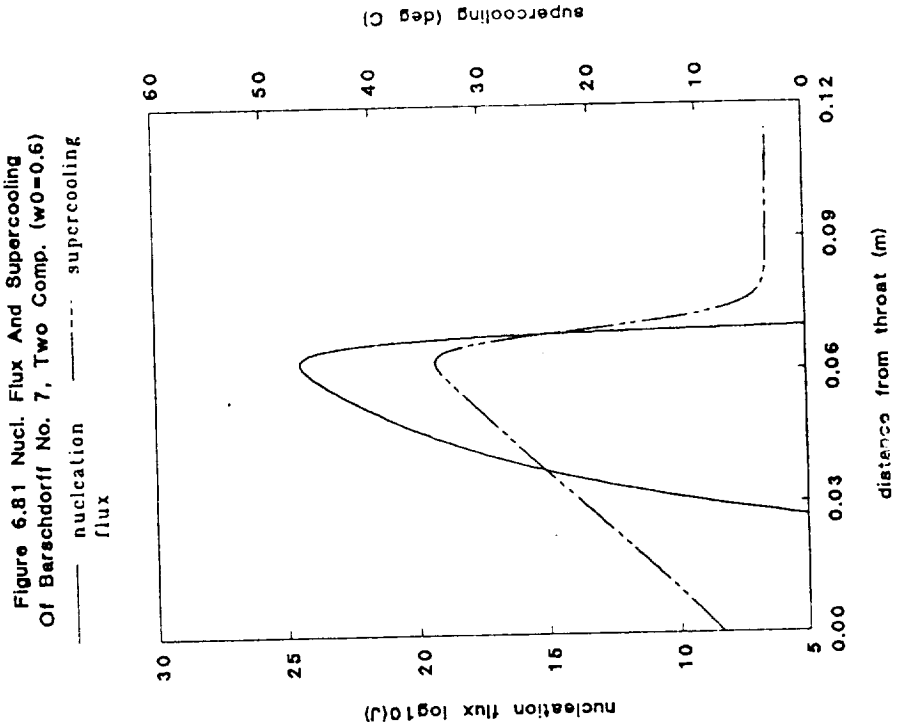


Figure 6.81 Nucl. Flux And Supercooling Of Barschdorff No. 7, Two Comp. (w0=0.6)

——— nucleation flux  - - - - - supercooling

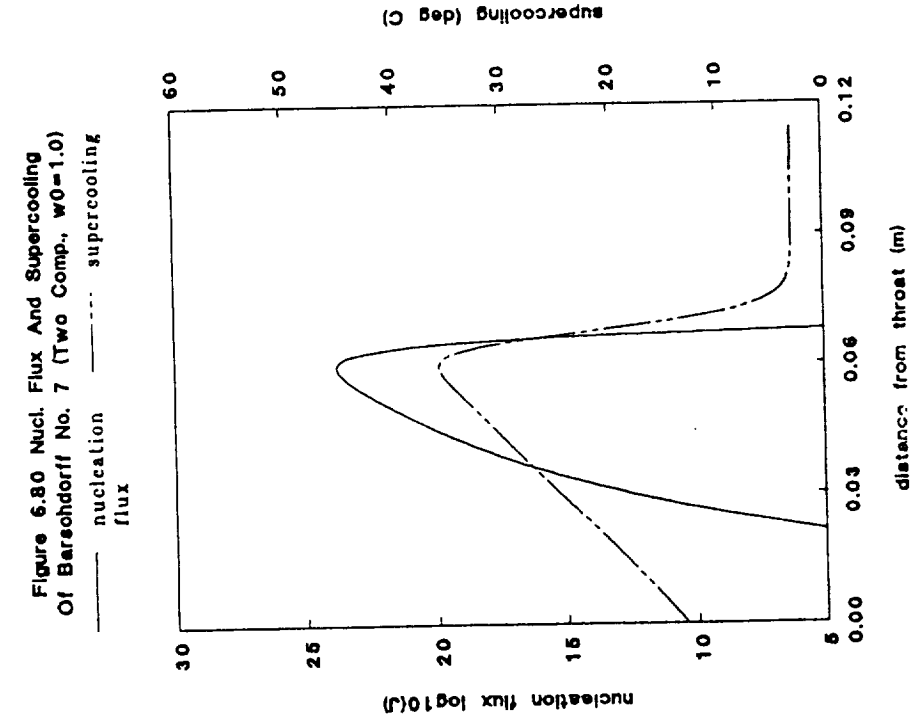


Figure 6.80 Nucl. Flux And Supercooling Of Barschdorff No. 7 (Two Comp., w0=1.0)

——— nucleation flux  - - - - - supercooling

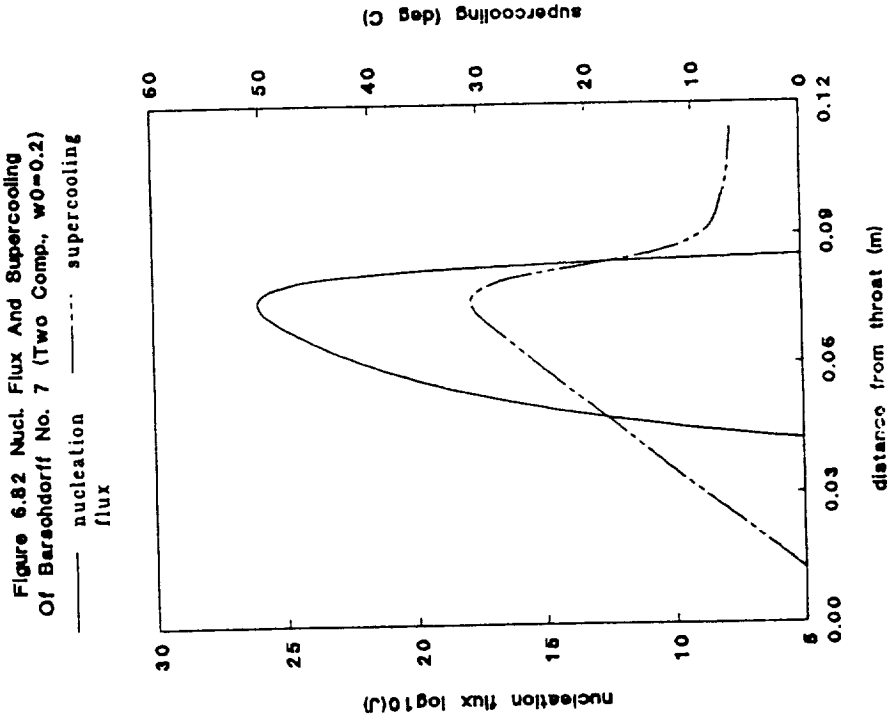


Figure 6.82 Nucl. Flux And Supercooling Of Barschdorff No. 7 (Two Comp., w0=0.2)

—— nucleation flux ——·—· supercooling

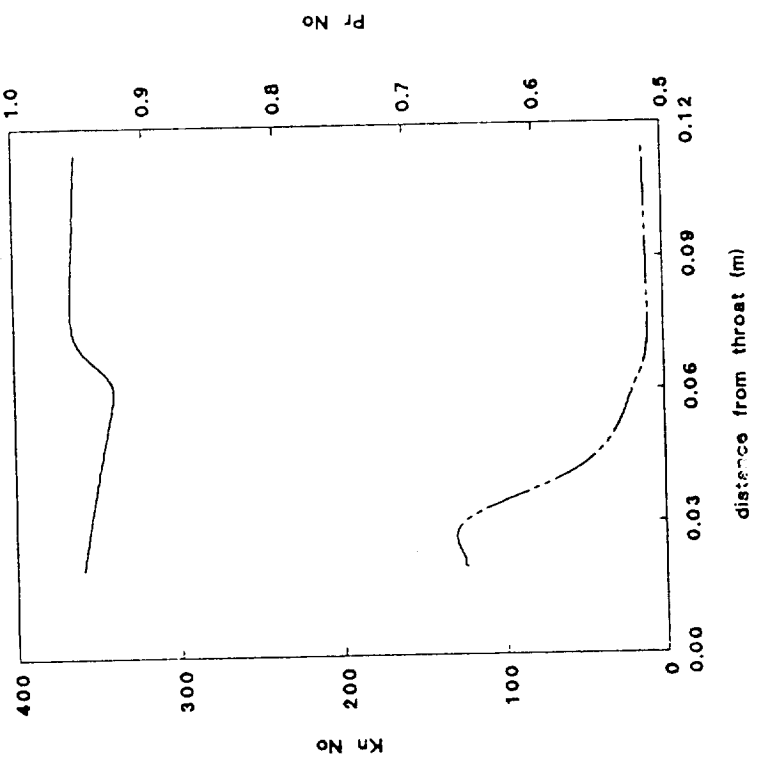


Figure 6.83 Knudsen No. And Prandtl No. Of Barschdorff No. 7, Two Comp. (w0=1.0)

—·—·— Kn No ——— Pr No

Figure 6.84 Knudsen No. And Prandtl No.
Of Barschdorff No. 7 (Two Comp., w0=0.6)

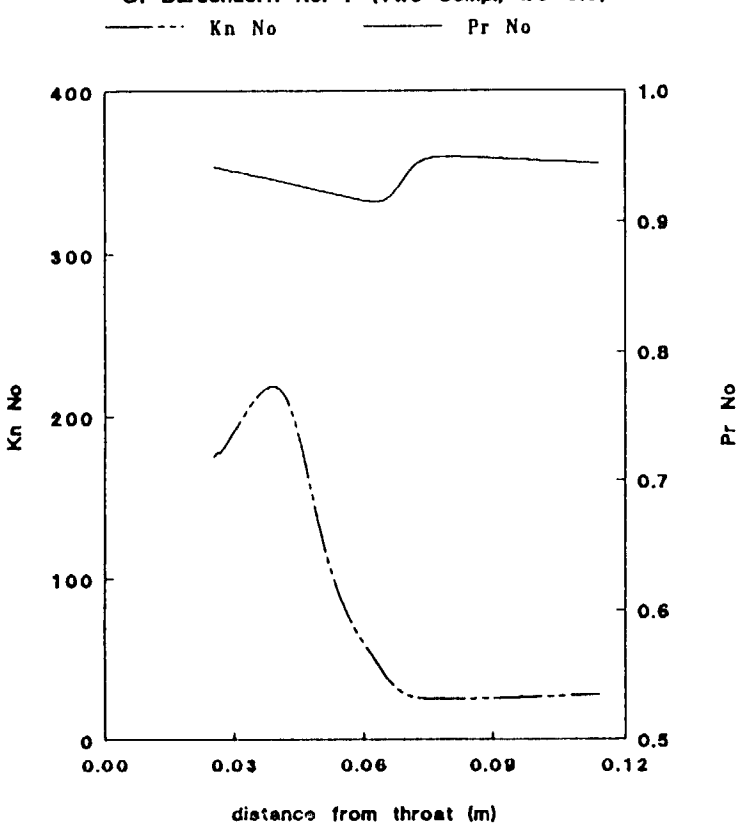


Figure 6.85 Knudsen No. And Prandtl No.
Of Barschdorff No. 7, Two Comp. (w0=0.2)

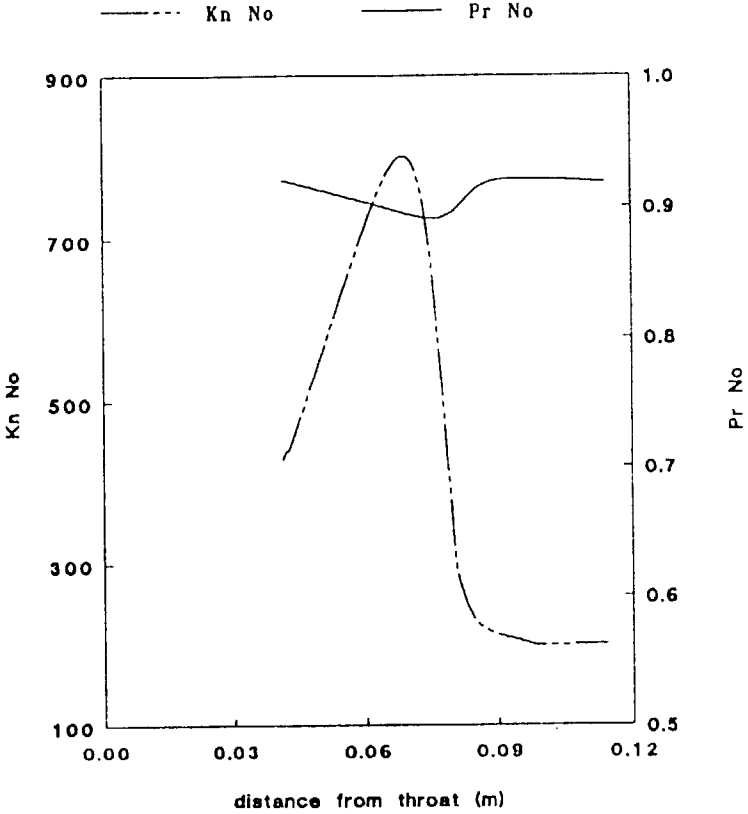

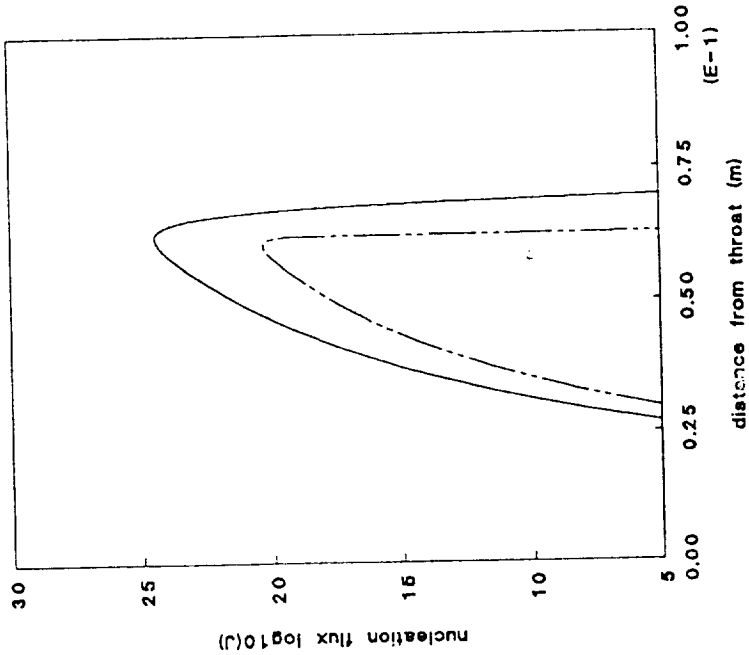


Figure 6.87 Two Components Of Nucl. Flux Of Barschdorff No. 7, Two Comp. (w0=0.6)

——— J1 ——·—·— J2

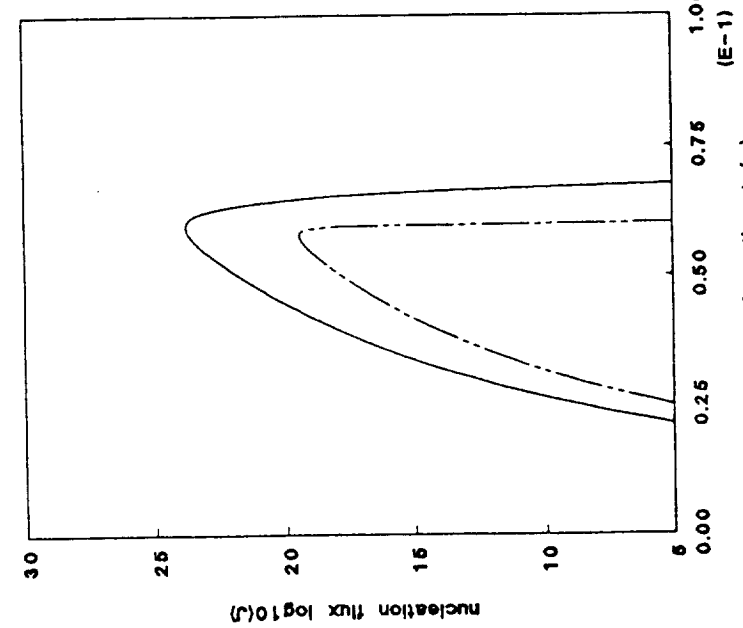


Figure 6.86 Two Components Of Nucl. Flux Of Barschdorff No. 7 (Two Comp., w0=1.0)

——— J1 ——·—·— J2

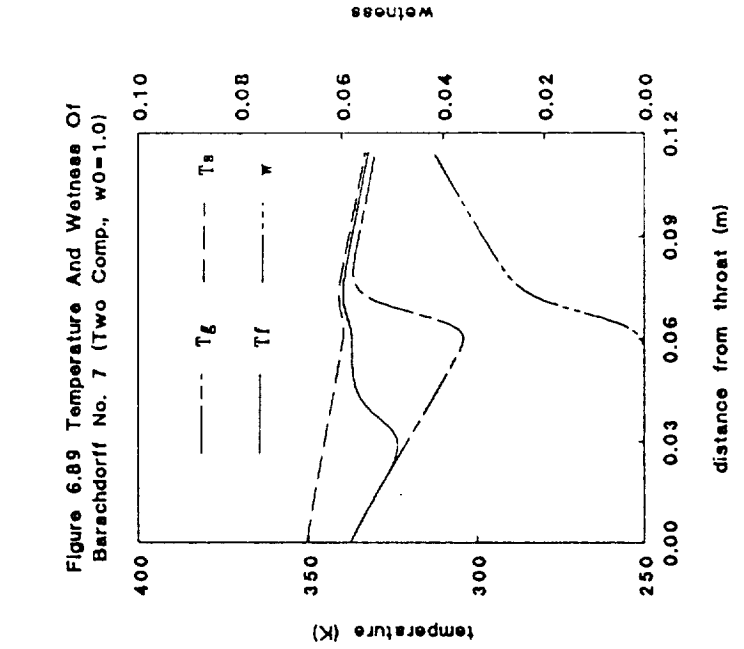


Figure 6.89 Temperature And Wetness Of Barschdorff No. 7 (Two Comp., w0=1.0)

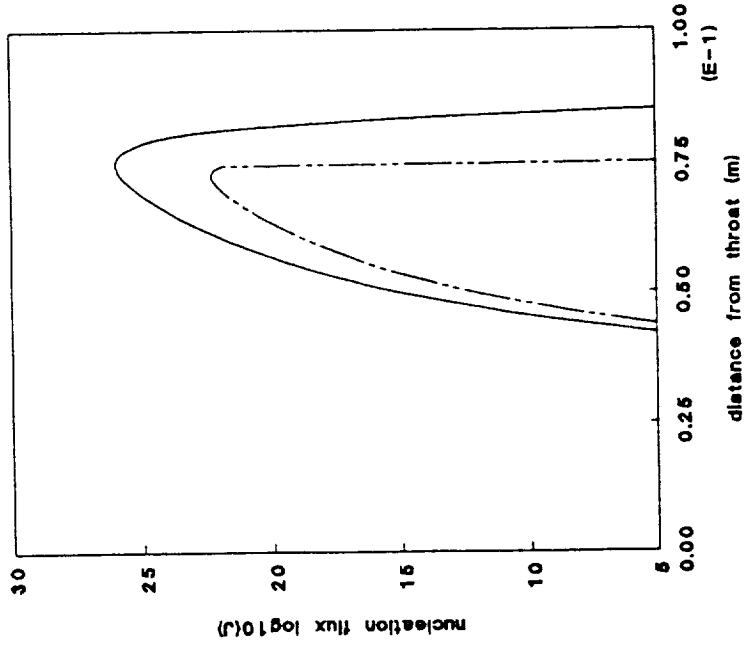


Figure 6.88 Two Components Of Nucl. Flux Of Barschdorff No. 7 (Two Comp., w0=0.2)

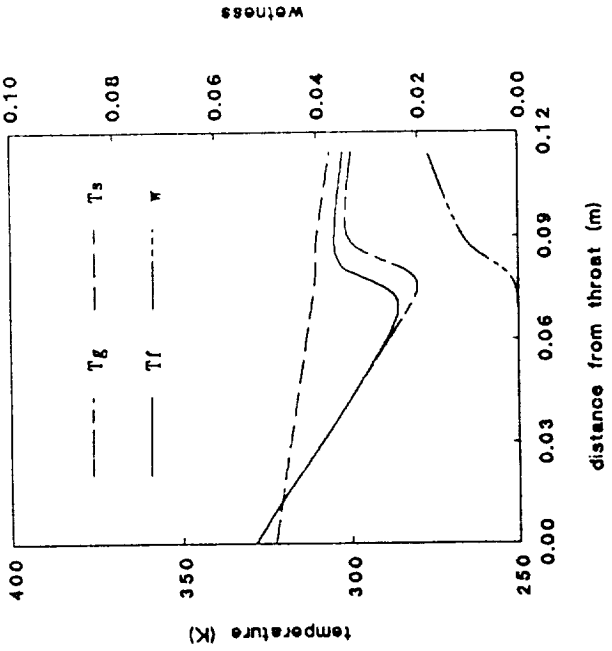


Figure 6.91 Temperature And Wetness Of Barschdorff No. 7 (Two Comp., w0=0.2)

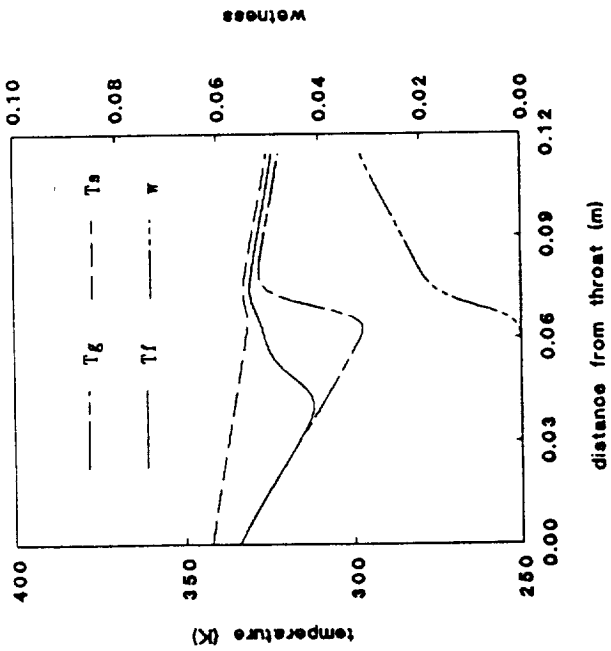


Figure 6.90 Temperature and Wetness Of Barschdorff No. 7 (Two Comp., w0=0.6)

Figure 6.92 Velocity and Expansion Rate
Of Barschdorff No. 7 (Two Comp., w0=1.0)

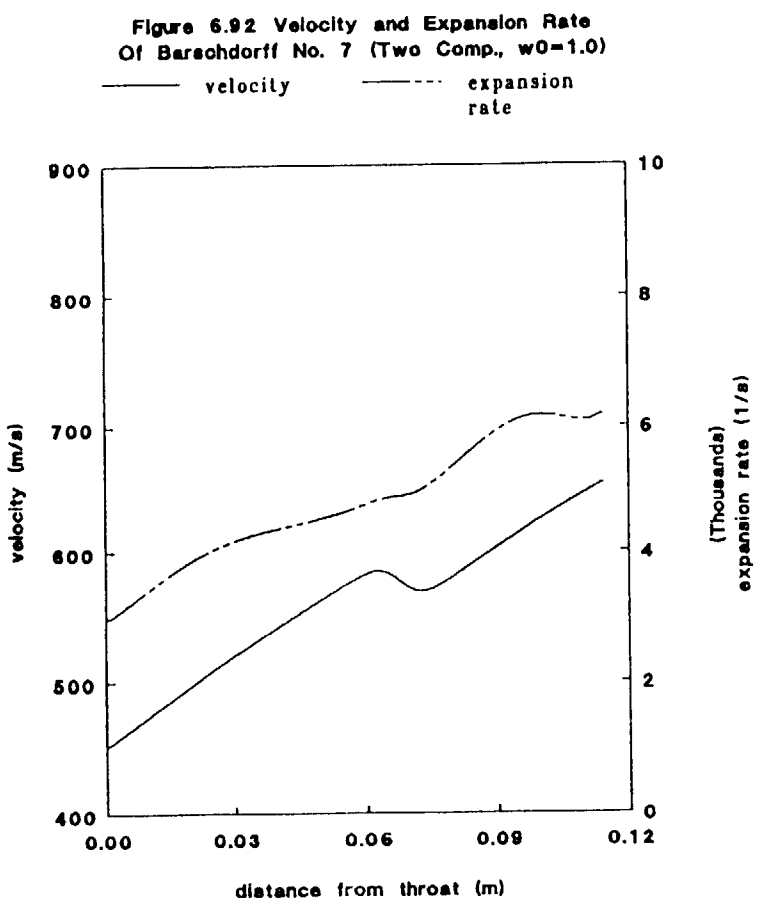


Figure 6.93 Velocity And Expansion Rate
Of Barschdorff No. 7, Two Comp. (w0=0.6)

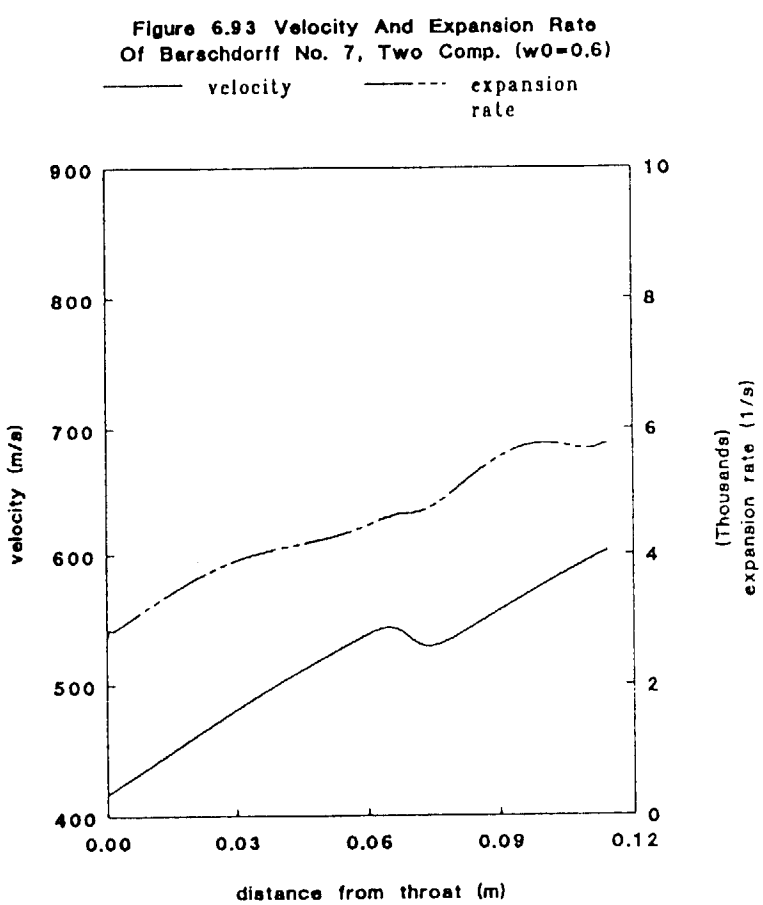

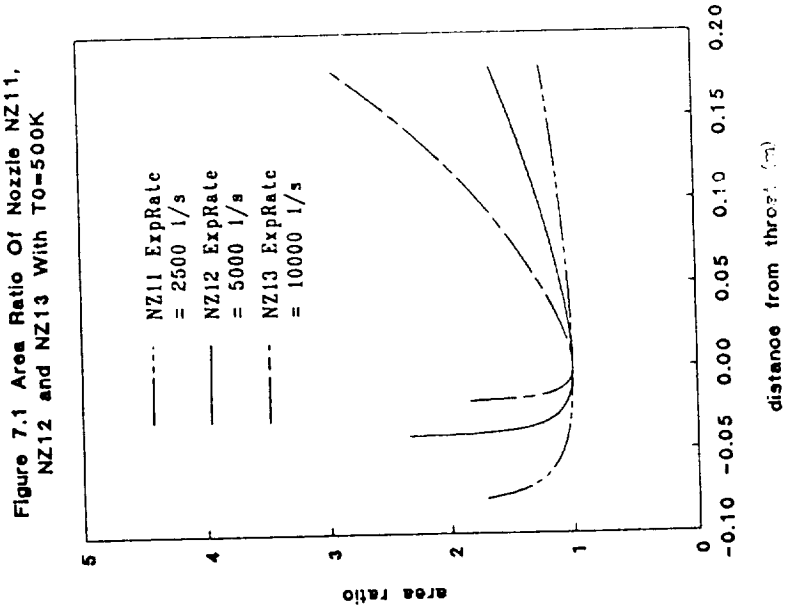


Figure 7.1 Area Ratio Of Nozzle NZ11, NZ12 and NZ13 With T0=500K

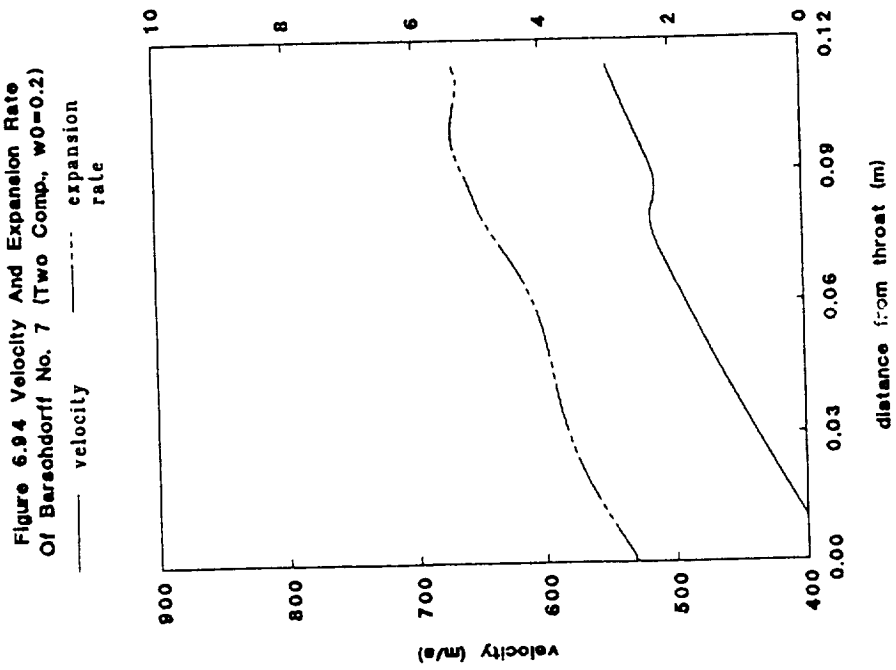


Figure 6.94 Velocity And Expansion Rate Of Barschdorff No. 7 (Two Comp., w0=0.2)

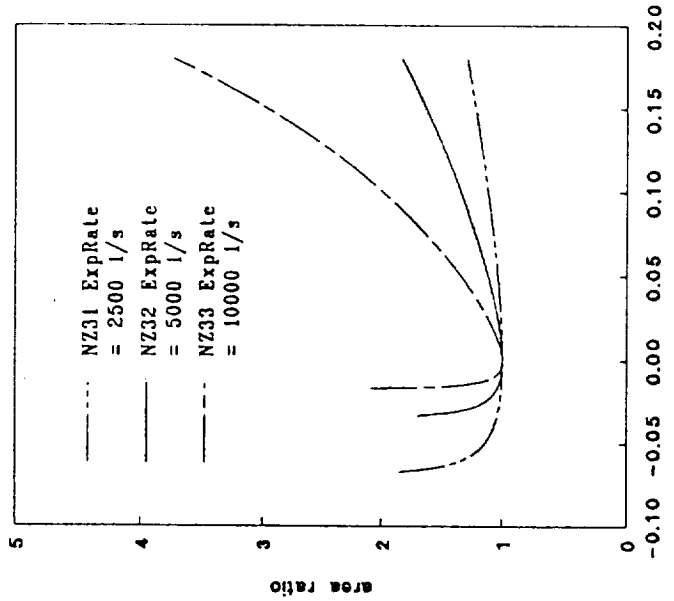


Figure 7.3 Area Ratio Of Nozzle NZ31, NZ32 And NZ33 With T0=350K

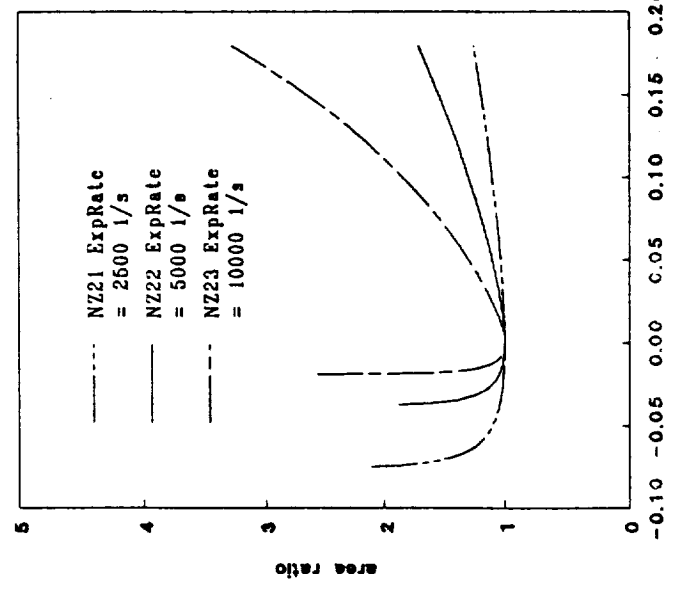


Figure 7.2 Area Ratio Of Nozzle NZ12, NZ22 And NZ23 With T0=425K